11-25-2015 12:00 AM

Fundamentals of the Biomechanical Characteristics Related to the Loading of Reverse Total Shoulder Arthroplasty Implants and the Development of a Wear Simulation Strategy

G Daniel G. Langohr
The University of Western Ontario

Supervisor
James A. Johnson
The University of Western Ontario

Recommended Citation

Langohr, G Daniel G., "Fundamentals of the Biomechanical Characteristics Related to the Loading of Reverse Total Shoulder Arthroplasty Implants and the Development of a Wear Simulation Strategy" (2015). *Electronic Thesis and Dissertation Repository*. 3436.
https://ir.lib.uwo.ca/etd/3436

FUNDAMENTALS OF THE BIOMECHANICAL CHARACTERISTICS RELATED TO THE LOADING OF REVERSE TOTAL SHOULDER ARTHROPLASTY IMPLANTS AND THE DEVELOPMENT OF A WEAR SIMULATION STRATEGY

(Thesis format: Integrated Article)

by

Gordon Daniel George <u>Langohr</u>

Graduate Program in Biomedical Engineering

A thesis submitted in partial fulfillment
of the requirements for the degree of
Doctor of Philosophy

The School of Graduate and Postdoctoral Studies
The University of Western Ontario
London, Ontario, Canada

© Gordon Daniel George Langohr 2015

Abstract

A greater understanding of reverse total shoulder arthroplasty (RTSA) in terms of articular contact mechanics and wear is essential for the optimization of current surgical technique and future implant design. Despite the prevalence of RTSA for shoulder reconstruction, there is little information in current literature regarding the effects of changes in implant parameters on articular contact mechanics and wear. The present work describes the use of in-vitro cadaveric studies, a computational model of the articular contact surfaces, and the development and implementation of a wear simulation strategy to assess RTSA contact mechanics and wear.

The articular loading characteristics of RTSA were assessed using an in-vitro shoulder joint motion simulator and a custom instrumented implant, including the effects of changes in implant configuration. Decreasing neck-shaft angle and cup depth was not found to affect joint load or muscle forces. Increasing glenosphere diameter increased adduction range of motion (ROM), but also slightly increased joint load.

The contact mechanics of RTSA were then investigated. The location of the contact patch and peak contact stress was typically in the inferior humeral cup quadrant, coincident with the location of clinical retrieval damage. Reducing neck-shaft angle and decreasing cup depth reduced contact area and increased peak contact stress, which may negatively impact implant performance. Increasing size came at no cost in terms of contact mechanics.

A wear simulation strategy was developed based on the loading and motion characteristics of the cadaveric study, and produced a mean wear rate of 201.1 ± 86.5 mm^3/Mc, which was higher than previously published data, and created damage in the cup inferior quadrant. The number of 'cycles' per year for RTSA reconstructed shoulders was estimated between 0.33-1.5 Mc/yr, suggesting a similar order of magnitude as the lower extremities.

The present work advances knowledge regarding RTSA biomechanics and tribology. Specific tradeoffs in terms of ROM and contact mechanics were observed for the reduction of both neck-shaft angle and cup depth, whereby increased motion came at the cost of

reduced contact area and increased peak contact stress. Increasing size improved ROM without any negative consequences on contact mechanics.

Keywords

Co-Authorship Statement

Chapter 1:   GDG Langohr – sole author

Chapter 2:   GDG Langohr – developed implant system, study design, data collection,
statistical analysis, wrote manuscript

JW Giles– developed implant system, study design, data collection

GS Athwal – study design, specimen preparation, reviewed manuscript

JA Johnson – study design, reviewed manuscript

Chapter 3:   GDG Langohr – developed model, study design, data collection,
statistical analysis, wrote manuscript

R Willing – model development, study design, reviewed manuscript

JB Medley – study design, reviewed manuscript

GS Athwal – study design, reviewed manuscript

JA Johnson – study design, reviewed manuscript

Chapter 4:   GDG Langohr – developed and implemented testing apparatus & wear
simulation strategy, study design, data collection, wrote manuscript

GS Athwal – study design, reviewed manuscript

JA Johnson – study design, reviewed manuscript

JB Medley – wear simulation strategy development, study design, reviewed
manuscript

Chapter 5:   GDG Langohr –study design, data collection, wrote manuscript

MW Griffiths - data collection

GS Athwal – study design, reviewed manuscript

JA Johnson – study design, reviewed manuscript

JB Medley – study design, reviewed manuscript

MG Teeter - CT scanned specimens

Chapter 6:   GDG Langohr - sole author

Acknowledgments

Table of Contents

List of Tables

List of Figures

xiii

List of Appendices

Chapter 1

1   Introduction

OVERVIEW

This primary chapter illustrates the glenohumeral joint in terms of its anatomy, soft tissues, physiology and kinematics. Insight into the need for replacement of the glenohumeral joint, both primary and reverse, is also described. Additionally, a review of previously described biomechanical studies regarding the joint loading of reverse total shoulder arthroplasty (RTSA) and the resulting changes in joint kinematics resulting from this procedure will be provided. Finally, the current state of literature regarding the finite element modeling and wear simulation of RTSA is also described. In summary, this introductory chapter outlines the motivation for the investigation of the specific biomechanical and clinical questions regarding RTSA, as well as the objectives and hypotheses regarding these investigations.

1.1   The Shoulder

The shoulder provides the largest range of motion of any joint in the human body, allowing for humeral orientation in a space larger than a hemisphere (Culham & Peat, 1993). In order to provide this impressive range of motion, the shoulder joint uniquely employs three articulations between three bones and includes a shallow 'ball on socket' type joint whereby the centre of rotation of the ball, or humeral head, is not captured (or constrained) by bony anatomy. Constraint of the native joint is primarily achieved by a variety of soft tissues including muscles, tendons, and ligaments; all of which work in unison to allow for achieving various states of humeral orientation (Jobe, Phipatanakul, & Coen, 2009). Because shoulder joint stability (resistance to dislocation) is achieved by the cooperative function of these aforementioned anatomic structures, the deficiency of any one of these elements due to injury or disease can result in sub-optimal joint function and shoulder kinematics (Neer, 1990).

The primary focus of this work is the glenohumeral joint, however in order to fully comprehend the biomechanical aspects of the shoulder, an understanding as to how each of the shoulder components contribute to the overall joint function is required. These structures can be broken into three categories; (i) osseous anatomy, (ii) passive soft tissues, and (iii) active musculature. The key anatomical features in each of these categories are outlined below, with particular attention as to how they impact the glenohumeral joint specifically.

1.1.1   Osseous Anatomy

1.1.1.1   Bony Structures

The shoulder is comprised of three bones; the scapula, the clavicle, and the humerus (Figure 1-1). While the glenohumeral joint allows relative motion between the humerus and the scapula, there are three other joints which allow scapular rotation relative to the torso occurring concomitantly to the glenohumeral relative rotation. These joints are the sternoclavicular joint, the acromioclavicular joint, and the scapulothoracic joint (Culham & Peat, 1993). The scapulothoracic joint involves the scapula gliding on the loose aereolar tissue between it and the thoracic rib cage and friction is reduced by bursa. The

focus of this work is mainly the glenohumeral joint, however an understanding as to how each aspect of the shoulder affects this articulation is required. Therefore, for the purpose of this literature review the joints which allow for scapulothoracic rotation will only be described in enough depth to portray the effect of these joints, which is to rotate the scapula during shoulder adduction-abduction.

The scapula forms the connection between the torso and the upper limb, and plays a large role in the anchoring of the soft tissue of the shoulder by serving as the attachment point for a variety of active and passive structures which act between the torso and the scapula and the scapula and the upper limb (Figure 1-2). Not only does the scapula act as a means of force transmission from the torso to the upper limb and vice versa, as previously mentioned it also simultaneously rotates in conjunction with the humerus allowing for the provisioning of the large range of motion at the shoulder (Rockwood, 2009).
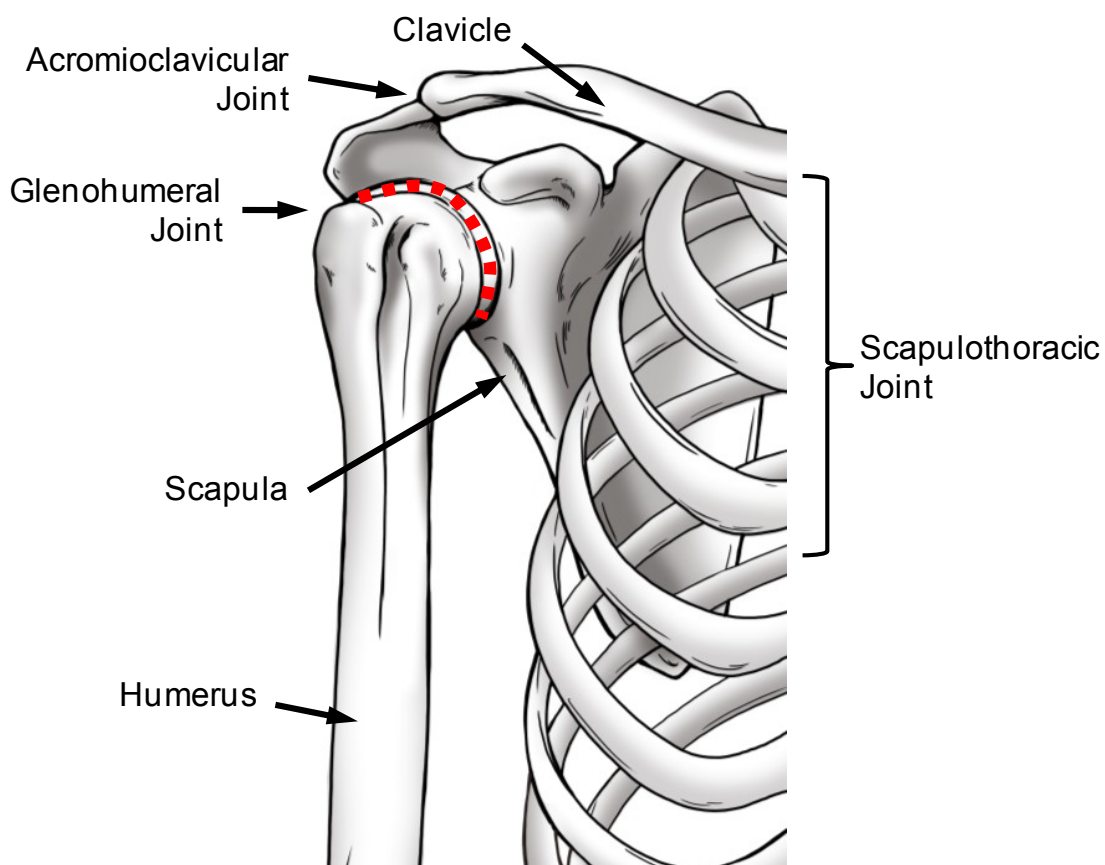
Figure 1-1: The shoulder joint

The glenohumeral joint is illustrated alongside the primary bony structures of the shoulder.
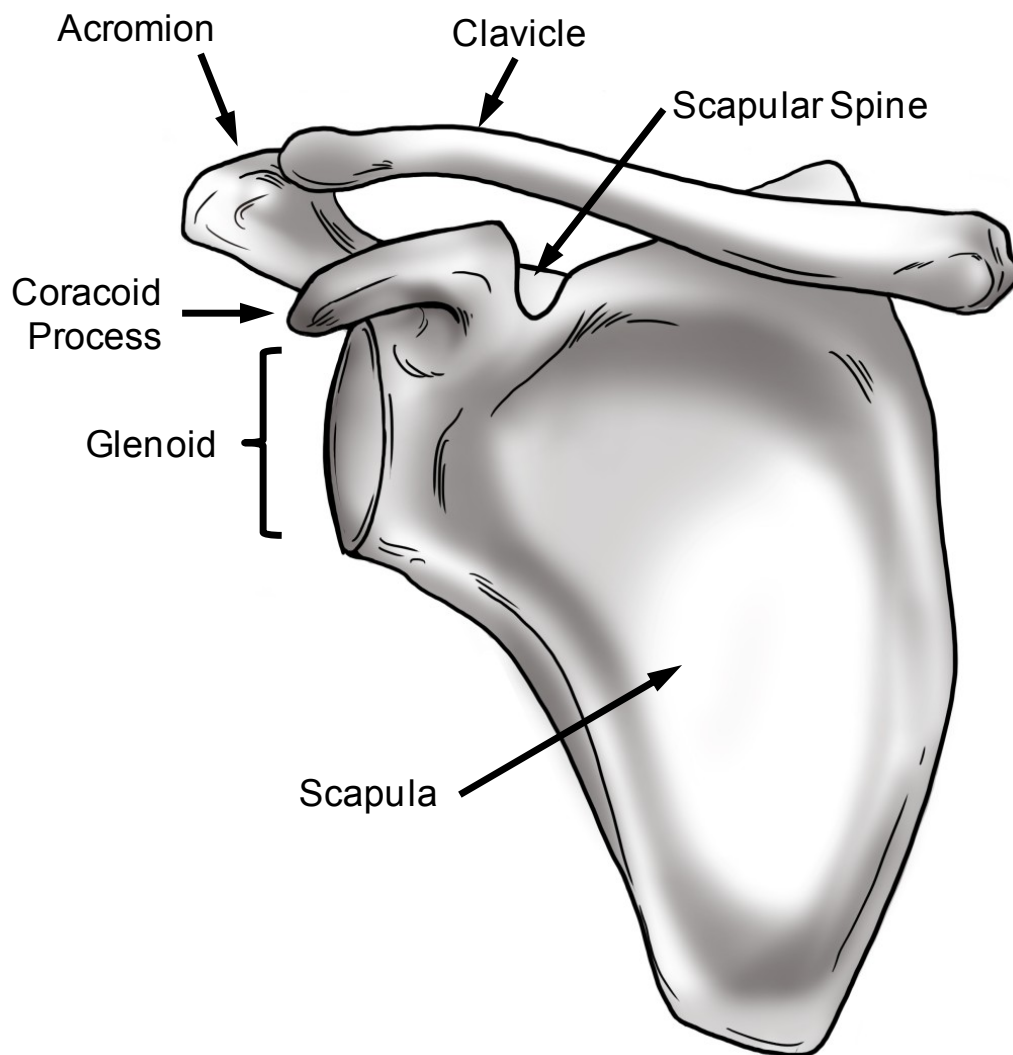
Figure 1-2: Anterior view of the osseous anatomy of a right scapula and clavicle

The acromion extends from the scapular spine and forms a bony arc superior to that of the humeral head when articulated with the scapula. It articulates with the clavicle during scapulothoracic rotation and is the one of the attachment sites of the deltoid and the trapezius muscles (as is shown later). The superior-lateral position of the acromion increases the mechanical advantage of the middle deltoid by increasing the moment arm of the muscle's line of action (Jobe et al., 2009).

The scapula articulates with the humerus via the concave pear-shaped glenoid which is located at the lateral edge of the scapular body (Figure 1-2). The glenohumeral joint is a synovial joint, and as such the glenoid is covered in hyaline cartilage exhibiting an increasing thickness at the peripheral margin which has the effect of increasing glenohumeral joint conformity and translational stability (L J Soslowsky, Flatow, Bigliani, & Mow, 1992). This effect is enhanced by a ring of fibrocartilaginous tissue located at the glenoid periphery, known as the glenoid labrum (Figure 1-3). By increasing the contact area between the glenoid and the humeral head, the labrum also reduces average contact stress of the articulation. The aim of the glenoid labrum is to increase the stability of the glenohumeral joint by increasing conformity and the depth of the concavity with which the humerus articulates in a similar sense to the more highly constrained articulation of the acetabulum and femur that employs bony constraint, while still maintaining a fairly large range of motion while avoiding hard impingement of the mating bony structures (Itoi, Morrey, & An, 2009). Although the glenoid labrum is not as effective as hard constraints by virtue of the flexibility of the structure under shear loading, it is unlikely that a hard constraint of the same geometry would permit similar ranges of motion.

The clavicle forms a connection between the torso and the scapula, which extends laterally from the sternum to the acromion with both it articulates. The purpose of the clavicle is to resist relative compression of the space which it spans, which would force together under muscle loading, and to help guide scapulothoracic rotation.
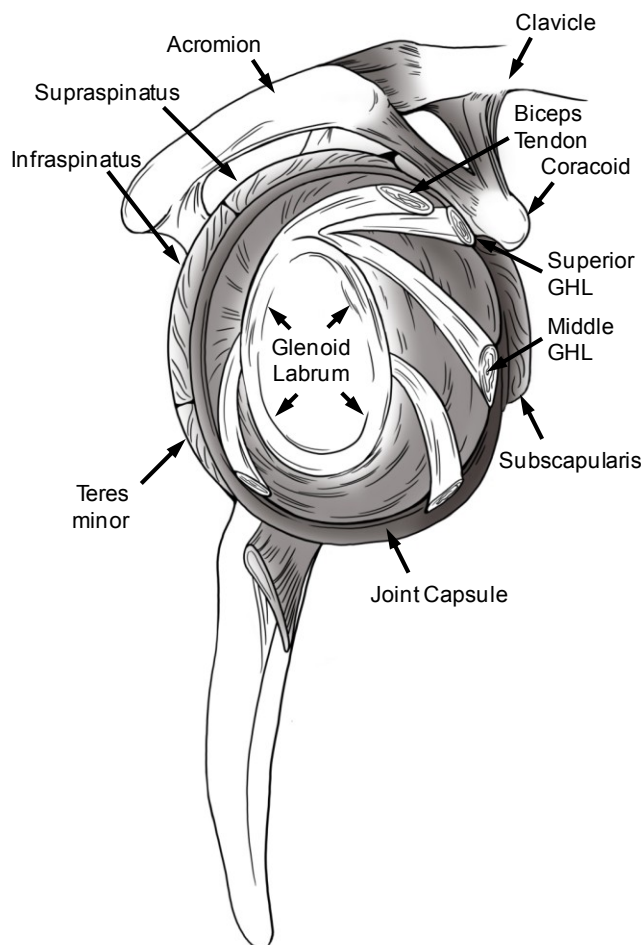
Figure 1-3: Lateral view of the glenoid labrum and soft tissue structures of the scapula.

This illustration exhibits the soft tissue structures pertinent to the present work including selected ligaments and musculature.

The humerus forms the proximal aspect of the upper limb, positioned between the scapula and the radius and ulna. Its proximal end includes a largely spherical surface which forms the humeral head that articulates with the glenoid and its distal end forms one side of the elbow (Figure 1-4). There is a relative rotation between the proximal and distal ends whereby the central axis of the humeral head, which forms approximately one-third of a sphere, is oriented in the superior-medial-posterior direction relative to the elbows flexion-extension axis (O'Brien, Voos, Neviaser, & Drakos, 2009). This orientation permits the humeral head, which is anatomically oriented in the lateral-anterior direction, to be more or less centered within the articular surface of the glenoid when the flexion-extension axis of the elbow (formed between the medial and lateral epicondyles) is oriented in the sagittal plane when the arm is in the at side position. This allows for optimal load transmission, range of motion, and stability of the glenohumeral joint (Itoi et al., 2009). Forming one half of a synovial joint, the humeral head is covered in cartilage of approximately constant thickness (L J Soslowsky, Flatow, Bigliani, Pawluk, et al., 1992).

The greater tuberosity of the humeral head is separated from the lesser tuberosity by the bicipital groove which guides the biceps tendon around the glenohumeral joint from its origin to insertion. The greater tuberosity is posterolateral and the lesser tuberosity is anterolateral, with both being located just lateral of the articular margin of the humeral head (Figure 1-4). The subscapularis muscle inserts on the lesser tuberosity whereas the supraspinatus inserts superiorly and the infraspinatus/teres minor insert posteriorly and posteroinferiorly on the greater tuberosity. In a similar way in which the acromion increases the deltoid moment arm, the greater tuberosity increases the distance from the centre of rotation to the deltoid muscle line of action by displacing the deltoid superolaterally via muscle wrapping at elevation angles lower than 60° (D C Ackland, Pak, Richardson, & Pandy, 2008; Jobe et al., 2009). The deltoid tuberosity serves as the insertion point for the deltoid muscle and is located at the approximate mid-shaft of the humerus.
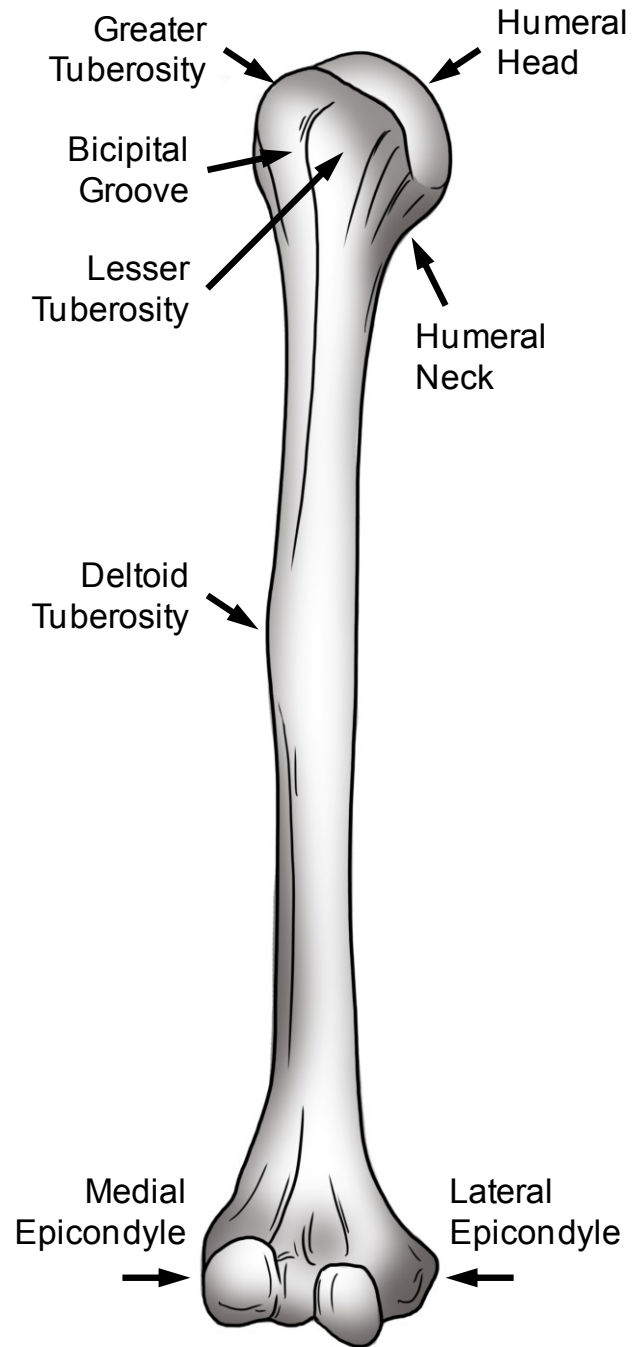
Figure 1-4: Osseous anatomy of a right humerus

1.1.1.2   Articulations

Bony articulations provide motion of the shoulder by permitting relative motion of articulating structures. The glenohumeral joint is the largest contributor to shoulder motion providing three degrees of freedom about the centre of rotation, which is located at the centre of the humeral head (An, Browne, Korinek, Tanaka, & Morrey, 1991; Howell & Galinat, 1989; Karduna, Williams, Williams, & Iannotti, 1997; Lippitt & Matsen, 1993). As previously described, the articular profiles that comprise each side of this joint include the pear-shaped cartilaginous covered concave glenoid and associated glenoid labrum, and the approximately spherical cartilage covered humeral head.

Adduction-abduction range of motion, which is defined as the angle of motion through the lowest angle and the largest humeral elevation angle achievable, is largely limited by impingement of the humeral greater tuberosity and the scapular acromion (Culham & Peat, 1993). The relative motion of the glenohumeral joint is predominantly rotation of the humerus about its centre of rotation, however there is some translation permitted as the radius of curvature of the glenoid is slightly larger than the humeral head, and the glenoid labrum can deform when the joint is placed under shear loading thereby permitting some sliding (Itoi et al., 2009; L J Soslowsky, Flatow, Bigliani, & Mow, 1992).

The acromioclavicular, sternoclavicular, and scapulothoracic joints serve to permit relative motion between the scapula and torso (Culham & Peat, 1993). These joints provide stability of the scapula during motion, while still allowing scapular rotation relative to the torso, the concomitant motion that is a large component of maintaining glenohumeral joint stability during humeral elevation by limiting the shear loading transverse to the glenoid surface that needs to be counteracted by the soft tissues of the shoulder (Lippitt & Matsen, 1993).

Although not a discrete articulation characterized by a cartilaginous coating and a joint capsule, the acromion and coracoid do tend to articulate with the humerus through interaction of the rotator cuff muscles and the acromion and coracoid structures and their

linking coracoaromial ligament (Culham & Peat, 1993). This interaction serves to stabilize the glenohumeral joint superiorly when subjected to anterior loading.

1.1.2   Passive Soft Tissues

Passive soft tissues, which include joint capsules and ligaments, act as shoulder stabilizers when tensioned via glenohumeral rotation, and in many cases aid in limiting range of motion at extreme joint angles. The glenohumeral joint capsule (Figure 1-3) is sufficiently loose to allow the large range of motion of the joint, but becomes adequately tensioned near the end limits of motion so as to passively restrict joint hyper mobility (Peat, 1986). The capsule connects the periphery of the glenoid labrum to the articular margin of the humeral head. The glenohumeral ligaments reinforce the joint capsule in the superior, anterior, and inferior aspects, and act to control glenohumeral motion by becoming tensioned during certain motion configurations (Burkart & Debski, 2002).

1.1.3   Active Musculature

In addition to passive soft tissues, active soft tissues also play a role in shoulder stabilization with the added role of also being responsible for arm positioning. The muscles can be grouped into three categories based on their origin and insertion sites; the scapulohumeral, humerothroracic, and scapulothoracic. For the purpose of this work, the scapulothoracic, or musculature that is responsible for rotation of the scapula with respect to the torso, will not be explicitly defined.

The scapulohumeral muscles include the deltoid, supraspinatus, subscapularis, infraspinatus, teres minor, and coracobrachialis (Figure 1-5). The deltoid is the one of the primary drivers of humeral abduction, and has been shown to produce about one-half the moment required to produce glenohumeral abduction (Hess, 2000). The deltoid is divided into three independent segments (or heads) to form the anterior, middle, and posterior deltoids. Due to their slightly varying lines of action, the anterior and posterior deltoids can produce humeral rotation in the flexion-extension and internal-external rotation planes in addition to abduction rotation (D. Ackland & Pandy, 2011).
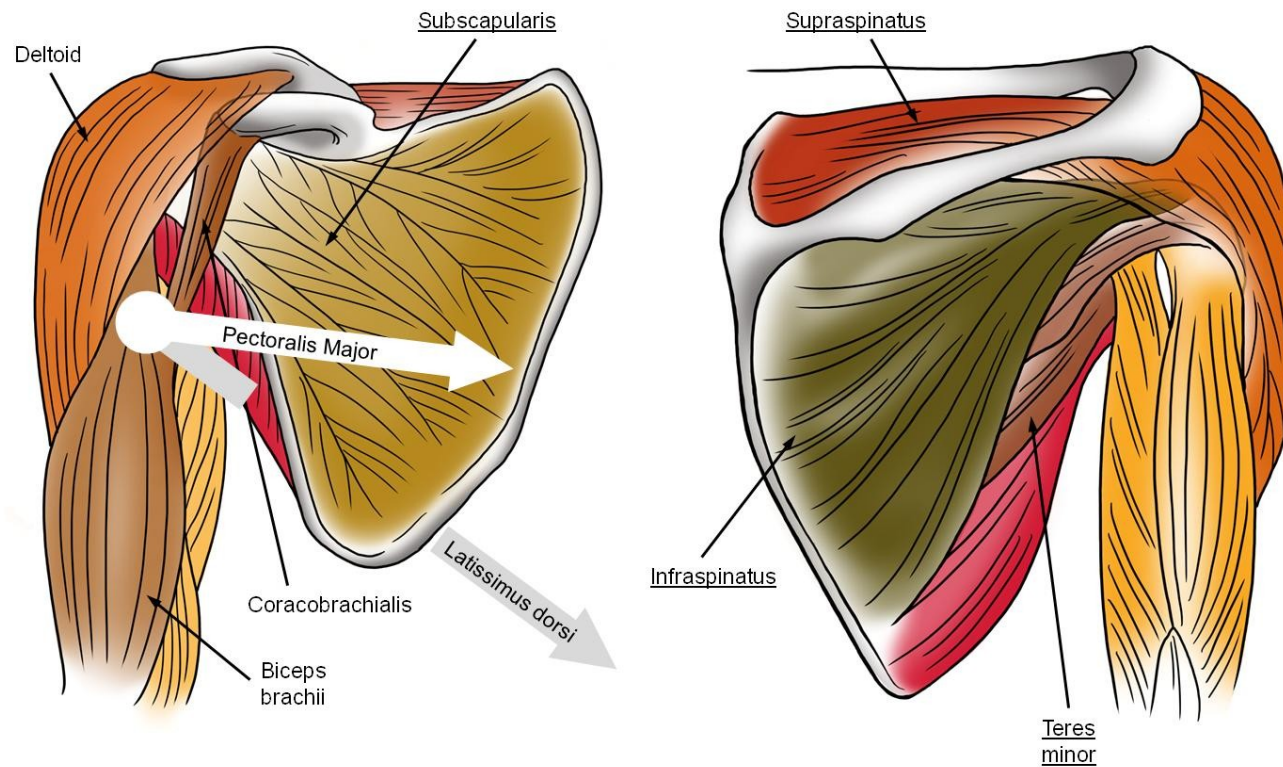
Figure 1-5: Scapulohumeral muscles of the shoulder

A right shoulder viewed from anterior (left) and posterior (right) with cuff muscles underlined. (Pectorialis major and lattissimus dorsi shown overlaid with arrows indicating lines of action.)

Four individual muscles of this category, the supraspinatus, subscapularis, infraspinatus, and teres minor, are included in the structure known as the rotator cuff (Figure 1-3). As its name belies, the rotator cuff surrounds the glenohumeral joint in all but the inferior aspect and provides stability to the joint during motion through the application of both adduction-abduction and internal-external rotation moments (Culham & Peat, 1993; Neer, 1990). These muscles typically act in conjunction with one another due to the integrative layout of their musculotendinous junctions and joint capsules (L. J. Soslowsky, Carpenter, Bucchieri, & Flatow, 1997).

The pectoralis major and latissimus dorsi originate on the torso and insert on the humerus, and as such are classified as humerothroracic muscles. The main purpose of these muscles is to adduct the humerus, with the pectoralis major and its anterior positioning additionally providing flexion and internal rotation, and the latissimus dorsi generating extension and internal rotation (D C Ackland et al., 2008; D. Ackland & Pandy, 2011).

1.2 Kinematics and Motion of the Shoulder

The large range of motion and multiple degrees of freedom of the shoulder allows for the placement of the hand over a large region. Humeral motions and the resulting humeral positions can be expressed using combinations or sequences of rotations of the humerus with respect to the scapula. These rotations include the plane of elevation which is the plane in which the humerus elevates in, the humeral elevation or the angle to which the humerus rotates in the plane of elevation, and the humeral axial rotation which is the angle with which the humerus rotates about its length in the plane of elevation and at the elevation angle it is positioned in (Figure 1-6).

Motion of the scapula during humeral elevation also occurs, and can be described as scapular rotation across the torso and away from the mid-line (Figure 1-7).
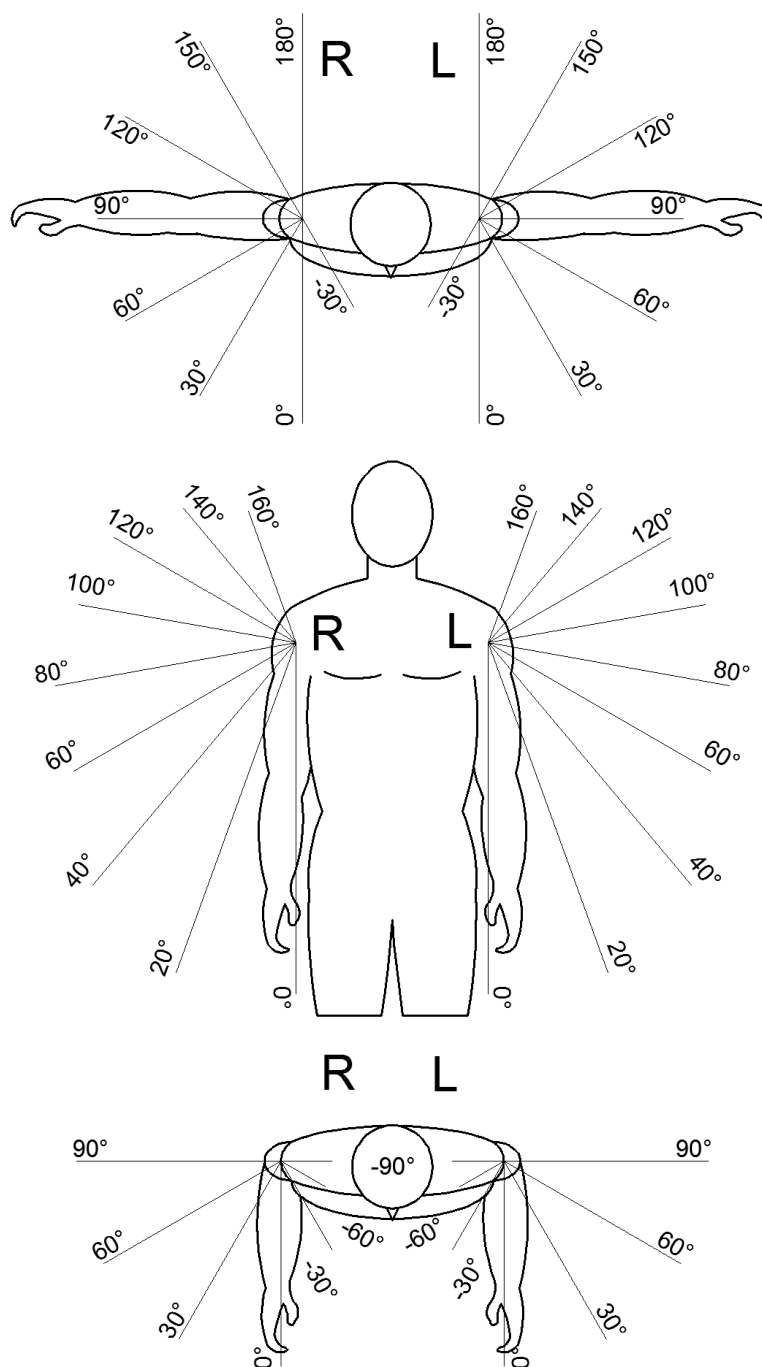
Figure 1-6: Humeral rotations used to describe position

Plane of elevation (top), elevation angle (middle), and axial rotation (bottom).
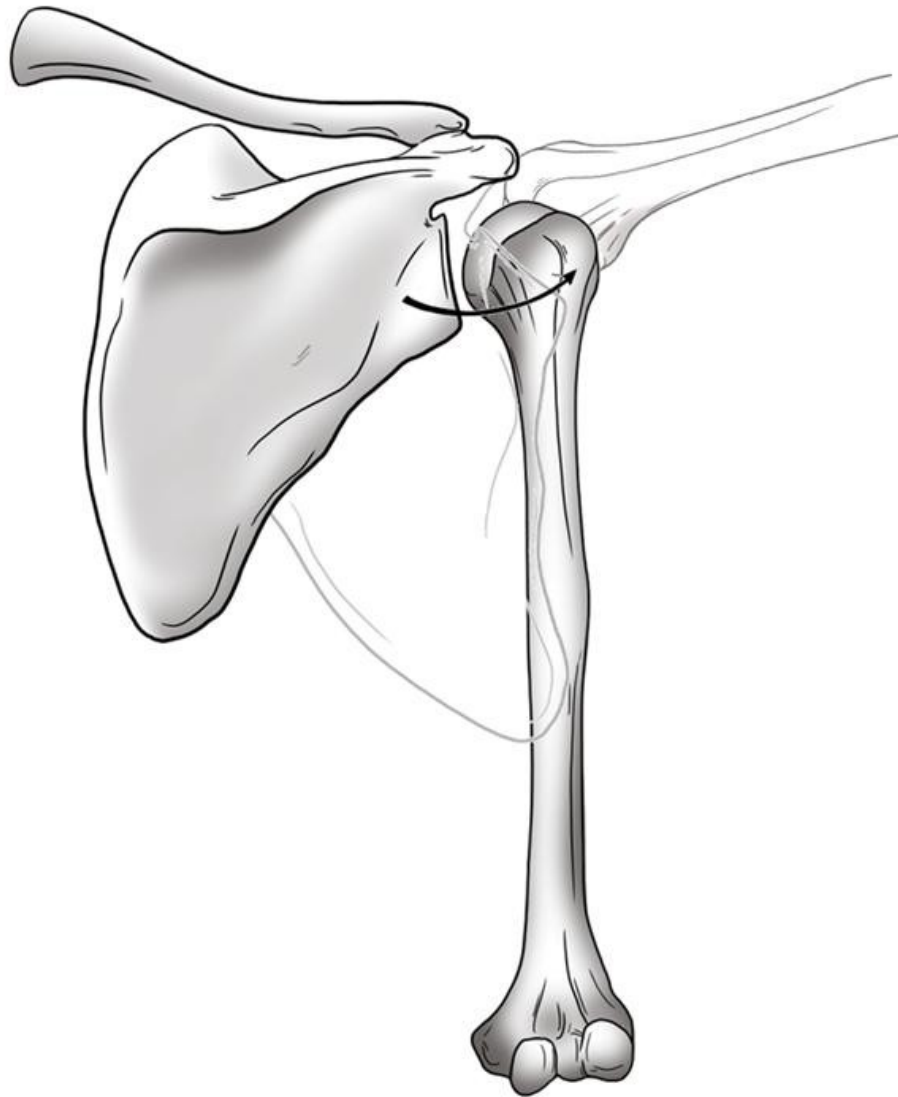
Figure 1-7: Rotation of the scapula in conjunction with humeral elevation

Arm at side position shown in solid with elevated humerus overlaid.

Humeral elevation is achieved through a combination of glenohumeral and scapulothoracic rotation, the ratio between which is known as the scapulohumeral rhythm. The most traditionally accepted relationship between these two rotations is the ratio of 2:1 (glenohumeral:scapulothoracic) throughout the full adduction-abduction range (Inman, Saunders, & Abbott, 1996). Maximum adduction-abduction range of motion is slightly less than 180° on average, and is dependant mainly on the bony structures of the scapula and humerus as well as the laxity of the joint (Itoi et al., 2009). Not only does the combined rotation of the scapula and the humerus during elevation increase the maximum range of motion of the shoulder, the rotation of the glenoid relative to the torso also reduces the shear loading observed by the joint (Itoi et al., 2009).

1.3 Reverse Total Shoulder Arthroplasty

Reverse total shoulder arthroplasty (RTSA) is an accepted treatment for end-stage rotator cuff tear arthropathy, as well as for fracture and failed shoulder arthroplasty (Castagna et al., 2013; Drake, OConnor, Edwards, O'Connor, & Edwards, 2010; Ek, Neukom, Catanzaro, & Gerber, 2013; Flury, Frey, Goldhahn, Schwyzer, & Simmen, 2011; Leung, Horodyski, Struk, & Wright, 2012; Nolan, Ankerson, & Wiater, 2011; Ortmaier et al., 2013; B. S. Werner, Boehm, & Gohlke, 2013).

RTSA has been growing in usage, representing approximately 50% of all total shoulder arthroplasties performed in 2012 out of 100 hospitals reviewed (Boguski, Miller, Carpenter, Mendenhall, & Hughes, 2013). RTSA is an established clinical procedure in the case of rotator cuff deficiency (Drake, OConnor, Edwards, O'Connor, & Edwards, 2010; Ek, Neukom, Catanzaro, & Gerber, 2013; Leung, Horodyski, Struk, & Wright, 2012; Nolan, Ankerson, & Wiater, 2011), as a revision procedure to primary total shoulder replacement (Castagna et al., 2013; Flury, Frey, Goldhahn, Schwyzer, & Simmen, 2011; Ortmaier et al., 2013; B. S. Werner, Boehm, & Gohlke, 2013), and in the repair of severely comminuted fractures of the proximal humerus.

1.3.1 RTSA Joint Reconstruction

RTSA reverses the anatomy of the native glenohumeral joint by replacing the concave glenoid with a convex glenosphere, and the convex humeral head with a concave humeral cup attached to a humeral stem (Figure 1-8).
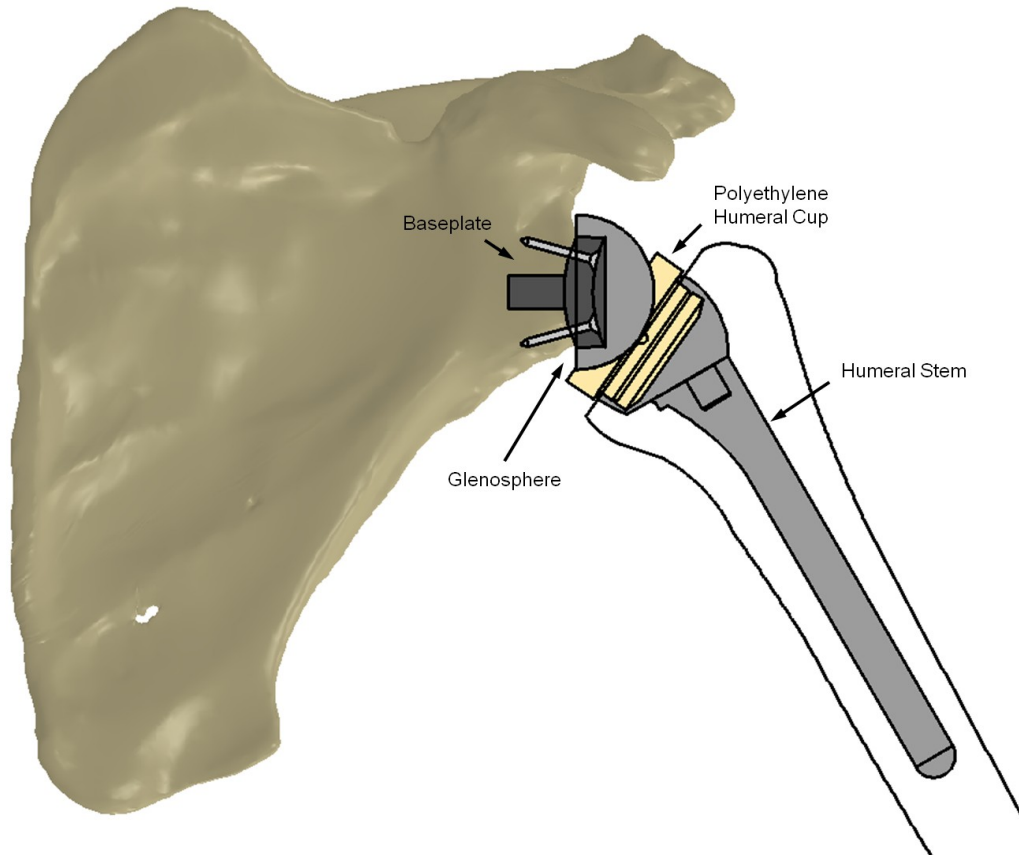
Figure 1-8: Reverse total shoulder arthroplasty implant
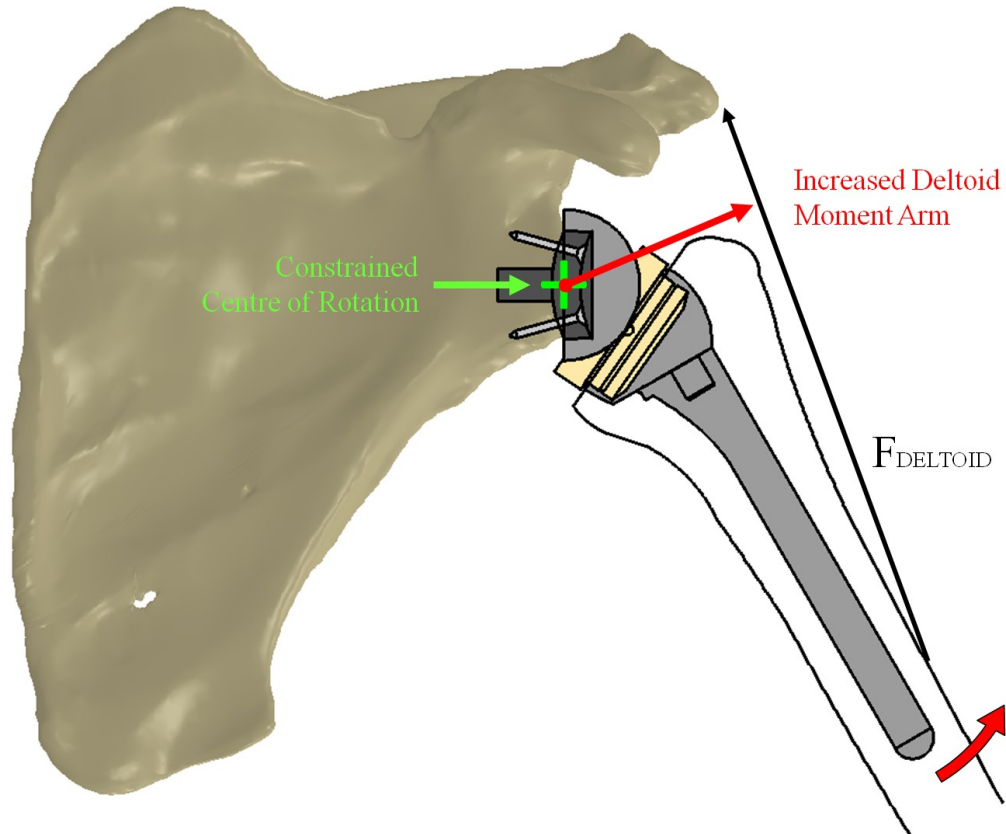
Figure 1-9: Effects of RSA reconstruction on shoulder biomechanics

RTSA constrains the joint centre of rotation (green) and increases the deltoid muscle moment arm (red) compared to the native joint.

In reversing and replacing the relatively unconstrained geometry of the native shoulder, RTSA constrains the centre of rotation of the reconstructed glenohumeral joint to the centre of the glenosphere (Figure 1-9). This arrests all translation of the humerus with respect to the scapula. The relocation of the joint centre of rotation medially from the centre of the humeral head to the centre of the glenosphere also acts to increase the moment arm of the deltoid muscle, which increases the effectiveness of this muscle in producing humeral elevation, or abduction (David C Ackland, Roshan-Zamir, Richardson, & Pandy, 2010).

1.3.2   RTSA Implant Performance

RTSA, shown in Figure 1-8 and Figure 1-9, has demonstrated good outcomes in terms of improvements in patient pain and function in the repair of rotator cuff deficient shoulders (Frankle et al., 2006). In a study of fifty-eight patients who received a Delta III RTSA, significant improvements were observed in both shoulder function and pain but a total complication rate of 50% was reported, with a 33% reoperation rate (C. M. L. Werner, Steinmann, Gilbart, & Gerber, 2005). Another study of sixty RTSA recipients reported a better success rate of 83% (Frankle et al., 2006).

Scapular notching, which occurs when the inferomedial edge of the polyethylene cup contacts the scapula inferiorly to the glenosphere, remains a concern. A study of forty-five RTSA recipients showed notching present in 26 cases, or 68% (Boileau, Watkinson, Hatzidakis, & Hovorka, 2006).

A study of fourteen RTSA clinical retrievals with a mean implantation time of 0.5 years reported that scratching and abrasion was present in all components, with material removal from the inferior aspect of the polyethylene cup observed using visual damage assessment in just under 50% of the retrievals (Nam et al., 2010), although the clinical significance of scapular notching is not yet fully understood.

Another study of seven clinical retrievals showed rim damage as a result of scapular impingement in all polyethylene cups, ranging in depth from 0.1 to 4.7 mm, for devices that had implanted for 1.3-3.3 years (Day et al., 2012). The authors report that the

predominant form of cup wear was from scapular impingement, rather than wear from the intended articulating surfaces.

1.3.3 RTSA Surgical Technique and Implant Configuration

In an effort to reduce the potential for scapular impingement and provide the maximum range of motion possible, both surgical techniques and implant configuration can be modified (Roche et al., 2009).

In terms of surgical technique, the location of the glenosphere as inferiorly as possible on the native glenoid aids in the prevention of contact between the cup and scapula by translating the articular surfaces inferiorly, thereby increasing the distance between the scapula and the inferomedial edge of the cup (Nicholson, Strauss, & Sherman, 2011; Roche et al., 2009). Lateral offset of the glenosphere can also be increased by use of bone graft or mechanical means, which shifts the centre of rotation laterally, and similar to inferior placement of the glenosphere, lateralization increases the distance between the scapula and the articulating surface. However, this can also reduce the mechanical advantage provided by moving the reconstructed joints centre of rotation laterally (Henninger et al., 2012).

Implant configuration can also be altered to reduce the chance of scapular impingement, although certain design parameters, such as humeral offset and typically N-S angle, are prescribed at the time of manufacture while others can be selected at the time of implantation.

1.3.3.1 RTSA Glenosphere Diameter

RTSA glenosphere diameter, or size, can be selected at the time of implantation (Figure 1-10). Implant systems commonly offer a smaller 36 or 38 mm and a larger 40 or 42 mm size, with the larger diameters used for patients of larger sizes.

Increasing glenosphere diameter attempts to decrease the risk of scapular impingement by moving the articular surface of the humeral cup further from the centre of rotation, which results in an increase in adduction (Berhouet, Garaud, & Favard, 2014; Chou, Malak, Anderson, Astley, & Poon, 2009; de Wilde, Poncet, Middernacht, & Ekelund,

2010; Gutiérrez et al., 2008; Gutiérrez, Keller, et al., 2008; Roche et al., 2009; Virani et al., 2013).

1.3.3.2   RTSA Neck-Shaft Angle

RTSA neck-shaft (N-S) angle is typically incorporated into the design of the implant and is not user-selectable at the time of implantation (Figure 1-11). Reducing the N-S angle can help reduce the chance of scapular impingement by decreasing the inferior overlap of the polyethylene cup under the glenosphere (de Wilde et al., 2010; Gutiérrez et al., 2008; Gutiérrez, Levy, et al., 2008; Virani et al., 2013).

Historically, the N-S angles of RTSA implants have been relatively high (155°-150°), although more recent designs have incorporated lower angles including both 145° and 135° angles. It is important to note that as the N-S angle is reduced, the shear component of the load applied to the cup can be increased by virtue of the rotation of the axis of the cup in the direction of abduction relative to the humeral component. Therefore, some implants which incorporate lower N-S angles sometimes also incorporate increased humeral offsets which attempt to increase the medial, or compressive, loads which could help reduce shear loading of the cup.

Significant increases in cup shear loading may result in the generation of high contact stresses at the edges of the articular surface, which may potentially promote wear and contribute to scapular notching via wear particle induced osteolysis through the promotion of active bone resorption (Terrier, Merlini, Pioletti, & Farron, 2009).
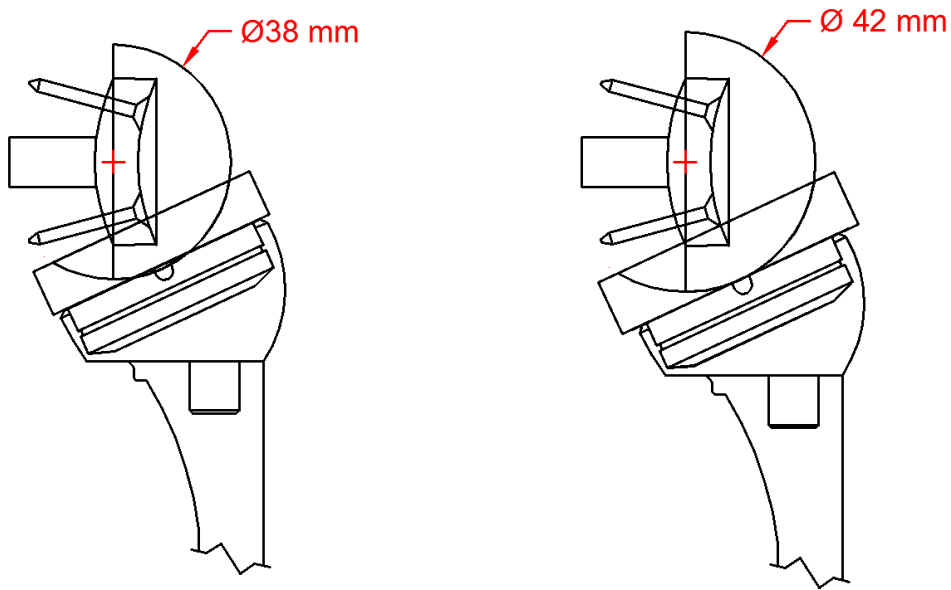
Figure 1-10: RTSA glenosphere diameter variants

Varying glenosphere diameters with 38 mm (left) and 42 mm (right) shown.
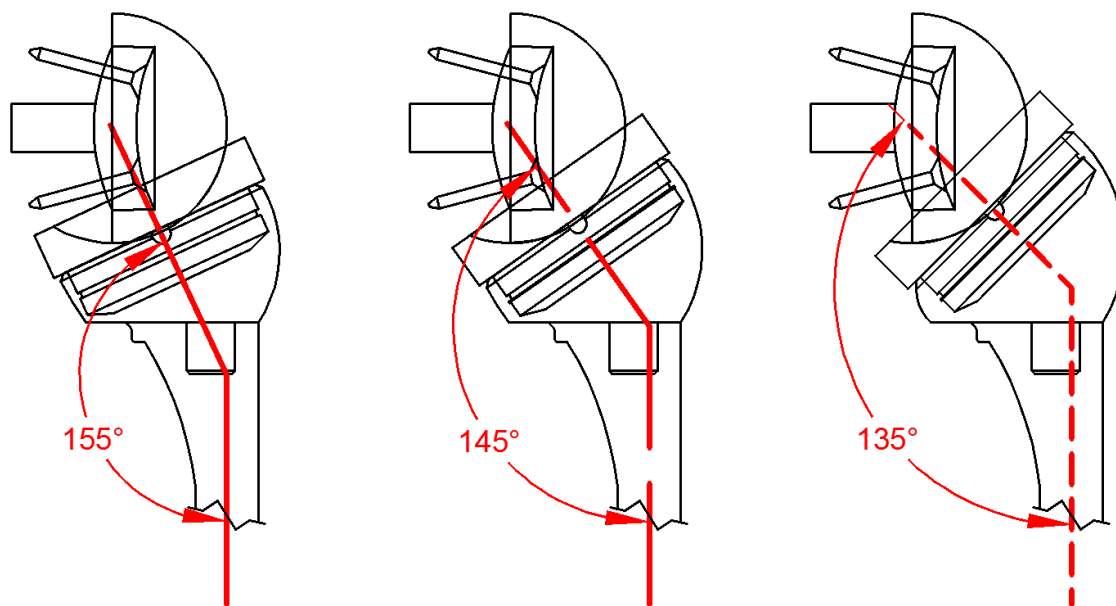
Figure 1-11: RTSA neck-shaft angle variants

Varying neck-shaft angles with the most common 155° N-S angle on the left progressing to the less common 135° N-S angle on the right.
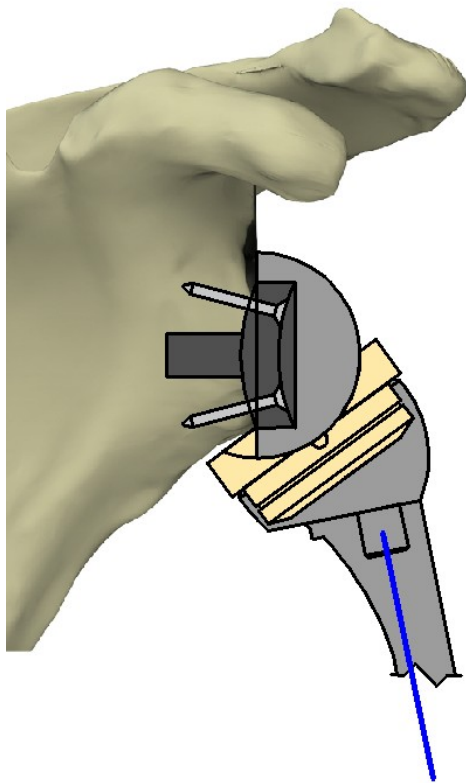
38 mm, 155° N-S Angle   **42 mm, 155° N-S Angle**   **38 mm, 135° N-S Angle**

Increased adduction ROM due to larger glenosphere diameter
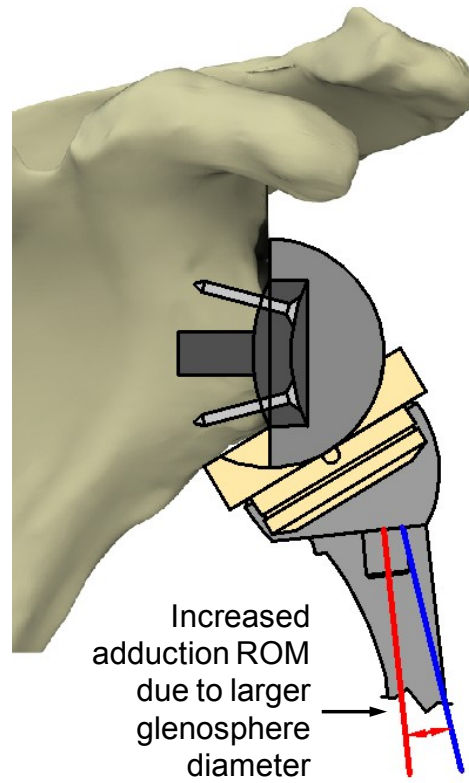
Increased adduction ROM due to reduced N-S angle
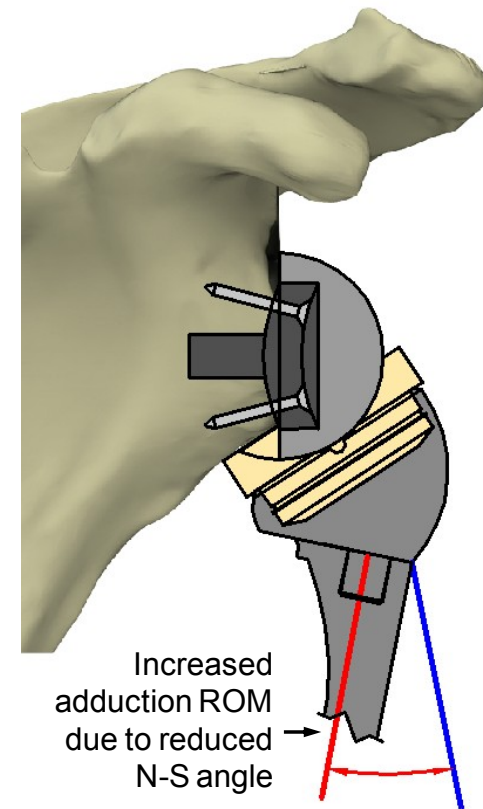
Figure 1-12: Scapular impingement at the inferiomedial edge of the polyethylene cup for various reverse total shoulder arthroplasty implant configurations

Standard configuration minimum adduction-adduction angle (left), increased ROM for 42 mm (middle) and 135° N-S angle (right).

1.3.3.3   RTSA Cup Constraint

More recently, some RTSA implant manufacturers have introduced humeral cups that produce varying constraint levels by having different depths. This allows the surgeon to try to select an implant construct that suits the specific needs of the patient (Figure 1-13).

Common options for cup depth include a standard "constraint" cup, a shallower low constraint cup that attempts to increase range of motion by reducing the chance of impingement, and a deeper higher constraint cup that aims to increase joint stability by increasing the force required to dislocate the reconstructed joint (Gutiérrez et al., 2009).

Decreasing cup depth has been shown to improve range of motion (Gutiérrez et al., 2009; Gutiérrez, Levy, et al., 2008) but this may also carry with it the risk of the articular contact patch migrating to the periphery of the cup.
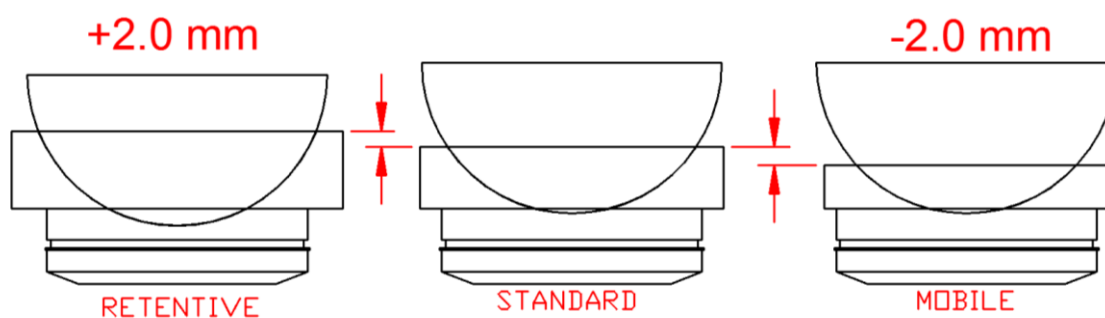
Figure 1-13: RTSA cup constraint variants

Varying humeral cup constraints ranging from normal (middle) to mobile (right) and retentive (left).

1.4   Biomechanical Studies of Total Shoulder Arthroplasty

The biomechanics of total joint arthroplasty reconstructed shoulders have been the subject of several studies, the focus of which has ranged from the assessment of post-operative range of motion to the determination of joint reaction forces during motion. These studies can be classified into one of three investigational approaches; computational, instrumented in-vivo, and in-vitro modeling.

1.4.1   Computational Modeling

1.4.1.1   Solid Body Rigid Motion

Computer-based modeling involving solid body rigid motion of the humerus and humeral implant with discrete surface to surface contact with the scapula and glenosphere has been used in the investigation of the effects of changes in implant parameters on a variety of outcomes.

Inferior positioning of the glenosphere was found to increase adduction range of motion and reduce adduction deficit (the reduction in maximum adduction angle that commonly occurs after RTSA) (de Wilde et al., 2010). Glenosphere lateralization was also reported to also increase adduction-abduction range of motion (Gutiérrez, Levy, et al., 2008).

Increasing glenosphere diameter was shown to increase adduction-abduction range of motion by reducing the "adduction deficit" (Gutiérrez et al., 2008; Gutiérrez, Levy, et al., 2008; Virani et al., 2013), and for glenosphere diameters larger than 45 mm, also increase the peak abduction angle (Roche et al., 2009).

Decreasing humeral cup depth was found to increase range of motion through reduced cup coverage, generating impingement at higher adduction and abduction angles (Gutiérrez et al., 2009; Gutiérrez, Keller, et al., 2008).

Reducing the N-S angle of the humeral component was also reported to increase adduction-abduction range of motion as a result of the relative rotation of the cup in

adduction-abduction relative to the humerus (de Wilde et al., 2010; Gutiérrez, Levy, et al., 2008).

1.4.1.2   Finite Element Analysis

Finite element methods have been employed to investigate a variety of RTSA related concepts. The effect of RTSA joint reconstruction on muscle moment arms and resultant joint forces has been investigated using a finite element model to show that glenohumeral joint loads can decrease as much as 50% compared to an anatomical prosthesis in the absence of all cuff muscles (Terrier, Reist, Merlini, & Farron, 2008). This was postulated to be a result of an increase in the deltoid muscle moment arms, and the lack of the cuff muscles which can act as antagonists to the deltoid during abduction. Net resultant RTSA joint loads during abduction reached peak levels of approximately 300 N for the inactive cuff case, and up to 450 N when only the supraspinatus was deactivated (Terrier et al., 2008).

Masjedi & Johnson (2010) also investigated RTSA joint contact forces using an inverse dynamic shoulder model which incorporated the kinematics recorded from 12 subjects who had been implanted with RTSA prostheses into a model which attempted to reproduce the motion virtually by estimating the required muscle forces required to achieve the measured kinematics. Estimated RTSA joint loads during abduction with a 0.5 kg weight in hand were reported to have reached peak values near 650 N (Masjedi & Johnson, 2010).

1.4.2   Instrumented In-Vivo Monitoring

At the present time, there is no literature to be found using in-vivo RTSA joint loading of wireless-capable instrumented implants. However, there are studies for the measurement of in-vivo joint loading of primary total shoulder arthroplasty (TSA) (Bergmann et al., 2007, 2011; Westerhoff, Graichen, Bender, Rohlmann, & Bergmann, 2009) and they have some relevance to the study of RTSA. While TSA is fundamentally different from RTSA in terms of joint constraint and the joint centre of rotation, and it is almost certain

that these differences will affect the joint loads of each type of implant, their study does provide some insight into the characteristics of glenohumeral joint loading.

A study including the measurement of TSA joint loading during activities of daily living reported glenohumeral joint forces of up to 144% body weight (BW) when lifting a 2 kg weight up to head height. Lifting a 1.5 kg weight was found to generate a glenohumeral joint load in the range of 90-125% BW (Westerhoff, Graichen, Bender, Halder, et al., 2009).

While the loading characteristics of RTSA implants are expected to be significantly different due to the inclusion of shear forces as a result of the constrained centre of rotation, the in-vivo TSA studies provide valuable insight into the general magnitude of glenohumeral joint loading that can be observed even during the lifting of relatively lightweight objects.

1.4.3   In-Vitro Cadaveric Studies

The physical implantation of RTSA components into cadaveric shoulders carries with it the strengths of including shoulder soft tissues which is often excluded in the case of solid body computer modeling studies in an effort to reduce model complexity, and has been used to study a variety of RTSA hypotheses.

Ackland et al (2010) have extensively used in-vitro cadaveric models to study a variety of topics regarding RTSA. They have shown how RTSA changes muscle moment arms after reconstruction (David C Ackland et al., 2010), and have inferred the joint contact forces required to hold both natural and RTSA reconstructed shoulders in static equilibrium at a variety of abduction angles (David C. Ackland, Roshan-Zamir, Richardson, & Pandy, 2011). They reported that the glenohumeral joint forces at various abduction angles in static equilibrium decreased approximately 50% from the native to RTSA reconstructed state, with peak RTSA loads reaching about 40% BW in abduction. The joint load was also deconstructed into compressive and shear loading to show the degree to which RTSA articulations are loaded transversely, with Ackland et al (2010) reporting joint load angles with respect to the glenosphere ranging from 63° to 18°.

Similarly, Kwon et al (2010) investigated RTSA joint loading throughout a variety of static positions in abduction. They reported peak joint loads of approximately 45% BW and peak shear forces of 30% BW during abduction in the scapular plane (Kwon, Forman, Walker, & Zuckerman, 2010).

Increasing glenosphere size was shown to increased abduction range of motion for 40 cadaveric RTSA reconstructed shoulders using an in-vitro apparatus which allowed for the measurement of joint angle (Berhouet et al., 2014). They also reported that glenosphere lateralization increased both maximum adduction and abduction. Another biomechanical cadaveric study showed that increasing glenosphere diameter improved range of motion, as did eccentric (or inferior) positioning of the glenosphere (Chou et al., 2009), both of which may reduce the incidence of scapular notching.

Clouthier et al (2013) investigated the stability of RTSA implants, and found that stability increased for higher abduction angles, inferiorly positioned glenospheres, and highly constrained cups. All of these factors were postulated to decrease the potential of implant dislocation.

A cadaveric study which investigated 155°, 145°, and 135° N-S angles reported that while reducing N-S angle can reduce adduction deficit, implant stability was also decreased (Oh et al., 2014).

1.5   Studies of the Tribology of Reverse Total Shoulder Arthroplasty Implants

Tribology is the science and technology of interacting surfaces in relative motion, and includes the investigation of contact stress, friction, lubrication, and wear. There has been some recent interest shown in the tribology of RTSA implants, including the finite element analysis of their contact mechanics compared to anatomical TSA prostheses in terms of the contact stress of the articular polyethylene (Terrier et al., 2009), as well as the wear testing of RSA implants (Haider, Sperling, & Throckmorton, 2013; Kohut, Dallmann, & Irlenbusch, 2012; Peers et al., 2015; Vaupel, Baker, Kurdziel, & Wiater,

2012), although the effects of changing RSA implant parameters on wear has not yet been fully investigated.

1.5.1   Computational Studies

Terrier et al (2009) developed a finite element polyethylene wear model of both anatomical and reversed shoulder prostheses that incorporated an inverse kinematics model which estimated joint contact forces through the determination of muscle forces required to achieve the kinematics of actual RTSA reconstructed shoulders. While their kinematic model predicted approximately 20x lower contact stresses for the reversed prosthesis compared to the anatomical, their wear model estimated that RTSA wear would be 44.6 mm^3 per year compared to 8.4 mm^3 for the anatomical (Terrier et al., 2009), and suggested that while wear has not historically been a cause for RTSA failure, it may have negative consequences on humeral stem fixation due to the potential for wear particle induced osteolysis.

1.5.2   In-Vitro Studies

The in-vitro RTSA wear studies that have previously been published are typically performed using a modified hip wear simulator while applying joint loads drawn from in-vivo load data obtained from instrumented primary TSA implants (Bergmann et al., 2011; Westerhoff, Graichen, Bender, Rohlmann, et al., 2009; Westerhoff, Graichen, Bender, Halder, et al., 2009).

Vaupel et al (2012) investigated the effects of the central placed in some glenosphere designs that is used for fixation on wear using a modified hip simulator with a biaxial rocking motion ±23° and alternated between abduction-adduction and flexion-extension motions every 0.25 million cycles (Mc) by changing both the fixtures and the input load profile. The load ranged from 20 N to 617 N (90% BW) and was centrally applied in adduction-abduction and ranged from 20 N to 927 N (135% BW) and was applied obliquely to the cup in flexion-extension to bringing the contact to the cup edge. They tested eight implant pairs with central holes in the glenosphere and eight without the central holes against custom-made non crosslinked polyethylene cups and did not detect

significant differences in wear between the RSA implants with and without holes (Vaupel et al., 2012). The same group performed a second study using the same protocol comparing non cross-linked and highly cross-linked polyethylene cups, and reported the wear rate of the highly cross-linked polyethylene cups to be approximately one-half that of the non cross-linked cups (Peers et al., 2015). Interestingly, this study apparently with identical conditions to those of Vaupel et al. had a much lower wear rate for the non crosslinked polyethylene.

Haider et al (2013) briefly described their wear study of Vitamin E doped highly cross linked compared to moderately cross lined polyethylene cups. Using an adapted AMTI hip simulator they applied 38°-79° of forward elevation in two separate planes (15° and 45°) throughout a rotation of 57° while loading the implants from 50-1700 N. No further wear protocol details were provided. They reported that the highly cross linked cups wore significantly less than their moderately cross linked counterparts; 3.42±0.22 mg/Mc compared to 17.9±0.85 mg/Mc respectively (Haider et al., 2013).

Kohut et al (2012) also investigated the wear of non-cross linked polyethylene humeral cups and compared that to a rather unconventional custom implant design with the glenosphere made of polyethylene and the humeral cup made of metal (cobalt alloy). Cross-linking of polyethylene offers an increased resistance to wear and is achieved using radiation exposure which facilitates the formation of cross-links between adjacent chains of molecules. Using an E-sim hip simulator (KUPA Präzisionsmaschinen GMBH, Grambach, Austria) they applied a load ranging from 250-1000 N while applying a motion profile including a 43° flexion-extension range, 11° abduction-adduction range, and a 13° range of internal-external rotation, although they did state that oblique loading was not simulated in their protocol. They reported wear rates between 16-20 mm^3/Mc, for a test period of 0.5 Mc, and did not note any significant difference between the conventional and their custom implant (Kohut et al., 2012).

1.6   Activity Levels of the Shoulder

In the lower limb, where the gait cycle can be used to characterize common repetitive motion, measurement of the number of times this motion is performed can be used to define an approximate number of cycles of use the lower extremities experience per year, which has been found to range between 1-2 Mc (Schmalzried et al., 1998; Silva, Shepherd, Jackson, Dorey, & Schmalzried, 2002).   The activity of the shoulder is comparatively more complex, and apart from arm swing during walking or activities like swimming, the glenohumeral joint is not typically functionally required to perform repetitive prescribed motions to provide locomotion. Therefore, the definition of a shoulder cycle becomes more difficult than for the locomotive structures of the human body.

For the purpose of orthopaedic implant wear testing, the relationship between the number of cycles and years implanted in-vivo is of interest in estimating the expected lifespan and performance of the device under investigation.

Zhou et al have described the development (Zhou, Hu, & Tao, 2006) and implementation of a system which is capable of measuring upper limb position (Zhou, Hu, Harris, & Hammerton, 2006; Zhou, Stone, Hu, & Harris, 2008), but there appears to be no mention of the use of this system to record and report the shoulder motion of human subjects.

Namdari et al (2012) described their study of shoulder range of motion during the performance of 10 activities of daily living using an electromagnetic tracking device. The results of their study provided insight into the range of motion required of the shoulder for a variety of different tasks, however the study provided no insight into the number of times such motions are performed on a daily basis (Namdari et al., 2012).

An investigation of the shoulder motion of healthy subjects who wore an ambulatory system with inertial sensors for a portion of the day was able to provide some data regarding the average daily shoulder activity (Coley, Jolles, Farron, & Aminian, 2008). The authors reported that the majority of the time spent during the day (96%) fell below

100° of abduction, and that the number of elevation cycles above 100° of abduction was less than 19 occurrences per hour on average for the 200 hours the system was worn by healthy volunteers.

1.7 Motivation

Despite the widespread use of RTSA, there are still aspects of the implant design that have not been fully investigated. Examination of the contact mechanics and the complete tribology of RTSA implants should have been done much sooner and is needed to better understand the performance of these relatively new prostheses. Also, such examination will yield insight into the future improvements of both RTSA implant design and the clinical techniques used to implant them.

While the effects of differing RTSA implant configurations on shoulder range of motion are relatively well described in the literature, the corresponding changes in contact mechanics are not well understood. For example, while the modification of RTSA neck-shaft angle may prove advantageous in terms of reducing adduction deficit, this improvement may need to be weighed against any potential negative consequences of this implant selection on the wear performance of the device in-vivo and the potential for osteolysis and implant loosening.

Furthermore, although several groups have initiated the exploration of RTSA wear using custom modified wear simulator apparatuses, the loads and motions that have been applied to the implants to date have been largely based on instrumented primary total shoulder in-vivo loading, which employs an inherently different articulation compared to that of the reverse shoulder prosthesis. A more careful investigation of the joint loads and unique loading characteristics of RTSA implants and the application of these findings to the development of a wear simulation strategy for these devices would provide a means by which to assess RTSA wear performance in a more clinically relevant manner.

Our current understanding in the area of RTSA tribology is limited to a finite element wear analysis comparing anatomical to reverse prostheses, and the work of four groups

who applied the loading principles of anatomical prostheses to their RTSA wear simulator studies. While this sets the groundwork for future work in this area, there exists opportunity to further study the unique loading characteristics of RTSA and apply this knowledge directly to the design and development of a wear simulation strategy in an effort to obtain the most clinically relevant results possible. This is not meant to suggest that the strategy presented in the present work is the only correct strategy for all future wear testing of RTSA implants. It is likely that a number of "standard" tests should be developed to test the safety of RTSA implants regarding wear issues. However, it does describe a process by which to develop a wear simulation strategy to be used to evaluate RTSA implants for one general scenario. This development process is presented in this work along with some early simulator wear results.

1.8 Objectives and Hypotheses

The goal of this dissertation was to develop a RTSA wear simulation strategy through i) the procurement of a more thorough understanding of the loads and unique loading characteristics of RTSA implants during motion, and ii) by applying this knowledge to the design and implementation of a custom RTSA wear simulator apparatus that would initiate wear assessment of RTSA devices.

Objectives:

1. To develop a means by which to further investigate the articular loads and joint loading characteristics of RTSA implants during abduction, specifically in terms of both load magnitude and direction, and then use this to ascertain the effects of the following RTSA implant characteristics on joint load, muscle force, and range of motion:
    a. Changes in implant neck-shaft angle.
    b. Varying cup depth.
    c. Modifications in glenosphere diameter.
2. To investigate the contact mechanics of RTSA implants during abduction, and to ascertain the effects of changes in implant configuration on articular contact area and stress. The specific aims are to:

a. Compare the location of articular contact and contact stress distribution to the wear morphology of RTSA implants.

b. Determine if changes in implant configuration (neck-shaft angle, cup depth, and glenosphere size) have related consequences on articular contact mechanics.

3. To develop a RTSA wear simulation strategy through the application of the knowledge obtained in Objective 1. The specific aims are to:

a. Investigate specifically the line of action of the load with respect to both the glenosphere and the polyethylene cup to determine the most appropriate way to apply loading during wear testing.

b. Design, develop, and implement a wear simulator to allow for the wear testing of RTSA implants in a clinically relevant manner.

c. Perform a pilot wear test to ascertain the wear rate and wear morphology produced by the wear simulation strategy developed and compare these to previously published wear studies and RTSA clinical retrievals.

4. To perform a full scale wear test on current commercially available Depuy Delta XTEND 38 mm diameter RTSA implants and compare these early wear results using the developed protocol to previously published data.

Hypotheses:

Hypothesis 1

a. Decreasing neck-shaft angle would i) not change joint load or muscle force due to the joint center of rotation not changing, and ii) increase adduction range of motion.

b. Decreasing cup depth would i) not alter joint load or muscle force, but ii) would increase adduction/abduction and internal/external rotation range of motion.

c. Increasing glenosphere diameter would increase ROM while not significantly altering joint loading due to the nearly identical joint centers of rotation.

Hypothesis 2

    a. During abduction, the joint load acting on the glenosphere would typically be superiorly directed, and the joint load acting on the humeral cup would be predominantly directed inferiorly.

    b. The resulting wear simulation strategy would produce wear rates of the same magnitude as previously published works, and generate cup wear in the inferior quadrant of the cup.

Hypothesis 3

    a. The location of both the contact patch and peak contact stresses would be located in the inferior cup quadrant coincident with the most common location of wear found on clinical retrievals..

    b. Higher neck-shaft angles, increased cup depth, and larger glenosphere diameters would provide improved RSA contact mechanics because of the resulting reduced cup shear loading, large range of motion without impingement and increased stability.

Hypothesis 4

The wear rate of the full scale wear test will be within the range of previously published wear rates and the wear region will occur in the inferior quadrant.

A secondary objective of this thesis was to estimate the average motion of an RTSA reconstructed shoulder is subjected to in-vivo. To accomplish this, a wearable upper limb motion tracking system was developed and implemented that was capable of measuring and recording shoulder position and motion. The system could be worn during the entire course of daily activity and the resulting data could be used to estimate the average number of cycles the shoulder performs on an annual basis and compare to the lower extremity. We hypothesized that: similar to the lower extremities, the estimated average number of shoulder cycles per year would range between 1-2 Mc.

1.9 Thesis Overview

Chapter 2 describes the investigation of RTSA joint loads and addresses the clinical questions of whether varying neck-shaft angles, cup depths, and glenosphere diameters alters joint loads and muscle forces throughout abduction which could alter wear testing protocol for differently configured prostheses.

Chapter 3 investigates the contact mechanics of RTSA implants during abduction and ascertains the effects of changes in implant configuration (neck-shaft angle, cup depth, and glenosphere diameter) on articular contact area and stress. The location of articular contact and contact stress distribution to the wear morphology of RTSA implants will also be compared to determine if changes in implant configuration have related consequences on articular contact mechanics.

Chapter 4 describes the further investigation of the characteristics of RTSA joint loads with respect to both the glenosphere and humeral cup, the incorporation of these results with the development of a RTSA wear simulation strategy, and a pilot wear study.

Chapter 5 describes the results of a wear test of standard 38 mm, 155° N-S angle, standard cup depth, Depuy Delta XTEND RTSA implants, and includes the quantification of both wear rate and wears morphology.

Chapter 6 provides a general cumulative discussion of this dissertation's work, and furnishes interplay and association of the conclusions in the different chapters included in this work.

Appendix B describes a wearable upper limb motion tracking system capable of measuring and recording shoulder position and motion that can be worn during the entire course of daily activity. The average number of cycles the shoulder performs on an annual basis will be estimated and compared to the lower extremity.

1.10 References

Ackland, D. C., Pak, P., Richardson, M., & Pandy, M. G. (2008). Moment arms of the muscles crossing the anatomical shoulder. Journal of Anatomy, 213(4), 383–390. http://doi.org/10.1111/j.1469-7580.2008.00965

Ackland, D. C., Roshan-Zamir, S., Richardson, M., & Pandy, M. G. (2010). Moment arms of the shoulder musculature after reverse total shoulder arthroplasty. The Journal of Bone and Joint Surgery, 92(5), 1221–1230. http://doi.org/10.2106/JBJS.I.00001

Ackland, D. C., Roshan-Zamir, S., Richardson, M., & Pandy, M. G. (2011). Muscle and joint-contact loading at the glenohumeral joint after reverse total shoulder arthroplasty. Journal of Orthopaedic Research, 29(12), 1850–1858. http://doi.org/10.1002/jor.21437

Ackland, D., & Pandy, M. (2011). Moment arms of the shoulder muscles during axial rotation. Journal of Orthopaedic Research, 29(5), 658–667.

An, K. N., Browne, A. O., Korinek, S., Tanaka, S., & Morrey, B. F. (1991). Three-dimensional kinematics of glenohumeral elevation. Journal of Orthopaedic Research, 9(1), 143–149. http://doi.org/10.1002/jor.1100090117

Bergmann, G., Graichen, F., Bender, A., Kaab, M., Rohlmann, A., & Westerhoff, P. (2007). In vivo glenohumeral contact forces—Measurements in the first patient 7 months postoperatively. Journal of Biomechanics, 40(10), 2139–2149. http://dx.doi.org/10.1016/j.jbiomech.2006.10.037

Bergmann, G., Graichen, F., Bender, A., Rohlmann, A., Halder, A., Beier, A., & Westerhoff, P. (2011). In vivo gleno-humeral joint loads during forward flexion and abduction. Journal of Biomechanics, 44(8), 1543–1552. http://dx.doi.org/10.1016/j.jbiomech.2011.02.142

Berhouet, J., Garaud, P., & Favard, L. (2014). Evaluation of the role of glenosphere design and humeral component retroversion in avoiding scapular notching during reverse shoulder arthroplasty. Journal of Shoulder and Elbow Surgery, 23(2), 151–158. http://doi.org/10.1016/j.jse.2013.05.009

Boguski, R. M., Miller, B. S., Carpenter, J. E., Mendenhall, S., & Hughes, R. E. (2013). Variation in use of reverse total shoulder arthroplasty across hospitals. Journal of Shoulder and Elbow Surgery, 22(12), 1633–1638. http://doi.org/10.1016/j.jse.2013.09.002

Boileau, P., Watkinson, D., Hatzidakis, A. M., & Hovorka, I. (2006). Neer Award 2005: The Grammont reverse shoulder prosthesis: Results in cuff tear arthritis, fracture

sequelae, and revision arthroplasty. Journal of Shoulder and Elbow Surgery, 15(5), 527–540. http://doi.org/10.1016/j.jse.2006.01.003

Burkart, A. C., & Debski, R. E. (2002). Anatomy and function of the glenohumeral ligaments in anterior shoulder instability. Clinical Orthopaedics and Related Research, 400, 32–39.

Castagna, A., Delcogliano, M., de Caro, F., Ziveri, G., Borroni, M., Gumina, S., De Biase, C. F. (2013). Conversion of shoulder arthroplasty to reverse implants: clinical and radiological results using a modular system. International Orthopaedics, 37(7), 1297–1305. http://doi.org/10.1007/s00264-013-1907-4

Chou, J., Malak, S. F., Anderson, I. A., Astley, T., & Poon, P. C. (2009). Biomechanical evaluation of different designs of glenospheres in the SMR reverse total shoulder prosthesis: range of motion and risk of scapular notching. Journal of Shoulder and Elbow Surgery, 18(3), 354–359. http://doi.org/10.1016/j.jse.2009.01.015

Clouthier, A.L., Hetzler, M.A., Fedorak, G.F., Bryant, J.T., Deluzio, K.J., Bicknell, R.T. (2013) Factors affecting the stability of reverse shoulder arthroplasty: a biomechanical study. Journal of Shoulder and Elbow Surgery, 22, 439-444. http://dx.doi.org/10.1016/j.jse.2012.05.032

Coley, B., Jolles, B. M., Farron, A., & Aminian, K. (2008). Arm position during daily activity. Gait and Posture, 28(4), 581–587. http://doi.org/10.1016/j.gaitpost.2008.04.014

Culham, E., & Peat, M. (1993). Functional anatomy of the shoulder complex. The Journal of Orthopaedic and Sports Physical Therapy, 18(1), 342–350.

Day, J. S., MacDonald, D. W., Olsen, M., Getz, C., Williams, G. R., & Kurtz, S. M. (2012). Polyethylene wear in retrieved reverse total shoulder components. Journal of Shoulder and Elbow Surgery, 21(5), 667–674. http://dx.doi.org/10.1016/j.jse.2011.03.012

de Wilde, L. F., Poncet, D., Middernacht, B., & Ekelund, A. (2010). Prosthetic overhang is the most effective way to prevent scapular conflict in a reverse total shoulder prosthesis. Acta Orthopaedica, 81(6), 719–726. http://doi.org/10.3109/17453674.2010.538354

Drake, G. N., OConnor, D., Edwards, T. B., O'Connor, D. P., & Edwards, T. B. (2010). Indications for Reverse Total Shoulder Arthroplasty in Rotator Cuff Disease. Clinical Orthopaedics and Related Research, 468(6), 1526–1533. http://doi.org/10.1007/s11999-009-1188-9

Ek, E. T., Neukom, L., Catanzaro, S., & Gerber, C. (2013). Reverse total shoulder arthroplasty for massive irreparable rotator cuff tears in patients younger than 65 years old: results after five to fifteen years. Journal of Shoulder and Elbow Surgery, 22(9), 1199–1208. http://doi.org/10.1016/j.jse.2012.11.016

Flury, M. P., Frey, P., Goldhahn, J., Schwyzer, H. K., & Simmen, B. R. (2011). Reverse shoulder arthroplasty as a salvage procedure for failed conventional shoulder replacement due to cuff failure--midterm results. International Orthopaedics, 35(1), 53–60. http://doi.org/10.1007/s00264-010-0990-z

Frankle, M., Levy, J. C., Pupello, D., Siegal, S., Saleem, A., Mighell, M., & Vasey, M. (2006). The reverse shoulder prosthesis for glenohumeral arthritis associated with severe rotator cuff deficiency. a minimum two-year follow-up study of sixty patients surgical technique. The Journal of Bone and Joint Surgery. American Volume, 88 Suppl 1(July 2015), 178–190. http://doi.org/10.2106/JBJS.D.02813

Gutiérrez, S., Comiskey, C. a, Luo, Z.-P., Pupello, D. R., Frankle, M. A.. (2008). Range of impingement-free abduction and adduction deficit after reverse shoulder arthroplasty. Hierarchy of surgical and implant-design-related factors. The Journal of Bone and Joint Surgery. American Volume, 90(12), 2606–2615. http://doi.org/10.2106/JBJS.H.00012

Gutiérrez, S., Keller, T. S., Levy, J. C., Lee III, W., Luo, Z.-P. P., (2008). Hierarchy of stability factors in reverse shoulder arthroplasty. Clinical Orthopaedics and Related Research, 466(3), 670–676. http://doi.org/10.1007/s11999-007-0096-0

Gutiérrez, S., Levy, J. C., Frankle, M. a., Cuff, D., Keller, T. S., Pupello, D. R., Lee, W. E. (2008). Evaluation of abduction range of motion and avoidance of inferior scapular impingement in a reverse shoulder model. Journal of Shoulder and Elbow Surgery, 17(4), 608. http://doi.org/http://dx.doi.org/10.1016/j.jse.2007.11.010

Gutiérrez, S., Luo, Z.-P. P., Levy, J., Frankle, M. A. (2009). Arc of motion and socket depth in reverse shoulder implants. Clinical Biomechanics, 24(6), 473–479. http://doi.org/10.1016/j.clinbiomech.2009.02.008

Haider, H., Sperling, J., & Throckmorton, T. (2013). A method for wear testing of reverse shoulder arthroplasty systems. Bone Joint J., Vol. 95-B, SUPP 34 (607).

Henninger, H. B., Barg, A., Anderson, A. E., Bachus, K. N., Burks, R. T., & Tashjian, R. Z. (2012). Effect of lateral offset center of rotation in reverse total shoulder arthroplasty: A biomechanical study. Journal of Shoulder and Elbow Surgery, 21(9), 1128–1135. http://doi.org/10.1016/j.jse.2011.07.034

Hess, S. A. (2000). Functional stability of the glenohumeral joint. Manual Therapy, 5(2), 63–71. http://doi.org/10.1054/math.2000.0241

Howell, S. M., & Galinat, B. J. (1989). The glenoid-labral socket. A constrained articular surface. Clinical Orthopaedics and Related Research, (243), 122–125.

Inman, V. T., Saunders, J. B., & Abbott, L. C. (1996). Observations of the function of the shoulder joint. 1944. Clinical Orthopaedics and Related Research, (330)(330), 3–12.

Itoi, E., Morrey, B. F., & An, K. (2009). Biomechanics of the shoulder. In A. J. Rockwood, F. A. Matsen, C. J. Wirth, & S. . Lippitt (Eds.), The shoulder (pp. 213–266). Philadelphia: Saunders Elsevier.

Jobe, C. M., Phipatanakul, W. P., & Coen, M. J. (2009). Gross Anatomy of the Shoulder. In C. A. Rockwood, F. A. M. 3rd, C. J. Wirth, & S. B. Lippitt (Eds.), The shoulder (4th ed, p. 38). Philadelphia: Saunders Elsevier.

Karduna, A. R., Williams, G. R., Williams, J. L., & Iannotti, J. P. (1997). Glenohumeral joint translations before and after total shoulder arthroplasty. A study in cadavera. The Journal of Bone and Joint surgery.American Volume, 79(8), 1166–1174.

Kohut, G., Dallmann, F., & Irlenbusch, U. (2012). Wear-induced loss of mass in reversed total shoulder arthroplasty with conventional and inverted bearing materials. Journal of Biomechanics, 45(3), 469–473. http://doi.org/10.1016/j.jbiomech.2011.11.055

Kwon, Y. W., Forman, R. E., Walker, P. S., & Zuckerman, J. D. (2010). Analysis of reverse total shoulder joint forces and glenoid fixation. Bulletin of the NYU Hospital for Joint Diseases, 68(4), 273–280.

Leung, B., Horodyski, M., Struk, A. M., & Wright, T. W. (2012). Functional outcome of hemiarthroplasty compared with reverse total shoulder arthroplasty in the treatment of rotator cuff tear arthropathy. Journal of Shoulder and Elbow Surgery, 21(3), 319. http://dx.doi.org/10.1016/j.jse.2011.05.023

Lippitt, S., & Matsen, F. (1993). Mechanisms of glenohumeral joint stability. Clinical Orthopaedics and Related Research, (291), 20–28.

Masjedi, M., & Johnson, G. R. (2010). Glenohumeral contact forces in reversed anatomy shoulder replacement. Journal of Biomechanics, 43(13), 2493–2500. http://doi.org/10.1016/j.jbiomech.2010.05.024

Nam, D., Kepler, C. K., Nho, S. J., Craig, E. V., Warren, R. F., & Wright, T. M. (2010). Observations on retrieved humeral polyethylene components from reverse total shoulder arthroplasty. Journal of Shoulder and Elbow Surgery, 19(7), 1003. http://doi.org/http://dx.doi.org/10.1016/j.jse.2010.05.014

Namdari, S., Yagnik, G., Ebaugh, D. D., Nagda, S., Ramsey, M. L., Williams, G. R., & Mehta, S. (2012). Defining functional shoulder range of motion for activities of daily living. Journal of Shoulder and Elbow Surgery, 21(9), 1177–1183. http://doi.org/10.1016/j.jse.2011.07.032

Neer, C. S. (1990). Shoulder reconstruction. Toronto: Saunders.

Nicholson, G. P., Strauss, E. J., & Sherman, S. L. (2011). Scapular Notching: Recognition and Strategies to Minimize Clinical Impact. Clinical Orthopaedics and Related Research. 469(9), 2521–2530. http://doi.org/10.1007/s11999-010-1720-y

Nolan, B. M., Ankerson, E., & Wiater, J. M. (2011). Reverse total shoulder arthroplasty improves function in cuff tear arthropathy. Clinical Orthopaedics and Related Research, 469(9), 2476–2482. http://doi.org/10.1007/s11999-010-1683-z

O'Brien, S. J., Voos, J. E., Neviaser, A. S., & Drakos, M. C. (2009). Developmental anatomy of the shoulder and anatomy of the glenohumeral joint. In A. Rockwood, A. Matsen, C. Wirth, & S. Lippitt (Eds.), The shoulder2 (4th ed, pp. 1–32). Philadelphia: Saunders Elsevier.

Oh, J. H., Shin, S.-J. J., McGarry, M. H., Scott, J. H., Heckmann, N., & Lee, T. Q. (2014). Biomechanical effects of humeral neck-shaft angle and subscapularis integrity in reverse total shoulder arthroplasty. Journal of Shoulder and Elbow Surgery, 23(0), -. http://dx.doi.org/10.1016/j.jse.2013.11.003"

Ortmaier, R., Resch, H., Matis, N., Blocher, M., Auffarth, A., Mayer, M., … Tauber, M. (2013). Reverse shoulder arthroplasty in revision of failed shoulder arthroplasty-outcome and follow-up. International Orthopaedics, 37(1), 67–75. http://doi.org/10.1007/s00264-012-1742-z;

Peat, M. (1986). Functional anatomy of the shoulder complex. Physical Therapy, 66(12), 1855–1865.

Peers, S., Moravek Jr., J. E., Budge, M. D., Newton, M. D., Kurdziel, M. D., Baker, K. C., … Wiater, J. M. (2015). Wear rates of highly cross-linked polyethylene humeral liners subjected to alternating cycles of glenohumeral flexion and abduction. Journal of Shoulder and Elbow Surgery, 24(1), 143–149. http://dx.doi.org/10.1016/j.jse.2014.05.001

Roche, C., Flurin, P.-H., Wright, T., Crosby, L. A., Mauldin, M., & Zuckerman, J. D. (2009). An evaluation of the relationships between reverse shoulder design parameters and range of motion, impingement, and stability. Journal of Shoulder and Elbow Surgery, 18(5), 734. http://dx.doi.org/10.1016/j.jse.2008.12.008

Rockwood, C. A. (2009). The shoulder (4th ed). Philadelphia: Saunders Elsevier.

Schmalzried, T. P., Szuszczewicz, E. S., Northfield, M. R., Akizuki, K. H., Frankel, R. E., Belcher, G., & Amstutz, H. C. (1998). Quantitative assessment of walking activity after total hip or knee replacement. The Journal of Bone and Joint Surgery. American Volume, 80(1), 54–59. http://doi.org/159

Silva, M., Shepherd, E. F., Jackson, W. O., Dorey, F. J., & Schmalzried, T. P. (2002). Average patient walking activity approaches 2 million cycles per year: pedometers under-record walking activity. The Journal of Arthroplasty, 17(6), 693–697. http://doi.org/10.1054/arth.2002.32699

Soslowsky, L. J., Carpenter, J. E., Bucchieri, J. S., & Flatow, E. L. (1997). Biomechanics of the rotator cuff. Orthopedic Clinics of North America, 28(1), 17–30.

Soslowsky, L. J., Flatow, E. L., Bigliani, L. U., & Mow, V. C. (1992). Articular geometry of the glenohumeral joint. Clinical Orthopaedics and Related Research, (285)(285), 181–190.

Soslowsky, L. J., Flatow, E. L., Bigliani, L. U., Pawluk, R. J., Ateshian, G. A., & Mow, V. C. (1992). Quantitation of in situ contact areas at the glenohumeral joint: a biomechanical study. Journal of Orthopaedic Research : Official Publication of the Orthopaedic Research Society, 10(4), 524–534. http://doi.org/10.1002/jor.1100100407

Terrier, A., Merlini, F., Pioletti, D. P., & Farron, A. (2009). Comparison of polyethylene wear in anatomical and reversed shoulder prostheses. The Journal of Bone and Joint surgery.British Volume, 91(7), 977–982. http://doi.org/10.1302/0301-620X.91B7.21999

Terrier, A., Reist, A., Merlini, F., & Farron, A. (2008). Simulated joint and muscle forces in reversed and anatomic shoulder prostheses. The Journal of Bone and Joint surgery.British Volume, 90(6), 751–756. http://doi.org/10.1302/0301-620X.90B6.19708

Vaupel, Z. M., Baker, K. C., Kurdziel, M. D., & Wiater, J. M. (2012). Wear simulation of reverse total shoulder arthroplasty systems: effect of glenosphere design. Journal of Shoulder and Elbow Surgery, 21(10), 1422–1429. http://dx.doi.org/10.1016/j.jse.2011.10.024

Virani, N. A., Cabezas, A., Gutiérrez, S., Santoni, B. G., Otto, R., & Frankle, M. (2013). Reverse shoulder arthroplasty components and surgical techniques that restore glenohumeral motion. Journal of Shoulder and Elbow Surgery, 22(2), 179–187. http://doi.org/10.1016/j.jse.2012.02.004

Werner, B. S., Boehm, D., & Gohlke, F. (2013). Revision to reverse shoulder arthroplasty with retention of the humeral component. Acta Orthopaedica, 84(5), 473–478. http://doi.org/10.3109/17453674.2013.842433

Werner, C. M. L., Steinmann, P. a, Gilbart, M., & Gerber, C. (2005). Treatment of painful pseudoparesis due to irreparable rotator cuff dysfunction with the Delta III reverse-ball-and-socket total shoulder prosthesis. The Journal of Bone and Joint Surgery. American Volume, 87(7), 1476–1486. http://doi.org/10.2106/JBJS.D.02342

Westerhoff, P., Graichen, F., Bender, a., Rohlmann, a., & Bergmann, G. (2009). An instrumented implant for in vivo measurement of contact forces and contact moments in the shoulder joint. Medical Engineering & Physics, 31(2), 207–213. http://doi.org/10.1016/j.medengphy.2008.07.011

Westerhoff, P., Graichen, F., Bender, A., Halder, A., Beier, A., Rohlmann, A., & Bergmann, G. (2009). In vivo measurement of shoulder joint loads during activities of daily living. Journal of Biomechanics, 42(12), 1840–1849. http://doi.org/10.1016/j.jbiomech.2009.05.035

Zhou, H., Hu, H., Harris, N. D., & Hammerton, J. (2006). Applications of wearable inertial sensors in estimation of upper limb movements. Biomedical Signal Processing and Control, 1(1), 22–32. http://doi.org/10.1016/j.bspc.2006.03.001

Zhou, H., Hu, H., & Tao, Y. (2006). Inertial measurements of upper limb motion. Medical and Biological Engineering and Computing, 44(6), 479–487. http://doi.org/10.1007/s11517-006-0063-z

Zhou, H., Stone, T., Hu, H., & Harris, N. (2008). Use of multiple wearable inertial sensors in upper limb motion tracking. Medical Engineering and Physics, 30(1), 123–133. http://doi.org/10.1016/j.medengphy.2006.11.010

<div align="center">Chapter 2</div>

2 The Effect of Neck-Shaft Angle, Cup Depth, and Glenosphere Diameter in Reverse Shoulder Arthroplasty on Muscle Force, Joint Load, and Range of Motion

<div align="center">**OVERVIEW**</div>

Little is known on the effects of reverse total shoulder arthroplasty (RSA) neck-shaft angle, cup depth, and glenosphere diameter on muscle and joint loads. Furthermore, ascertaining the changes to RSA implant loading when changing these implant variables is of interest in the development and implementation of a RSA wear simulation strategy, since if loads significantly change for implants of varying geometrical configurations, then the loading profile applied to the implants during testing must be variable depending on implant diameter. The purpose of this biomechanical study was to investigate the effects of humeral neck-shaft angle, cup depth, and glenosphere diameter on joint load, load angle, and total deltoid force required for active abduction, and ROM in internal (IR)/external rotation (ER) and abduction using a custom, instrumented RSA implant system capable of measuring joint load and varying neck-shaft angle (155°/145°/135°), cup depth (deep, normal, shallow), glenosphere diameter (38/42mm) and glenoid offset (neutral/lateral) and a shoulder motion simulator.[1]

2.1 Introduction

Reverse shoulder arthroplasty (RSA) is an established surgical treatment for severe symptomatic rotator cuff tear arthropathy (Castagna et al., 2013; Drake, OConnor, Edwards, O'Connor, & Edwards, 2010; Ek, Neukom, Catanzaro, & Gerber, 2013; Flury, Frey, Goldhahn, Schwyzer, & Simmen, 2011; Leung, Horodyski, Struk, & Wright, 2012; Nolan, Ankerson, & Wiater, 2011; Ortmaier et al., 2013; Werner, Boehm, & Gohlke, 2013). As the name implies, RSA reverses the natural geometric anatomy of the glenohumeral joint. As such, selection of optimal implant characteristics and size cannot be directly guided by attempting to replicate the native geometry. Currently, the most common humeral neck-shaft (N-S) angles are in the range of 150°-155° although more recent designs have incorporated lower neck-shaft angles as low as 135°. Some RSA implant systems also offer varying cup depths, typically a deeper more constrained cup and a shallower less constrained cup. The diameter of the glenosphere and articulating polyethylene cup is one such characteristic. Current commercially available RSA implant designs offer sizes ranging from 32 to 53 mm in diameter, with the most widely used offerings providing two size options including either a smaller 36 or 38 mm or a larger 40 to 42 mm diameter glenosphere/polyethylene insert pairing.

The results of altering humeral N-S angle on shoulder range of motion (ROM) have been studied using computer-based solid models (de Wilde, Poncet, Middernacht, & Ekelund, 2010; Gutiérrez et al., 2008; Virani et al., 2013) and physical solid sawbone models (Gutiérrez, Levy, et al., 2008), although none of these studies have investigated the resulting effects on joint force and muscle load for varying N-S angles. Generally, these works report that reducing the humeral N-S angle increases adduction range of motion by virtue of the rotation of the humeral cup relative to the humeral shaft in the direction of abduction, thereby allowing the humerus to achieve an angle closer to the torso without the inferiomedial edge of the cup contacting the inferior aspect of the glenoid (de Wilde et al., 2010; Gutiérrez et al., 2008; Gutiérrez, Levy, et al., 2008; Virani et al., 2013).

The depth of the humeral cup has been shown to have an inverse relationship with humeral ROM using both computer based and physical models whereby as cup depth is reduced, ROM increases due to the reduced potential for contact of the periphery of the cup with the scapula (Gutiérrez et al., 2009; Gutiérrez, Keller, et al., 2008). Joint stability is also altered with changes in cup depth, with deeper humeral cups providing a greater resistance to dislocation than shallower cups (Gutiérrez, Keller, et al., 2008). Clouthier et al (2013) also showed that deeper, more constrained humeral cups increased the resistance of the articulation to dislocation.

The effects of changing RSA glenosphere diameter on shoulder ROM have been investigated using computer models (de Wilde et al., 2010; Gutiérrez et al., 2009; Gutiérrez et al., 2008; Roche et al., 2009; Virani et al., 2013), physical models (Chou, Malak, Anderson, Astley, & Poon, 2009; Gutiérrez, Keller, et al., 2008), and in an in-vitro cadaveric study (Berhouet, Garaud, & Favard, 2014). The results of solid bone model studies, that do not include soft tissues and use angles of impingement as the outcome variable, report that larger glenospheres provide greater ROM in both abduction (Berhouet et al., 2014; Chou et al., 2009; de Wilde et al., 2010; Gutiérrez et al., 2008; Gutiérrez, Levy, et al., 2008; Roche et al., 2009; Virani et al., 2013) and internal/external rotation (Virani et al., 2013), and can increase the force required to dislocate the joint (Gutiérrez, Keller, et al., 2008).

However, there remains a lack of information regarding the effect of humeral N-S angle, cup depth, and glenosphere diameter on muscle and joint loads, which would provide further insight into the influence of this parameter on the long-term performance of RSA.

The purpose of this in-vitro biomechanical cadaveric simulator study was to investigate the effects of RSA humeral N-S angle, cup depth, and glenosphere diameter on the total deltoid force required for active abduction, the resulting articular joint load and load angle, and ROM in internal/external rotation and abduction, for three humeral N-S angles (155°, 145°, & 135°), three cup depths (deep, normal, & shallow), and two common glenosphere sizes (38 & 42 mm).

We hypothesized that reducing humeral N-S angle would i) increase adduction ROM, and ii) not significantly affect the resultant joint loads and muscle forces since all N-S angles share identical centers of rotation. We hypothesized that in terms of cup depth i) decreasing depth would increase ROM and increasing cup depth would reduce ROM, and ii) not significantly affect the resultant joint loads and muscle forces since all cup depths share identical centers of rotation. We hypothesized that increasing glenosphere diameter would i) increase ROM in both internal/external rotation and abduction, ii) not significantly affect the resultant joint loads and muscle forces, and iii) increase the joint load angle (or shear component) due to the increased stability and ability of the deeper cup to resist applied shear loading.

2.2   Materials & Methods

2.2.1   Custom Instrumented RSA Implant

A custom modular implant system was designed for use in this study that included a load sensor, which allowed joint load measurement, and different humeral N-S angles, cup depths, glenosphere offsets and diameters (Figure 2-1). The custom glenosphere was hollowed to allow insertion of a six degrees-of-freedom (DOF) load cell (NANO25, ATI-IA, Apex, NC) before attachment to the glenoid base plate, which was recessed into the glenoid vault to allow neutral glenosphere positioning. Neutral was defined with the glenoid base plate placed on the inferior rim of the glenoid with the center of rotation at the glenoid articular surface.
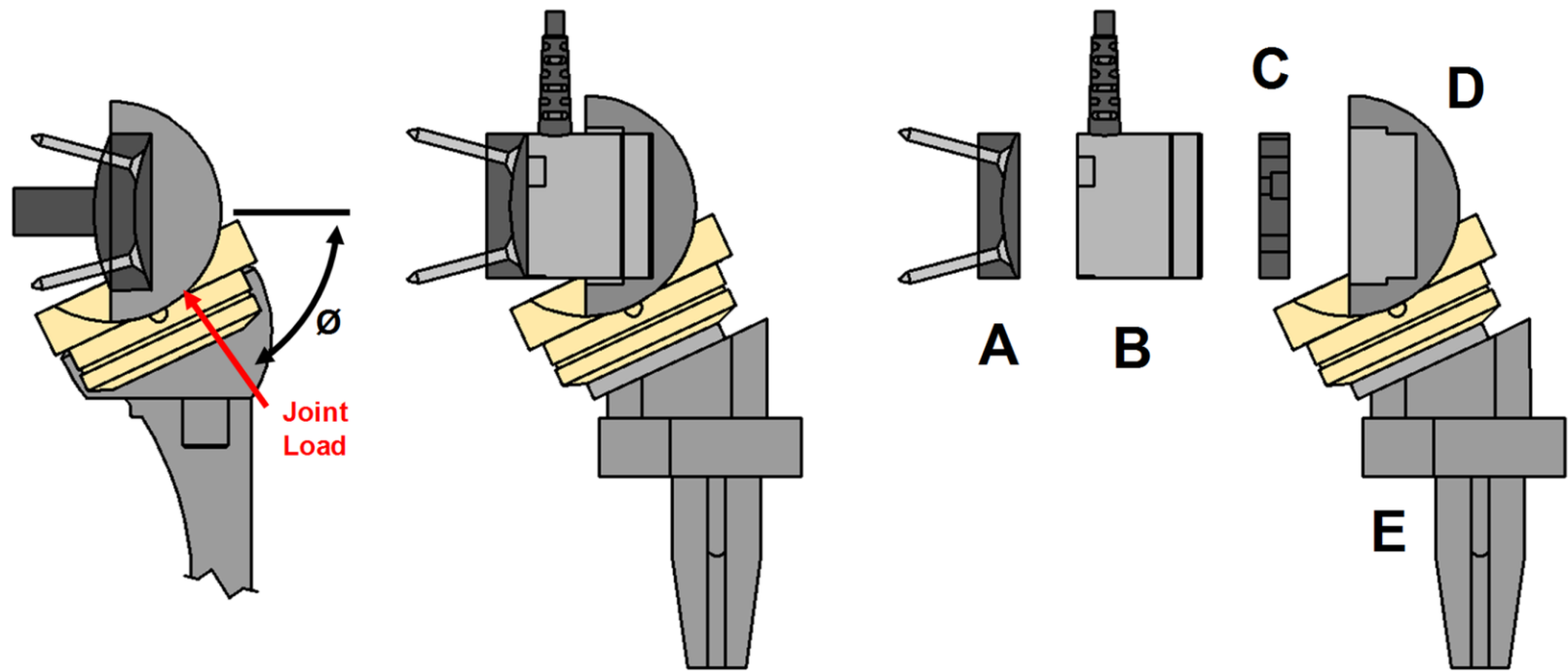
Figure 2-1: A cross-sectional side view of a typical commercially available reverse shoulder arthroplasty (RSA) system (left). *Our custom designed modular RSA implant (middle), with exploded view of the glenoid (right) showing the (A) custom base plate, (B) 6 degrees of freedom load cell, (C) glenosphere lateral offset spacer, (D) hollow glenosphere (38 & 42 mm sizes), and (E) custom humeral component.*

2.2.2   Specimen Preparation and Simulator Testing Apparatus

The custom RSA was implanted into the cadaveric shoulder after simulating a complete superior rotator cuff tear. The humeral component was cemented at 0° version relative to the transepicondylar axis. The glenoid component was implanted such that the center of rotation of the 0 mm offset implant was located at the articular margin of the glenoid baseplate, with the inferior rim of the baseplate located at the inferior rim of the glenoid. The three deltoid heads were sutured at their insertion, and the subscapularis and infraspinatus/teres minor musculotendious junctions were secured using a running locking stitch.

The remainder of specimen preparation was completed as described by Giles et al. (Giles et al., 2013), including fixation of optical motion trackers to the scapula (OptoTrak^{TM} Certus, NDI, Waterloo, ON) and insertion of an instrumented intramedullary humeral rod. The scapula was cemented to the simulator and all muscles were connected to load actuators through physiologically accurate lines-of-action which mimicked that of the native shoulder. The simulator produced independent muscle loading that was controlled via a multi-PID control system(Giles, Ferreira, Athwal, & Johnson, 2013), which provided accurate and repeatable muscle driven active glenohumeral motion with associated scapular rotation.

2.2.3   Experimental Testing Protocol

Two separate studies were conducted to examine the effect of i) N-S angle and cup depth and ii) glenosphere diameter. Individual studies were performed to allow for all the required implant configurations to be investigated in a single testing day such that the viability of the specimen was ensured throughout all trials.

2.2.3.1   Study 1: Humeral N-S Angle and Cup Depth

For study 1, the custom instrumented RTSA was implanted in seven fresh-frozen cadaveric shoulders (age: 71 ± 9 yrs). Three possible implant neck-shaft angle configurations comprised of 155°, 145°, and 135° were evaluated while all other implant

characteristics were maintained in their normal state (normal cup depth and neutral glenosphere and humeral offset), and three possible cup depths were evaluated (deep, normal, and shallow) while maintaining all other implant parameters in their normal state (155° N-S angle & neutral glenosphere and humeral offset). For each combination, active abduction was simulated from 0° (or as close as possible in the presence of an adduction deficit) to 90° of humerothoracic abduction at 1°/sec. Scapular rotation was applied at a 2:1 glenohumeral-to-scapulothoracic relationship (Inman, Saunders, & Abbott, 1996).

Commercially available 38 mm size polyethylene humeral inserts (Delta XTEND, Depuy, Warsaw, IN) were affixed to the humeral component of the modular RSA implant system having a N-S angle of either 155°, 145°, or 135° (Figure 2-2). All other implant parameters were normally configured (neutral version and 12.5 mm humeral offset). Cup depth was also varied including deep, normal, and shallow depths (Figure 2-2). Changing both N-S angle and cup depth did not alter the relationship between the humerus and the centre of rotation.

2.2.3.2   Study 2: Glenosphere Diameter

For study 2, the custom RTSA was implanted into another set of six fresh-frozen human cadaveric shoulders (60 ± 21 yrs). Four implant configurations, which represented all possible combinations of glenosphere diameter (38, 42 mm) and glenosphere offset (neutral, +10mm lateral offset), were evaluated in random order. For each combination, active abduction was simulated from 0° (or as close as possible in the presence of an adduction deficit) to 90° of humerothoracic abduction at 1°/sec. Scapular rotation was applied at a 2:1 glenohumeral-to-scapulothoracic relationship(Inman, Saunders, & Abbott, 1996).

Commercially available polyethylene humeral inserts (Delta XTEND, Depuy, Warsaw, IN) of either 38 or 42 mm size were affixed to the humeral component with the geometry of a neutrally configured clinical RSA. Neutral was defined as a neutral version humeral component with a 155° head-neck angle and a 12.5mm lateral offset humeral stem as in a

classic Grammont-style implant. Additionally, a 10mm spacer could be placed between the load cell and the glenosphere to allow for 10 mm of lateralization (Figure 2-3) to assess for interactions between glenosphere offset and diameter. Following commercial devices, when the glenosphere diameter was increased from 38 to 42 mm, the apparent cup thickness also increased by approximately +2.5 mm (Figure 2-3), due to a 2 mm increase in glenosphere radius, and a 0.5 mm increase in the distance from the deepest point of the cup to the cup-humeral component mating surface.

Internal/external rotational ROM was assessed by constraining the humeral rod at 0° of flexion-extension and abduction, while permitting free humeral axial rotation. Active internal rotation (IR) ROM was assessed by ramp loading the subscapularis, infraspinatus, and anterior deltoid to 38, 6, and 6 N, respectively and recording the maximum IR attained (Escamilla, Yamashiro, Paulos, & Andrews, 2009). External rotation (ER) ROM loaded the infraspinatus, subscapularis, and posterior and middle deltoids to 27, 9, 8 and 6 N, respectively (Escamilla et al., 2009). Passive IR/ER ROM was assessed by applying a 0.8 Nm torque to the humeral shaft while the deltoids and rotator cuff tendons were tone loaded to 5 and 7.5 N respectively, and recording the maximum rotation (Giles, Ferreira, Athwal, & Johnson, 2013). The maximum rotation limit was defined as 90°. Finally, passive abduction ROM was measured via manual adduction/abduction of the humerus to the point of bony or soft tissue impingement.
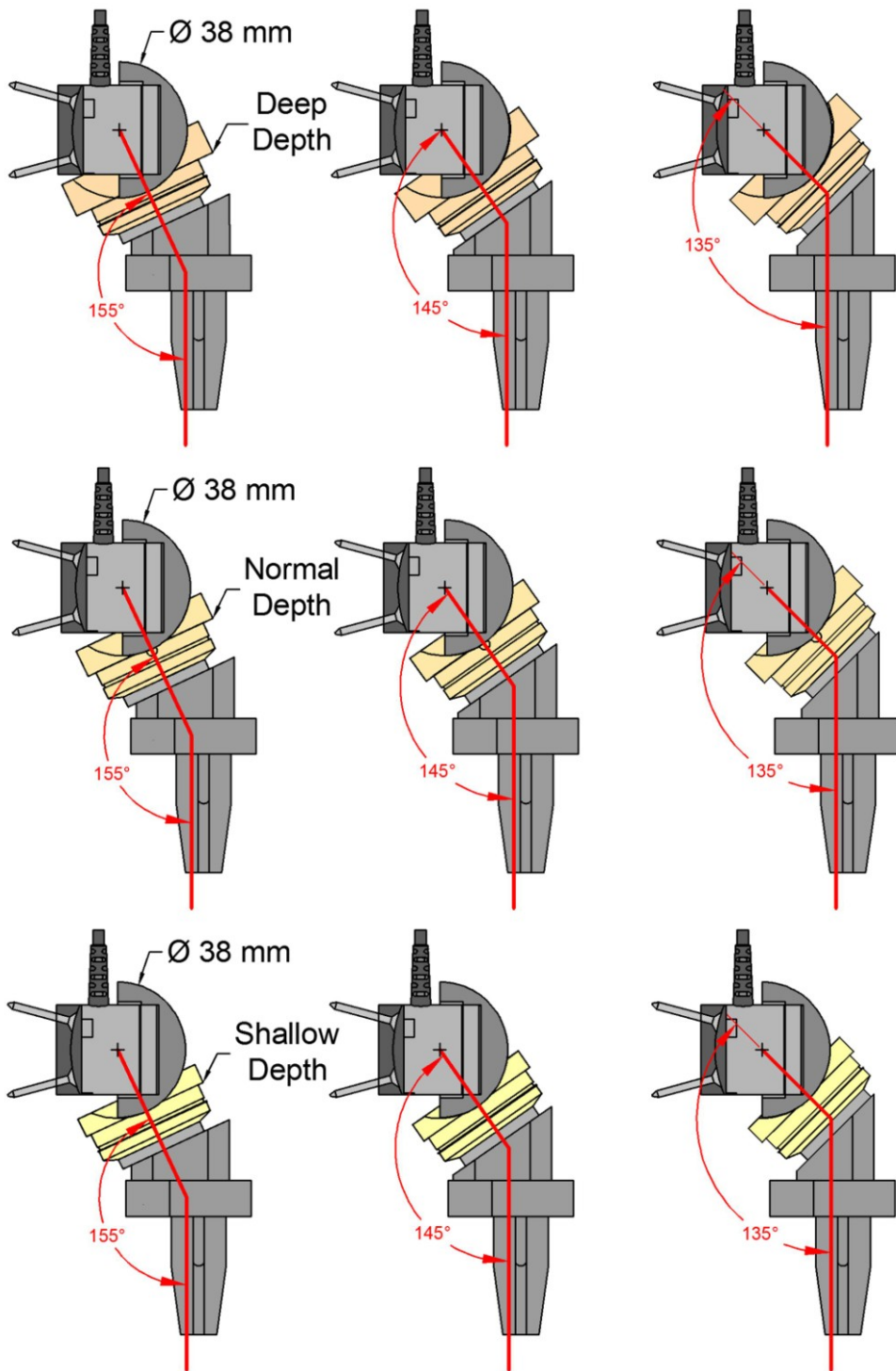
Figure 2-2: Humeral neck-shaft angles (left: 155°, middle: 145°, right: 135°) and cup depths (top: deep, middle: normal bottom: shallow) that were investigated.
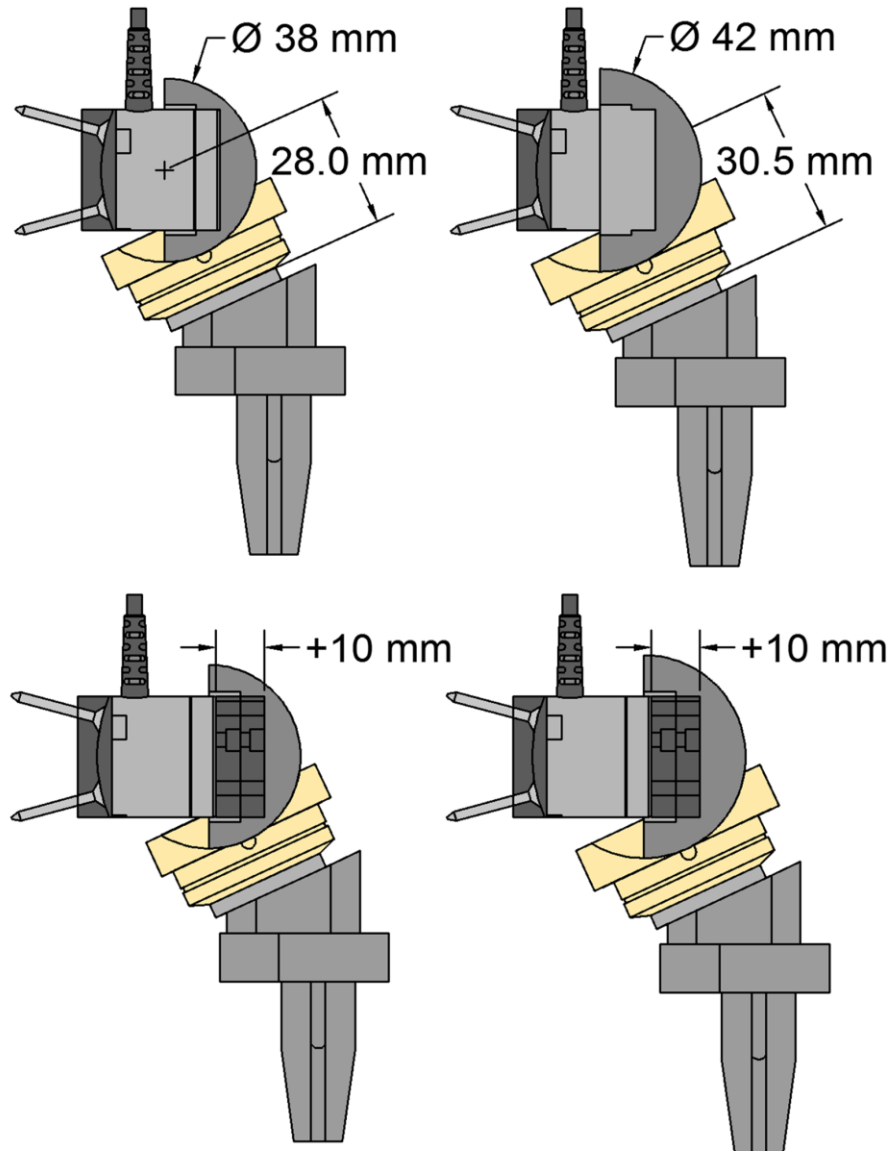
Figure 2-3: Glenosphere sizes (left: 38 mm, right: 42mm) and +10mm of glenosphere lateral offset (top: neutral, bottom: lateral) that were investigated.

2.2.4   Outcome Variables and Statistical Analyses

The effects of N-S angle, cup depth, and glenosphere diameter on active abduction were assessed using resultant joint load, total deltoid muscle force, and joint load angle. Transforming the load cell data to the center of the glenosphere provided resultant joint load. Summation of the three deltoid heads yielded total deltoid muscle force. Load angle was calculated using the transformed superior and lateral forces in the scapular plane, 0° corresponded to purely compressive forces and load angle increased with increasingly superior joint loads. All outcome variables were assessed at 5° increments between 22.5° and 82.5° of humeral-thoracic abduction, over which active motion was recorded for all implant variations.

For study 1, two 2 two-way (N-S angle, abduction angle; cup depth, abduction angle) repeated measures ANOVA (RM-ANOVA) was carried out for each outcome variable. For study 2, a three-way (glenosphere diameter, lateral offset, abduction level) RM-ANOVA was performed for each of the outcomes. Pairwise comparisons and analyses of interactions were performed for any cases demonstrating a significant effect ($p<0.05$). Power analyses carried out for each outcome variable found six specimens were sufficient to achieve at least 80% power for each outcome.

Implant configuration effects on passive abduction ROM was evaluated using total angular range and adduction deficit, and active and passive IR/ER ROM was assessed using the independent internal and external rotations. For study 1, paired t-tests were used to assess differences, and for study 2, a two way (glenosphere diameter, glenosphere lateralization) repeated measures ANOVA (RM-ANOVA) was performed for each of the ROM outcome variables.

2.3   Results

2.3.1   Resultant Joint Load

The mean resultant joint loads as a function of abduction angle for all glenosphere sizes and lateralizations are shown in Figure 2-4. The results of the two-way RM-ANOVA for

study 1 showed that both N-S angle and cup depth had no significant effects on resultant joint load (p=0.906 and p=0.149 respectively), although abduction angle showed significant effects (p<0.001 and p=0.038 respectively). The results from the three way RM-ANOVA for study 2 showed that glenosphere diameter (p=0.009), lateralization (p<0.001) and abduction level (p=0.003) all produced significant main effects on joint loading (Figure 2-4). Increasing glenosphere diameter increased RSA joint load (Table 2-1), on average by 5±9% and 10±17% at the neutral and lateralized glenosphere positions, respectively.

2.3.2   Total Deltoid Force

Neither N-S angle nor cup depth was found to have a significant effect on total deltoid force (p=0.067 and p=0.292 respectively), although for study 1 abduction angle was found to have significant effects on total deltoid force (p<0.001 and p=0.014 respectively). Significant main effects on total deltoid force were produced by glenosphere diameter (p=0.019), glenosphere lateralization (p=0.005) and abduction level (p=0.004). Increasing glenosphere size increased the required total deltoid force to achieve active abduction (Figure 2-5, Table 2-1). The average increases in total deltoid force when the glenosphere size was increased from 38 to 42mm for the neutral and lateral positions were 3 ± 7% and 3 ± 3%, respectively.

2.3.3   Resultant Joint Load Angle

The level of abduction had affected joint load angle (p<0.001). All other parameters (N-S angle, cup depth, and glenosphere size) had no significant effects. For study 1, load angles ranged from 22-60° at 22.5° abduction to 6-35° at 82.5° abduction for all N-S angles investigated, and from 20-56° at 22.5° abduction to 2-29° at 82.5° abduction. For study 2, load angles ranged from 45-53° at 22.5° abduction to 24-28° at 82.5° abduction for all glenosphere diameters and positions tested. Mean differences in joint load angle were less than 4.0° for all N-S angles, 0.7° for all cup depths, and 0.1° between 38 mm and 42 mm sizes (p>0.8, Table 2-1).
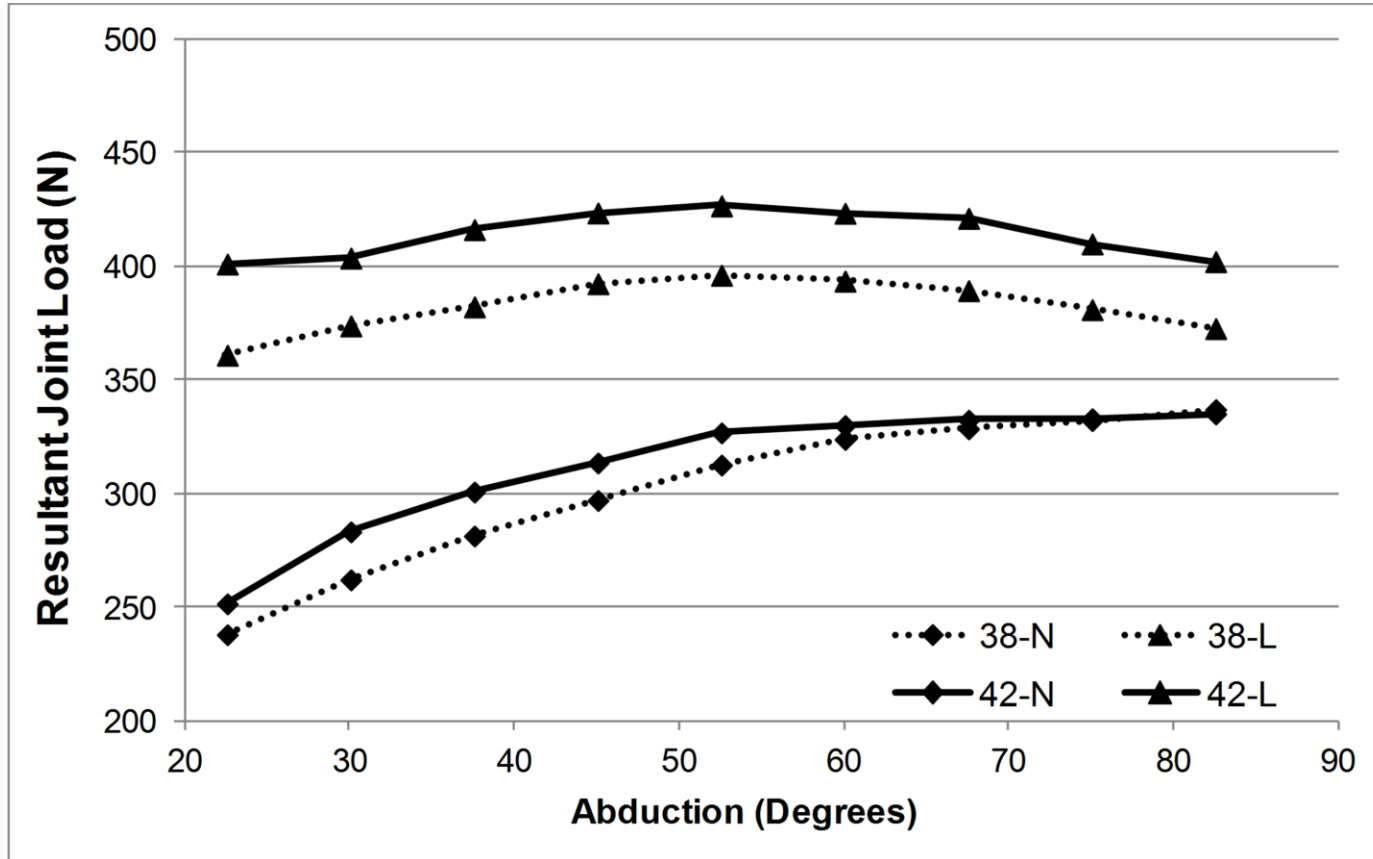
Figure 2-4: The mean joint loads throughout active abduction for both glenosphere diameters (38, 42 mm) and glenosphere positions (neutral and +10mm lateral) versus abduction angle are shown.

The standard deviations (omitted for clarity ranged from 38 to 138 N.
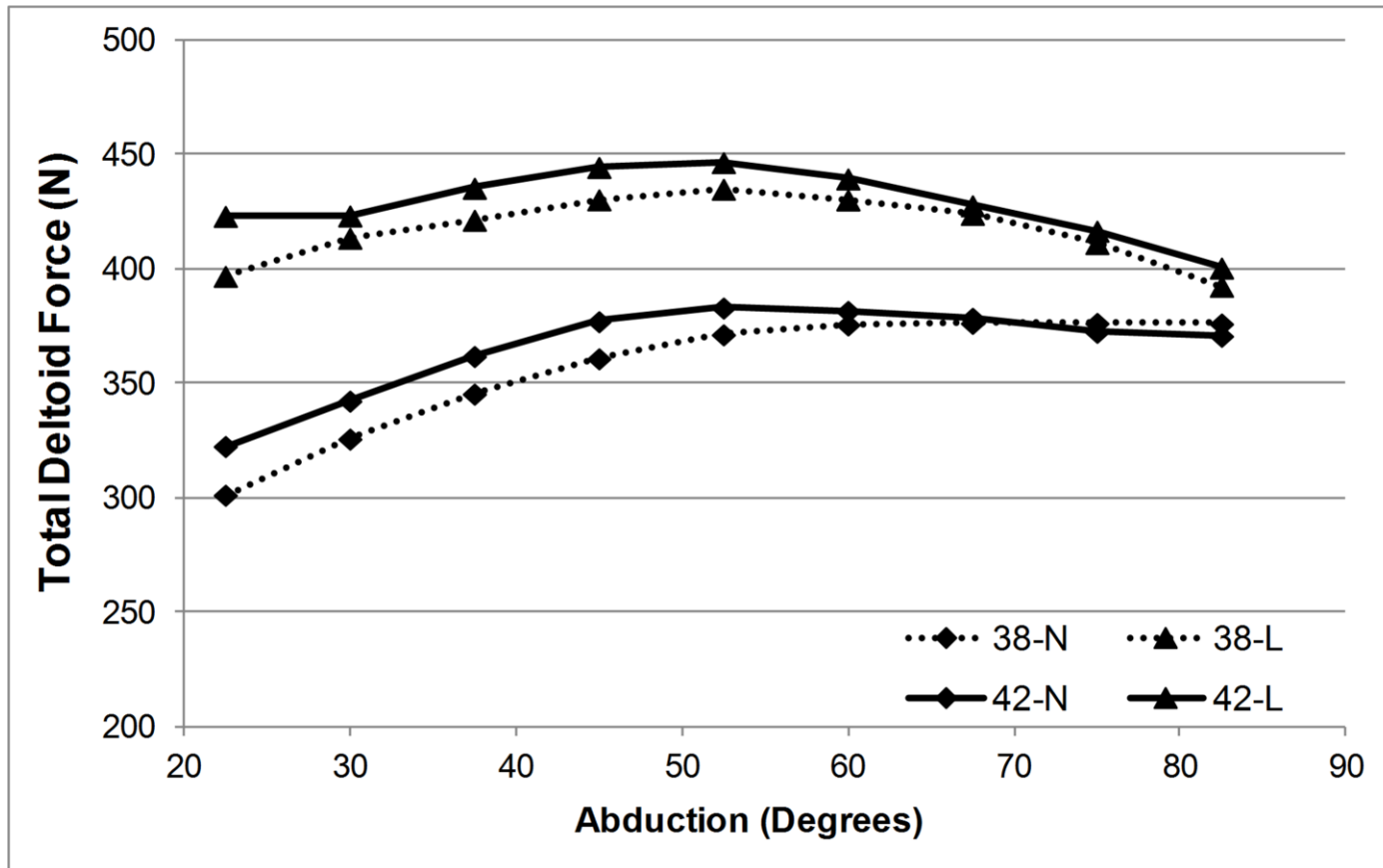
Figure 2-5: The mean total deltoid force throughout active abduction for both cup sizes (38, 42 mm) and glenosphere positions (neutral and +10mm lateral) versus abduction angle are shown.

The standard deviations (omitted for clarity) ranged from 23 to 70 N.

2.3.4   Internal and External Rotation ROM

For active IR ROM, significant effects were not detected for both N-S angle and cup depth (p>0.38 and p>0.15 respectively), however significant effects were detected for glenosphere diameter (p<0.001). Increased glenosphere size decreased active internal rotation at both the neutral and lateral glenosphere positions by an average of $2 \pm 3°$ and $6 \pm 7°$, respectively; however, only the lateral position was significant (p=0.127, p=0.014, Figure 2-6A, Table 2-1). For active ER ROM, no significant effects were detected for N-S angle, cup depth, or glenosphere size (p>0.27, p>0.07, and p>0.05 respectively). Lateralization of the glenosphere had no significant effects on active IR or ER ROM (p>0.09). For passive IR ROM, no significant effects were detected for N-S angle or cup depth (p>0.54 and p>0.14 respectively), however glenosphere diameter was found to have a significant effect; as size was increased, IR ROM decreased (p=0.002, Figure 2-6B). At both neutral and lateral glenosphere positions, increasing the glenosphere diameter from 38 to 42 mm significantly reduced passive IR ROM by an average of $6 \pm 6°$ and $12 \pm 6°$, respectively (p=0.048, p=0.004, Table 2-1). For passive ER ROM, N-S angle was not found to have significant effects (p>0.21), however a significant difference was detected between the shallow and deep cups (p=0.039). No significant effects were detected for passive ER ROM when glenosphere size was changed (p>0.05). On average, the deep humeral cup provided $5.8 \pm 5.09°$ less passive ER ROM than the mobile cup (Figure 2-7B).

Table 2-1: Mean (+1 SD) change in outcome variables between 38 mm and 42 mm glenosphere diameters (* $p<0.05$).

Glenosphere Position	Joint Load (N)	Total Deltoid Load (N)	Joint Load Angle (°)	Internal Rotation [Active/Passive] (°)		External Rotation [Active/Passive] (°)		Min Abduction Angle (°)	Peak Abduction Angle (°)
NEUTRAL	12 ± 21*	9 ± 22*	0 ± 2	-2 ± 3	-6 ± 6*	1 ± 6	0 ± 10	-1 ± 1*	8 ± 9*
LATERAL	6 ± 9*	11 ± 15*	0 ± 0	-6 ± 4*	-12 ± 6*	2 ± 5	-1 ± 1	1 ± 2	6 ± 9
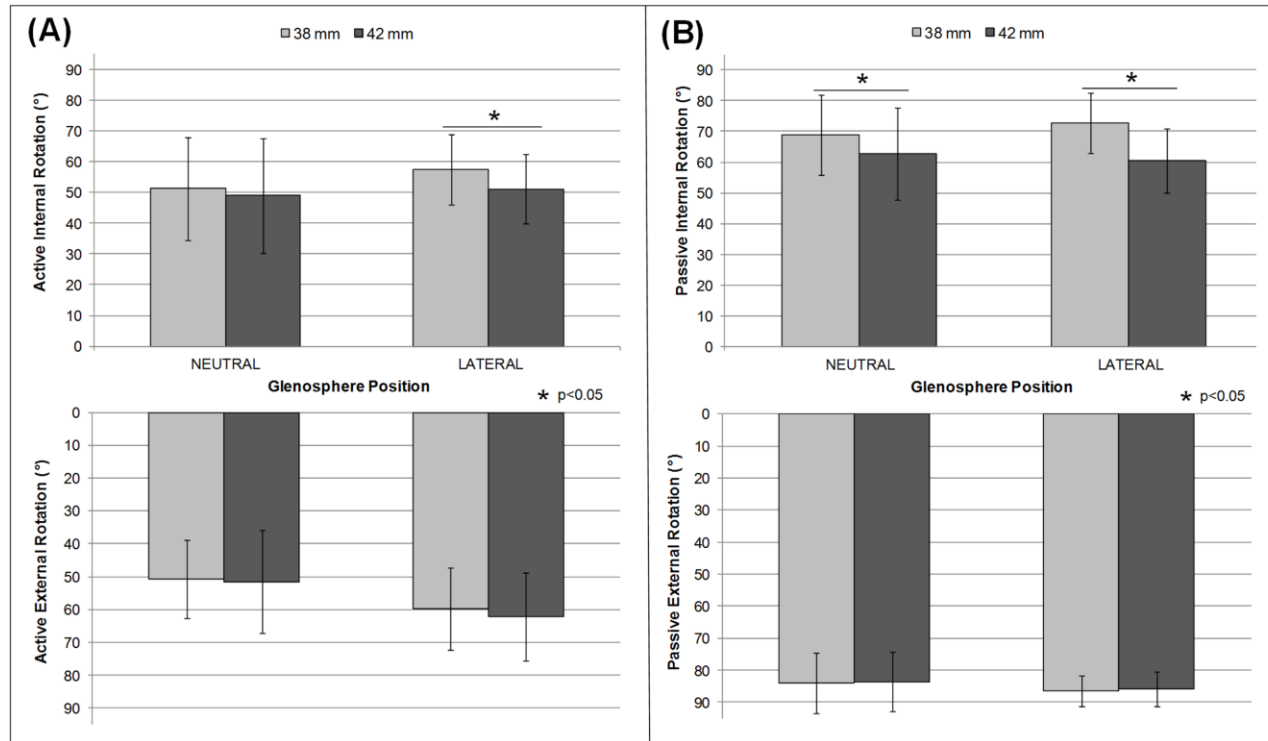
Figure 2-6: Mean (+ 1 SD) for (A) active IR (top) and ER (bottom) ROM and (B) passive IR (top) and ER (bottom) for all glenosphere diameters (38, 42 mm) and positions (neutral, lateral) investigated.
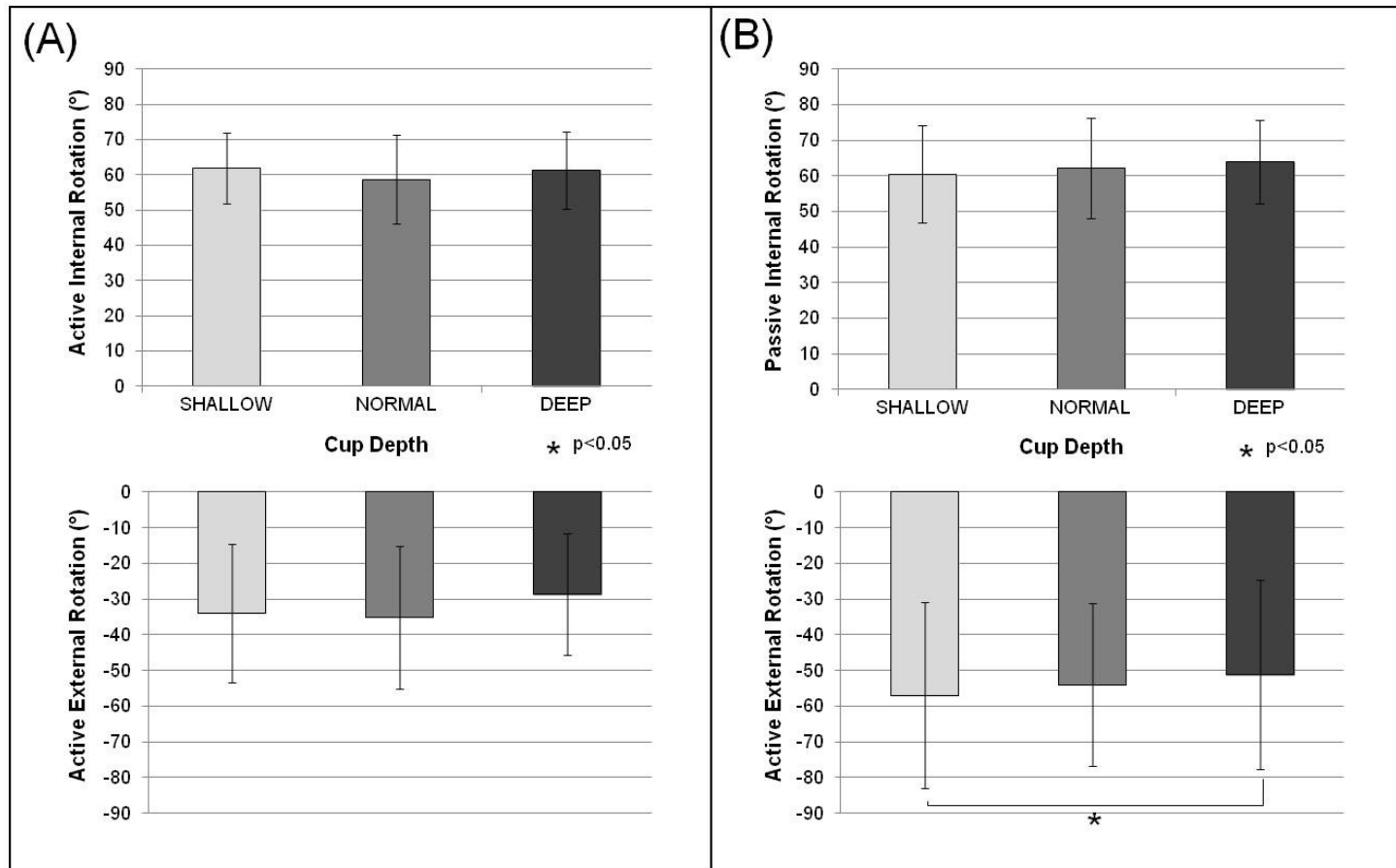
Figure 2-7: Mean (+ 1 SD) for (A) active IR (top) and ER (bottom) ROM and (B) passive IR (top) and ER (bottom) for all cup depths (Shallow, Normal, Deep) investigated.

2.3.5   Abduction Range of Motion

Reducing N-S angle from 155° to 145° and from 155° to 135° significantly increased adduction range of motion (p=0.014 and p=0.018 respectively), with the reduction from 155° to 145° and 155° to 135° providing an additional 4.3 ± 4.2° and 3.8 ±3.8° of adduction respectively (Figure 2-8). There was no significant difference detected between the 145° and 135° N-S angles. No significant effects were observed for peak abduction angle (p>0.09).

Cup depth was not found to have significant effects on either adduction or abduction ROM (p>0.45 for all).

The results of the two way RM-ANOVA for adduction angle showed that glenosphere lateralization produced significant main effects (p<0.03), and also interacted significantly with glenosphere diameter (p<0.002). Increasing glenosphere lateralization significantly decreased the adduction deficit (improved adduction) by an average of -6 ± 3° and -3 ± 2° for the 38 and 42 mm glenosphere diameters respectively (p<0.001, p=0.002, Figure 2-9). The pairwise comparison for the interaction between glenosphere offset and diameter, showed that in the neutral glenosphere position, increasing the glenosphere diameter from 38 to 42 mm significantly increased maximum adduction angle by an average of 1 ± 1° (p=0.03), while no significant differences were detected at the lateral glenosphere position (p=0.34).

The maximum angle of abduction was significantly affected by glenosphere lateralization (p=0.043). Lateralizing the glenosphere increased the maximum abduction angle achievable (Figure 2-9). Increasing glenosphere diameter only significantly affected peak abduction angle at the neutral glenosphere position (p=0.04, Table 2-1), resulting in an average increase of 8 ± 9°, while no significant differences were detected at the lateral position (p=0.08). Lateralizing the glenosphere significantly increased peak abduction angle by an average of 21 ± 8° and 19 ± 7° for the 38 and 42 mm glenosphere diameters respectively (p<0.001 for both).
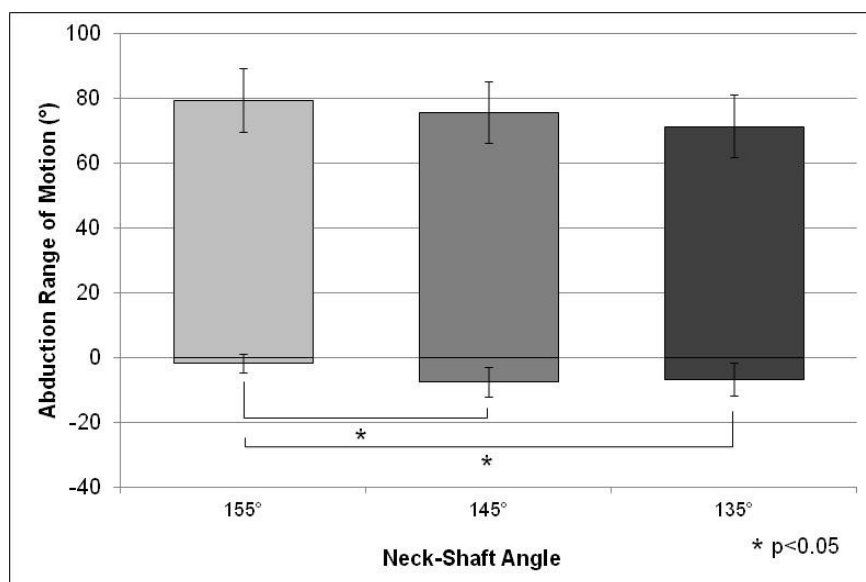
Figure 2-8: Mean (+ 1 SD) abduction ranges of motion for all neck-shaft angles (155°, 145°, 135°) investigated.
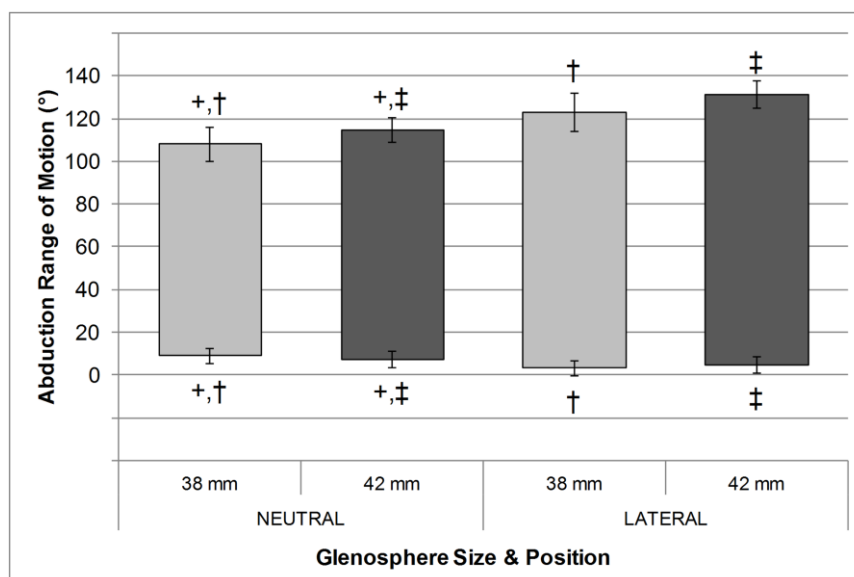
Figure 2-9: Mean (+ 1 SD) abduction ranges of motion for all glenosphere diameters (38, 42 mm) and positions (neutral, lateral) investigated.

Significance (p<0.05) denoted by '+' for size comparison at neutral offset, and '†' and '‡' for neutral to lateral comparisons for 38 and 42 mm glenosphere diameters, respectively.

2.4   Discussion

Decreasing N-S angle in RSA is known to increase adduction ROM, a direct result of the rotation of the humeral cup in the direction of abduction relative to the humeral shaft, which results in reduced scapular impingement in adduction (Gutiérrez et al., 2008; Gutiérrez, Levy, et al., 2008). The results of the present study agree with these previous findings, with both the 145° and 135° N-S angle providing greater adduction ROM than the 155° N-S angle. Interestingly, there was no difference detected between the 145° and 135° N-S angles, and this may have been a result of soft tissues constraining further adduction as geometrically the lower 135° N-S angle should have provided more adduction ROM if the limiting factor was scapular impingement (Figure 2-10).

Interestingly, cup depth was not found to have a significant impact on abduction ROM, which had been previously shown to occur (Gutiérrez et al., 2009; Gutiérrez, Keller, et al., 2008). One potential reason for this could be the inferior glenosphere placement in the present study, which may have mitigated the risk of scapular impingement between the inferiomedial edge of the cup and the scapula.

Increasing RSA glenosphere diameter is known to increase abduction ROM. This effect is mainly due to the larger radial distance from the centre of rotation to the articular surface of the humeral cup, which then passes under the medial glenosphere plane more inferiorly, resulting in a reduction in the occurrence of scapular impingement (Chou et al., 2009; de Wilde et al., 2010; Gutiérrez et al., 2009; Gutiérrez et al., 2008; Gutiérrez, Keller, et al., 2008; Roche et al., 2009; Virani et al., 2013). The selection of glenosphere size, however, is often based on patient size. Currently available RSA prostheses provide a limited range of glenosphere and humeral polyethylene sizes, typically offering one smaller and one larger option. These sizing options are in contrast to the often multiple size offerings seen with anatomic shoulder arthroplasty.

However, the effect of these implant characteristics on RSA performance in terms of joint loading and muscle forces is currently not fully investigated. As such, it is not known

whether a greater range of implant options would optimize implant performance in individual patients.

The specific aim of this study was to elucidate the effect of N-S angle, cup depth, and glenosphere size on: joint loading (resultant load & load angle), and total deltoid force, in addition to shoulder active and passive ROM. Furthermore, since glenosphere lateralization is also known to affect scapular impingement and notching, this parameter was also included in study 2 to investigate any interactions between it and glenosphere size. The resultant joint load was not affected by N-S angle nor cup depth, which is reasonable since all these implant configurations share identical centers of rotation. Resultant joint load was significantly affected by glenosphere diameter; however, the differences were relatively small, with maximum increases of less than 10%. It was not expected that glenosphere size would significantly affect joint load, since the glenohumeral centre of rotation for both sizes are nearly identical, with the only significant difference being the radial distance to the articulating surface. If articular bearing friction forces were significant, this increase in the friction force's moment arm could impact joint loads by requiring greater muscle forces to overcome the additional resistance of the articulation to motion. This, in addition to the slight humeral offset induced when the glenosphere diameter was increased in the present study is the most likely reason for the significant, albeit relatively small increase in joint load observed when the glenosphere size was increased.
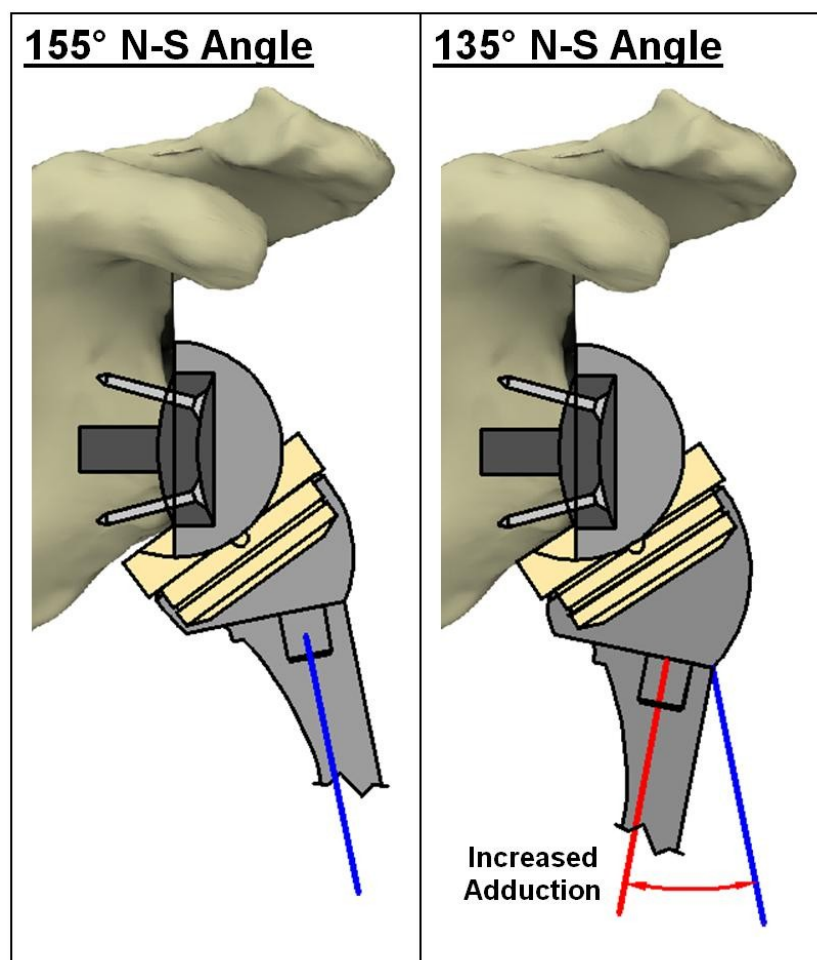
Figure 2-10: An example of scapular impingement in adduction for 155° (left) and 135° (right) N-S angles.

The potential reduction in the adduction deficit is shown as a result of the rotation of the humeral cup relative to the humerus in the direction of abduction.

The main abductor muscle group following RSA is the deltoid, as such, total deltoid force during abduction is an important outcome when configuring RSA devices. In the present study, neither N-S angle nor cup depth affected deltoid force, however total deltoid force increased as glenosphere size increased, and although the differences were significant, the increases were small with an average increase of only 3% when the load on the three deltoid groups was combined. Hence, although the required deltoid force increased with increased glenosphere size, the clinical significance of this increase is unknown. It can be theorized that insertions of excessively large glenospheres may have more substantial changes in deltoid force that may be more important.

It is reasonable that the required deltoid force for abduction would increase with increased cup size if the friction effects were substantial at the larger articular moment arm, as previously described; however, the increase in deltoid load was smaller than the increase in joint load under the same conditions. This may have been due to the slight humeral lateralization that occurred when the glenosphere diameter was increased, resulting in an increased deltoid muscle moment arm, which may have reduced the force required for active motion for the 42 mm glenosphere compared to the 38 mm.

RSA joint load angle is an important factor in the magnitude and type of loading applied to the glenosphere and subsequently the glenoid base plate, which can affect glenosphere fixation. No significant effects were detected for varying N-S angles or cup depths, again likely due to the identical centers of rotation of these variants. It is plausible that increased glenosphere diameter could affect joint load angle, since the deeper 42 mm humeral polyethylene insert may allow the articulation to carry more out of plane loading than the shallower 38 mm humeral insert. In the present study, however, increasing the glenosphere diameter did not seem to have any effect on joint load angle.

Active and passive internal rotation ROM was negatively affected when glenosphere diameter was increased in the present study. This contradicts results presented by Virani et al (2013), whose computational model, without soft tissue or muscle simulation, reported an increase in combined IR/ER of approximately 12° when glenosphere

diameter was increased from 36-42 mm. Similar to the mechanism by which increasing glenosphere size increases abduction ROM, we expected that IR/ER ROM would also be increased in our model. In order to investigate our contrary findings, we developed a computer 3D shoulder model using CT specimen data and implanted RSA geometry as described in our protocol. The same reduction in IR ROM encountered using our dynamic cadaveric model could not be reproduced in our computer generated model, which used bone impingement as its end point. We believe that this means that the reductions in IR ROM observed in our simulator cadaveric study are not a result of implant or bony impingement. Rather, we postulate that the decrease in IR ROM was due to the remaining posterior shoulder joint capsule being forced to wrap further around the larger 42 mm implant assembly resulting in increased capsular tensioning, which occurred during internal rotation, thus restricting terminal IR ROM. This is an important finding, as it underlines the importance of soft tissues when modeling and conducting RSA. This finding is especially interesting considering that it has been shown that ROM limitations that are encountered intra-operatively (Schwartz et al., 2014), whether due to soft tissue or bone impingement, persist post-operatively. The soft tissue effect encountered with internal rotation was not encountered for external rotation. This is likely due to the extensive releases of the anterior shoulder soft tissues that are done during RSA implantation.

Overall, active IR/ER ROM typically achieved 50-60° of rotation. Increasing glenosphere diameter reduced IR by up to 5°, likely due to increased capsular tension because of the larger prosthesis. Therefore, when increasing glenosphere size, soft tissue tension in both IR and ER should be intra-operatively assessed to prevent excessive tensioning and reduced rotational ROM. Should a terminal restriction in IR ROM be encountered intraoperatively due to capsular tightness, it is reasonable to consider further releases of the posterior capsular tissues.

The maximum adduction angle is often prescribed by scapular impingement at the inferior most edge of the humeral cup. The use of a 42 mm implant moves the cup edge in the inferior direction resulting in increased adduction (Figure 2-11). Similarly, lateral

positioning of the glenosphere also reduces adduction impingement. The results of the present study showed a significant reduction in minimum abduction angle when glenosphere size was increased only at a neutral glenosphere position. In the lateral position, cup size had no effect due to the elimination of scapular impingement by lateralization of the glenosphere. On the whole, the reduction in minimum abduction angle in the neutral position averaged about 1.5°, which is close to several published computer solid body modeling studies (Gutiérrez et al., 2008; Gutiérrez, Keller, et al., 2008; Virani et al., 2013). Chou et al (2009) reported about 4x the reduction in minimum abduction angle moving from a 36 to 44 mm diameter glenosphere; however, their smallest glenosphere diameter was 2 mm smaller and their range between the smallest and largest diameters was twice that of the present study. The smaller 36 mm and larger 44 mm glenospheres may have produced the larger difference they observed, as the smaller prosthesis has the potential to impinge earlier in adduction than a 38 mm, and the larger prosthesis may have provided greater adduction than the 42 mm sizes included in the present study. The maximum abduction angle was significantly increased when increasing the glenosphere size from 38 to 42 mm at the neutral position. Similar to minimum abduction angle, no significant differences were detected in the lateral position. Maximum abduction angle was increased an average of 8° when in the neutral position, which was similar to Chou et al (2009).

The present study used cadaveric specimens, which affects replication of in-vivo motion and loading. However, this is mitigated by the fact that in RSA the majority of passive soft tissues, the largest concern in cadaveric studies, are not present and as such were released as part of the study protocol. The arm mass in the present study was also scaled to accommodate the muscle force capabilities of the shoulder simulator apparatus; however, the presented loads were scaled appropriately and are expected to be an accurate representation due to the proportionality of joint loads and muscle forces to arm mass. Also, RSA recipients may have different rotator cuff functionality, which is not precisely correlated to the EMG data used to guide muscle activation in the present study. Finally, as occurs clinically due to inherent RSA design, when cup size was increased,

apparent cup thickness also increased by approximately 2.5 mm, which effectively applies a humeral lateralization of approximately 0.9 mm, although it is unlikely that a difference as small as 0.9 mm would significantly contribute to changes in the outcome variables of the present study.

The strengths of the present study include the direct measurement of the six degrees of freedom joint loads at the glenosphere for each RSA implant configuration investigated, using a custom designed prosthesis system, during both active and passive shoulder motion. Previous studies have measured loading through instrumented scapular mounts, which introduces error when loads are then translated to the glenohumeral joint. The present study also uses a shoulder simulator apparatus, which was capable of real-time feedback controlled active shoulder motion, rather than relying on passive user-driven motions.
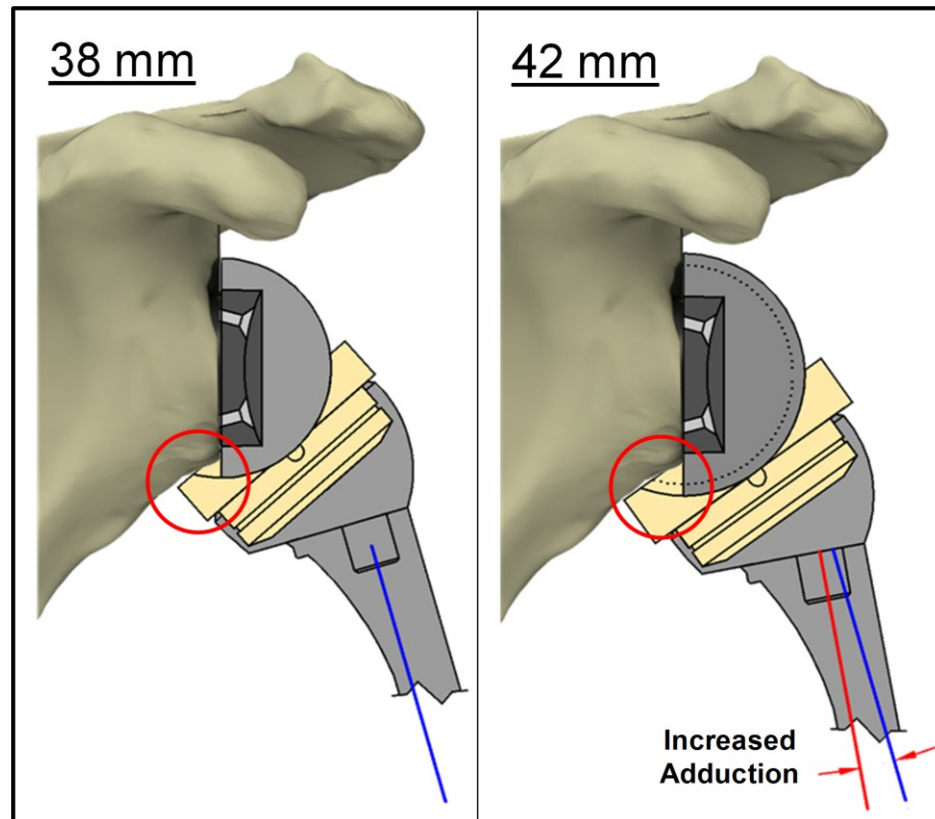
Figure 2-11: An example of scapular impingement in adduction for 38 mm (left) and 42 mm (right) glenosphere sizes.

The potential reduction in the adduction deficit is shown. The 38 mm glenosphere diameter is shown overlaid (dotted line) on the 42 mm cup size for clarity of comparison.

2.5 Conclusions

This study provides further insights into the effects of RSA implant configurations. First, the N-S angles and cup depths in this study did not affect joint load or deltoid force, however the glenosphere diameters tested did have a significant effect on joint load, and total deltoid force required for active abduction. Increases in joint load may have an impact on implant performance, and increased deltoid forces may contribute to a reduction in shoulder function over time. Second, joint load angle was not significantly affected by N-S angle, cup depth, or glenosphere diameter, even though it was expected that the deeper 42 mm implant would be able to accommodate greater shear loading due to a deeper cup geometry. Third, internal rotation ROM in adduction was reduced as glenosphere size increased, which was likely a result of increased tensioning of the remaining posterior capsule wrapping around the larger implant geometry. Therefore, soft tissue tension should be assessed when upsizing glenosphere diameter. Finally, in agreement with other studies, decreasing N-S angle and increasing glenosphere size increased abduction ROM, as a result of moving the cup articular surface further from the glenosphere center of rotation. Furthermore, lateral positioning of the glenosphere increased abduction ROM, and as a result diminished the effectiveness of increased diameter due to the elimination of scapular structure directly medial to the glenospheres inferior edge. Although this would aid in the prevention of cup damage due to scapular impingement, this also came at a cost of increased joint load, which may also have negative consequences on articular wear and long term clinical performance.

These findings are of importance to both future RSA implant design, as well as the laboratory testing of these devices. The current data shows that for varying N-S angles and cup depths, different loading protocols are not required. And although increasing glenosphere diameter significantly increased joint load, this difference was small.

2.6   References

Berhouet, J., Garaud, P., & Favard, L. (2014). Evaluation of the role of glenosphere design and humeral component retroversion in avoiding scapular notching during reverse shoulder arthroplasty. Journal of Shoulder and Elbow Surgery, 23(2), 151–158. http://doi.org/10.1016/j.jse.2013.05.009

Castagna, A., Delcogliano, M., de Caro, F., Ziveri, G., Borroni, M., Gumina, S., … De Biase, C. F. (2013). Conversion of shoulder arthroplasty to reverse implants: clinical and radiological results using a modular system. International Orthopaedics, 37(7), 1297–1305. http://doi.org/10.1007/s00264-013-1907-4

Chou, J., Malak, S. F., Anderson, I. A., Astley, T., & Poon, P. C. (2009). Biomechanical evaluation of different designs of glenospheres in the SMR reverse total shoulder prosthesis: range of motion and risk of scapular notching. Journal of Shoulder and Elbow Surgery, 18(3), 354–359. http://doi.org/10.1016/j.jse.2009.01.015

Clouthier, A.L., Hetzler, M.A., Fedorak, G.F., Bryant, J.T., Deluzio, K.J., Bicknell, R.T. (2013) Factors affecting the stability of reverse shoulder arthroplasty: a biomechanical study. Journal of Shoulder and Elbow Surgery, 22, 439-444. http://dx.doi.org/10.1016/j.jse.2012.05.032

De Wilde, L. F., Poncet, D., Middernacht, B., & Ekelund, A. (2010). Prosthetic overhang is the most effective way to prevent scapular conflict in a reverse total shoulder prosthesis. Acta Orthopaedica, 81(6), 719–726. http://doi.org/10.3109/17453674.2010.538354

Drake, G. N., OConnor, D., Edwards, T. B., O'Connor, D. P., & Edwards, T. B. (2010). Indications for Reverse Total Shoulder Arthroplasty in Rotator Cuff Disease. Clinical Orthopaedics and Related Research, 468(6), 1526–1533. http://doi.org/10.1007/s11999-009-1188-9

Ek, E. T., Neukom, L., Catanzaro, S., & Gerber, C. (2013). Reverse total shoulder arthroplasty for massive irreparable rotator cuff tears in patients younger than 65 years old: results after five to fifteen years. Journal of Shoulder and Elbow Surgery, 22(9), 1199–1208. http://doi.org/10.1016/j.jse.2012.11.016

Escamilla, R. F., Yamashiro, K., Paulos, L., & Andrews, J. R. (2009). Shoulder muscle activity and function in common shoulder rehabilitation exercises. Sports Medicine (Auckland, N.Z.), 39(8), 663–685. http://doi.org/10.2165/00007256-200939080-00004

Flury, M. P., Frey, P., Goldhahn, J., Schwyzer, H. K., & Simmen, B. R. (2011). Reverse shoulder arthroplasty as a salvage procedure for failed conventional shoulder replacement due to cuff failure--midterm results. International Orthopaedics, 35(1), 53–60. http://doi.org/10.1007/s00264-010-0990-z

Giles, J. W., Ferreira, L. M., Athwal, G. S., & Johnson, J. A. (2013). Validation of a Novel In-Vitro Simulator for Real-Time Control of Active Shoulder Movements in Various Planes of Motion (Vol. Volume 1B:, p. pp. V01BT31A001). http://doi.org/doi:10.1115/SBC2013-14067

Gutiérrez, S., Comiskey, C. a, Luo, Z.-P., Pupello, D. R., Frankle, M.A. (2008). Range of impingement-free abduction and adduction deficit after reverse shoulder arthroplasty. Hierarchy of surgical and implant-design-related factors. The Journal of Bone and Joint Surgery. American Volume, 90(12), 2606–2615. http://doi.org/10.2106/JBJS.H.00012

Gutiérrez, S., Keller, T. S., Levy, J. C., Lee III, W., Luo, Z.-P. (2008). Hierarchy of stability factors in reverse shoulder arthroplasty. Clinical Orthopaedics and Related Research, 466(3), 670–676. http://doi.org/10.1007/s11999-007-0096-0

Gutiérrez, S., Levy, J. C., Frankle, M. a., Cuff, D., Keller, T. S., Pupello, D. R., … Lee, W. E. (2008). Evaluation of abduction range of motion and avoidance of inferior scapular impingement in a reverse shoulder model. Journal of Shoulder and Elbow Surgery, 17(4), 608. http://dx.doi.org/10.1016/j.jse.2007.11.010

Gutiérrez, S., Luo, Z.-P. P., Levy, J., Frankle, M.A. (2009). Arc of motion and socket depth in reverse shoulder implants. Clinical Biomechanics, 24(6), 473–479. http://doi.org/10.1016/j.clinbiomech.2009.02.008

Leung, B., Horodyski, M., Struk, A. M., & Wright, T. W. (2012). Functional outcome of hemiarthroplasty compared with reverse total shoulder arthroplasty in the treatment of rotator cuff tear arthropathy. Journal of Shoulder and Elbow Surgery, 21(3), 319. http://dx.doi.org/10.1016/j.jse.2011.05.023

Nolan, B. M., Ankerson, E., & Wiater, J. M. (2011). Reverse total shoulder arthroplasty improves function in cuff tear arthropathy. Clinical Orthopaedics and Related Research, 469(9), 2476–2482. http://doi.org/10.1007/s11999-010-1683-z

Ortmaier, R., Resch, H., Matis, N., Blocher, M., Auffarth, A., Mayer, M., … Tauber, M. (2013). Reverse shoulder arthroplasty in revision of failed shoulder arthroplasty-outcome and follow-up. International Orthopaedics, 37(1), 67–75. http://doi.org/10.1007/s00264-012-1742-z

Roche, C., Flurin, P.-H., Wright, T., Crosby, L. A., Mauldin, M., & Zuckerman, J. D. (2009). An evaluation of the relationships between reverse shoulder design parameters and range of motion, impingement, and stability. Journal of Shoulder and Elbow Surgery, 18(5), 734. http://dx.doi.org/10.1016/j.jse.2008.12.008

Schwartz, D. G., Cottrell, B. J., Teusink, M. J., Clark, R. E., Downes, K. L., Tannenbaum, R. S., & Frankle, M. A. (2014). Factors that predict postoperative motion in patients treated with reverse shoulder arthroplasty. Journal of Shoulder and Elbow Surgery, 23(9):1289-95. http://dx.doi.org/10.1016/j.jse.2013.12.032

Virani, N. A., Cabezas, A., Gutiérrez, S., Santoni, B. G., Otto, R., & Frankle, M. (2013). Reverse shoulder arthroplasty components and surgical techniques that restore glenohumeral motion. Journal of Shoulder and Elbow Surgery, 22(2), 179–187. http://doi.org/10.1016/j.jse.2012.02.004

Werner, B. S., Boehm, D., & Gohlke, F. (2013). Revision to reverse shoulder arthroplasty with retention of the humeral component. Acta Orthopaedica, 84(5), 473–478. http://doi.org/10.3109/17453674.2013.842433

Chapter 3

3 The Effect of Neck-Shaft Angle, Humeral Cup Depth, and Glenosphere Diameter on the Contact Mechanics of Reverse Total Shoulder Arthroplasty

OVERVIEW

Implant design parameters can be changed during reverse shoulder arthroplasty (RSA) to improve range-of-motion and stability, however, little is known regarding their impact on articular contact mechanics. The purpose of this finite element study was to investigate RSA contact mechanics during abduction for different neck-shaft angles, glenosphere sizes, and polyethylene cup depths. [2]

3.1 Introduction

Reverse shoulder arthroplasty (RSA) is an accepted treatment for end-stage rotator cuff tear arthropathy, as well as for fracture and failed shoulder arthroplasty (Castagna et al., 2013; Drake, OConnor, Edwards, O'Connor, & Edwards, 2010; Ek, Neukom, Catanzaro, & Gerber, 2013; Flury, Frey, Goldhahn, Schwyzer, & Simmen, 2011; Leung, Horodyski, Struk, & Wright, 2012; Nolan, Ankerson, & Wiater, 2011; Ortmaier et al., 2013; Werner, Boehm, & Gohlke, 2013). RSA implants typically incorporate a low-coverage ball-in-socket articulation which, during shoulder motion, is regularly subjected to shear loading (Ackland, Roshan-Zamir, Richardson, & Pandy, 2011; Kwon, Forman, Walker, & Zuckerman, 2010). Increased shear loading has been shown in total hip arthroplasty to result in migration of the articular contact patch towards the rim of the cup with associated increases in articular contact stress (Hua et al., 2014). This effect would be exacerbated in RSA due the comparatively lower cup depth which reduces the distance between the contact patch and the rim.

In certain instances, the inferior edge of the polyethylene cup may come into contact with the scapula resulting in scapular impingement, which causes damage and excessive wear to the inferomedial rim of the cup (Day et al., 2012; Nam et al., 2010). To avoid impingement, yet still maintain a good range of motion, surgical techniques and RSA implant design parameters can be modified (Roche et al., 2009). Inferior placement of the glenosphere and increasing glenosphere diameter helps mitigate the risk of scapular impingment by offsetting the articular surface inferiorly and increasing the distance between the scapula and the inferomedial edge of the polyethylene cup (Langohr, Giles, Athwal, & Johnson, 2015; Nicholson, Strauss, & Sherman, 2011; Roche et al., 2009). Reducing RSA neck-shaft angle and decreasing cup depth also reduces the chance of scapular impingment by decreasing the inferior overlap of the polyethylene cup under the glenosphere, thereby reducing the potential for contact with the scapula (Gutiérrez et al., 2009; Nicholson et al., 2011; Oh et al., 2014). However, while such alterations to RSA implant parameters reduce the risk of scapular impingement, they can also increase articular shear loading. This may result in the generation of high contact stresses that

promote excessive wear, and potentially contribute to scapular notching via wear particle induced osteolysis (Terrier, Merlini, Pioletti, & Farron, 2009). There has been some recent interest shown in the wear testing of RSA implants (Haider, Sperling, & Throckmorton, 2013; Peers et al., 2015; Vaupel, Baker, Kurdziel, & Wiater, 2012), although the effects of changing RSA implant parameters on wear has not been fully investigated.

In RSA the location of the contact patch on the polyethylene cup is mainly a product of i) joint load angle, which is prescribed by a variety of factors including but not limited to arm position, muscle activity, and inertial effects, ii) implant neck-shaft (N-S) angle, iii) glenosphere diameter, and iv) cup constraint, the latter three of which are controlled by implant design geometry. Neck-shaft angles vary between current RSA implant systems, most commonly ranging between 135° to 155°. Lower angles provide greater adduction range of motion by rotating the humeral cup in the direction of abduction relative to the humeral shaft, reducing the angle at which scapular impingement can occur (de Wilde, Poncet, Middernacht, & Ekelund, 2010; Gutiérrez et al., 2008; Gutiérrez, Levy, et al., 2008; Virani et al., 2013). In terms of glenosphere diameter, typically a smaller 36 or 38 mm and a larger 40 or 42 mm are offered, with larger sizes used for patients with larger bone geometries (Berhouet, Garaud, & Favard, 2014; Chou, Malak, Anderson, Astley, & Poon, 2009; de Wilde et al., 2010; Gutiérrez et al., 2008; Gutiérrez, Levy, et al., 2008; Roche et al., 2009; Virani et al., 2013). Cup depth can also vary from a standard to either a deeper more constrained, or a shallower less constrained polyethylene insert; the former attempts to improve stability by increasing the force required to dislocate the joint, and the latter purports to increase mobility by reducing impingement (Gutiérrez et al., 2009).

While the effects of changing neck-shaft angle, glenosphere diameter, and polyethylene cup depth have been investigated for shoulder range of motion, the influence of changing these implant design characteristics on contact mechanics, and thus potentially the long-term performance of RSA, have yet to be investigated. Therefore, the objective of the present study was to use finite element analysis (FEA) to evaluate the effect of RSA neck-shaft angle, glenosphere diameter, and polyethylene cup depth on RSA contact

mechanics over the range of joint load angles that are to be expected during abduction and in the absence of scapular impingement. This will provide further insight into the effects of changing these parameters, and may show that improving implant range of motion (ROM) may come at the cost of less favorable contact mechanics, and thus the long-term performance of RSA. Our hypothesis was that higher neck-shaft angles, larger glenosphere diameters, and increased cup constraint would provide improved RSA contact mechanics because of the resulting reduced cup shear loading and increased cup depth.

3.2   Materials & Methods

In order to investigate the contact mechanics of RSA implants having varying design parameters the resultant joint load angles with respect to both the glenosphere and humeral cup (Figure 3-1) during the abduction of cadaveric RSA reconstructed shoulders were determined. This calculation was done by using the joint compression and shear data reported by Ackland et al (Ackland et al., 2011) and Kwon et al (Kwon et al., 2010) during the abduction of unloaded arms. The angle of abduction was converted to humeroscapular angle using the 2:1 ratio between humeral and scapular rotation employed by both studies. This provided specific resultant joint load angles for each of the fourteen abduction angles (Ackland et al., 2011; Kwon et al., 2010) that were required to satisfy static equilibrium for each respective humeroscapular rotation. The resultant joint load angles could then be applied to prostheses having varying glenosphere diameters, neck-shaft angles, and polyethylene cup depths, since the centre of rotation does not change with an RSA implant, and as a result the load angle to satisfy static equilibrium is also unchanged.

3.2.1   Finite Element Modeling

Finite element RSA prosthesis models were developed in Abaqus v6.12-2 (Simulia Corp, Providence, RI, USA) having varying neck-shaft angles (155º, 145º, 135º), glenosphere diameters (38 mm, 42 mm), and humeral polyethylene cup depths of shallow (S), normal (N), deep (D) as shown in Figure 3-1. The "normal" cups were assigned depths which

represented current clinically available prostheses (8.75 mm for the 38 mm and 9.25 mm for the 42 mm diameters [Delta Extend, Depuy, Warsaw, IN]), the depth of the "shallow" cups was reduced by 2 mm, and the depth of the "deep" cups was increased by 2 mm, representative of clinically available Depuy prostheses.

The hemispherical glenosphere was assigned CoCr material properties (E=210 GPa, v=0.3). The humeral cup was given the same spherical contact radius as the glenosphere, a cup depth corresponding to the desired level of cup constraint, and assigned linear elastic UHMWPE material properties (E=650 MPa, v=0.44) (Pruitt, 2005). Both the glenosphere and humeral cup were meshed using linear hexahedral elements (C3D8R) having an average side length of approximately 0.3 mm, deemed suitable by a mesh convergence study. Penalty-based contact was defined between the glenosphere and the humeral cup articulations using surface-to-surface discretization, and the coefficient of friction was specified as 0.04 (Willing & Kim, 2009).

The humeral components were articulated against the glenosphere, which was fixed in position, by applying a constant load of 400 N at the joint load angle obtained from the discretization of data reported by in vitro testing (Ackland et al., 2011; Kwon et al., 2010), as previously described, that corresponded to physiological abduction angles (15º-120º). A constant applied load was selected to allow direct comparison between implant parameters at all abduction angles. The 400 N load corresponded to the largest load observed during abduction as reported by Kwon et al (Kwon et al., 2010).
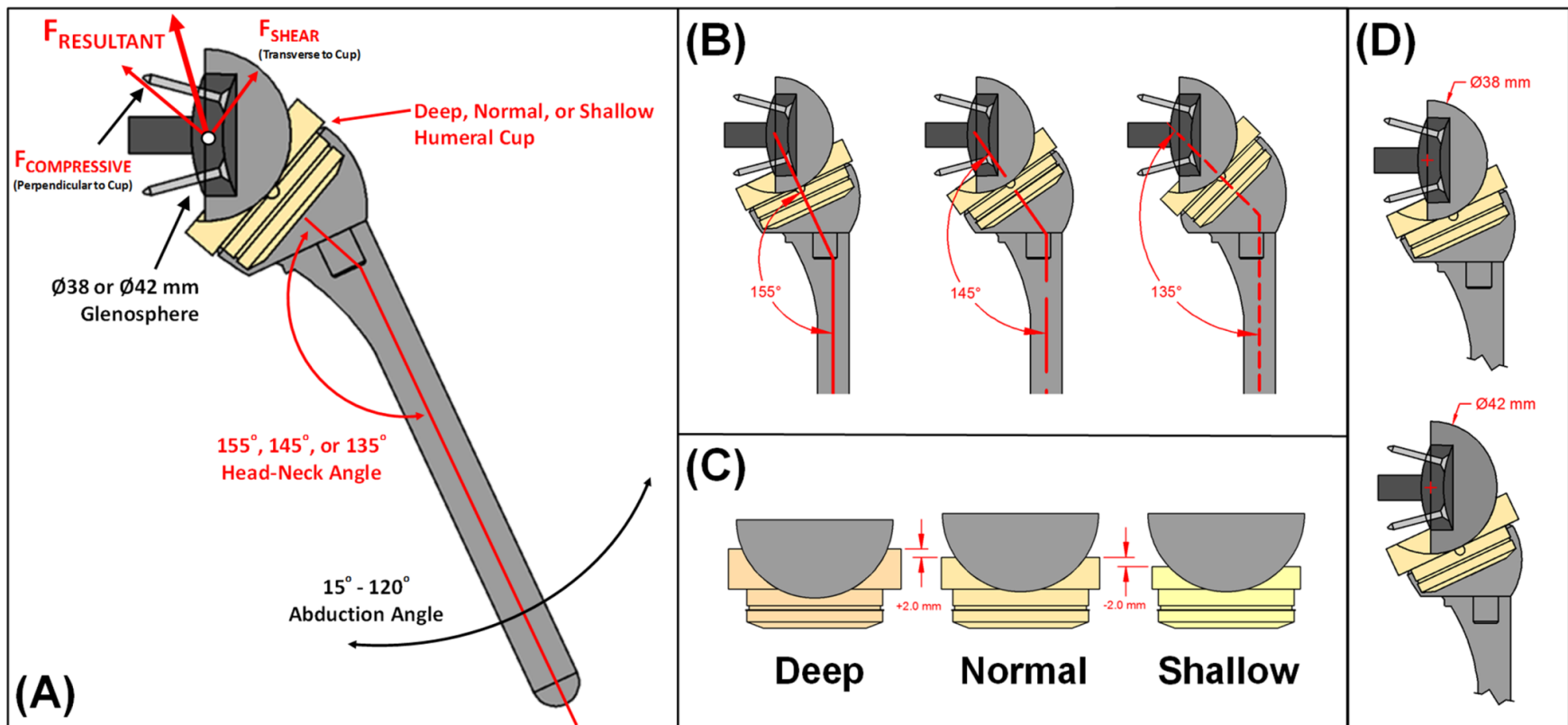
Figure 3-1: Finite element model developed (A) showing boundary and loading conditions for RSA prostheses having varying glenosphere diameters, (B) neck-shaft angles, (C) humeral cup depths, and (D) glenosphere diameters.

3.2.2   Experimental Testing Protocol & Outcome Variables

For each of the eighteen RSA implant configurations, finite element analyses (FEA) were performed without modelling any scapular impingement so as to allow for the investigation of the effects of changes in these configurations on contact mechanics only. The effects of all RSA implant parameters investigated were assessed using joint contact area and maximum contact stress. All outcome variables were assessed from either 20° to 120° at 20° increments or 15° to 120° at 15° increments of humeral-thoracic abduction, which were the ranges and intervals reported by Ackland et al and Kwon et al (Ackland et al., 2011; Kwon et al., 2010). The average of both the contact area and maximum contact stress for each independent RSA configuration were then calculated using all abduction angles investigated to allow for comparison of the effects of changes in RSA implant parameters.

3.3   Results

3.3.1   Finite Element Model to Hertzian Contact Theory Comparison

To provide insight into the accuracy of the results from our FEA modeling, a second FEA was performed for a cobalt alloy sphere (38 mm diameter) and load of 400 N in contact with a flat polyethylene geometry. This geometry, while not conforming as in the RSA configuration, allowed for the computational contact area and stress results to be compared to the contact area and stress determined mathematically using Hertzian contact theory (Johnson, 1985). Material properties, mesh spacing and friction coefficient were kept the same. While the contact morphology of this articulation is different from that of the RSA articulation of the primary model, the contact areas and maximum contact stresses were similar to some of the levels obtained with the 135° N-S angle at higher abduction levels. When the results of the second FEA were compared to Hertzian contact theory, the model was found to to exhibit acceptably low error; predicting contact area within 6.2% and maximum contact stress within 0.6% of the theoretical Hertzian values.

3.3.2   Articular Contact Area and Maximum Contact Stress

The humeral cup contact areas were inferomedially located, except for the 145° and 155° N-S implants at low abduction angles, which were more centrally located (Figure 3-2). As the abduction angle increased, and the N-S angle was reduced, the contact patch moved more inferomedially, most markedly for the 135° N-S implant.

Analysis of the polyethylene cup contact stress distribution showed that the location of the maximum contact stress was consistently found at the inferior-most point of joint contact, which except for the 145° and 155° N-S angles at low abduction, occurred at the inferomedial cup edge (Figure 3-3). For the cases where the maximum contact stress was not located on the inferiomedial cup edge, it occurred at the inferior-most edge of the contact patch, which was coincident with the inferiomedial edge of the glenosphere.

As the abduction angle of the RSA model was increased, joint contact area generally remained consistent, except for certain configurations using the deep cup, which increased slightly. Maximum contact stress exhibited similar, albeit inverse, trends to contact area as abduction angle increased; as abduction angle increased, maximum contact stress increased slightly, except again for certain configurations which incorporated the deep cup, some of which showed slight decreases in maximum contact stress (Table 3-1). Certain configurations were more sensitive to abduction angle, and generated lower contact areas and higher maximum contact stresses, particularly for the 135° N-S angle with the shallow and normal cup depths, and the 145° N-S angle with the shallow cup at high abduction angles.
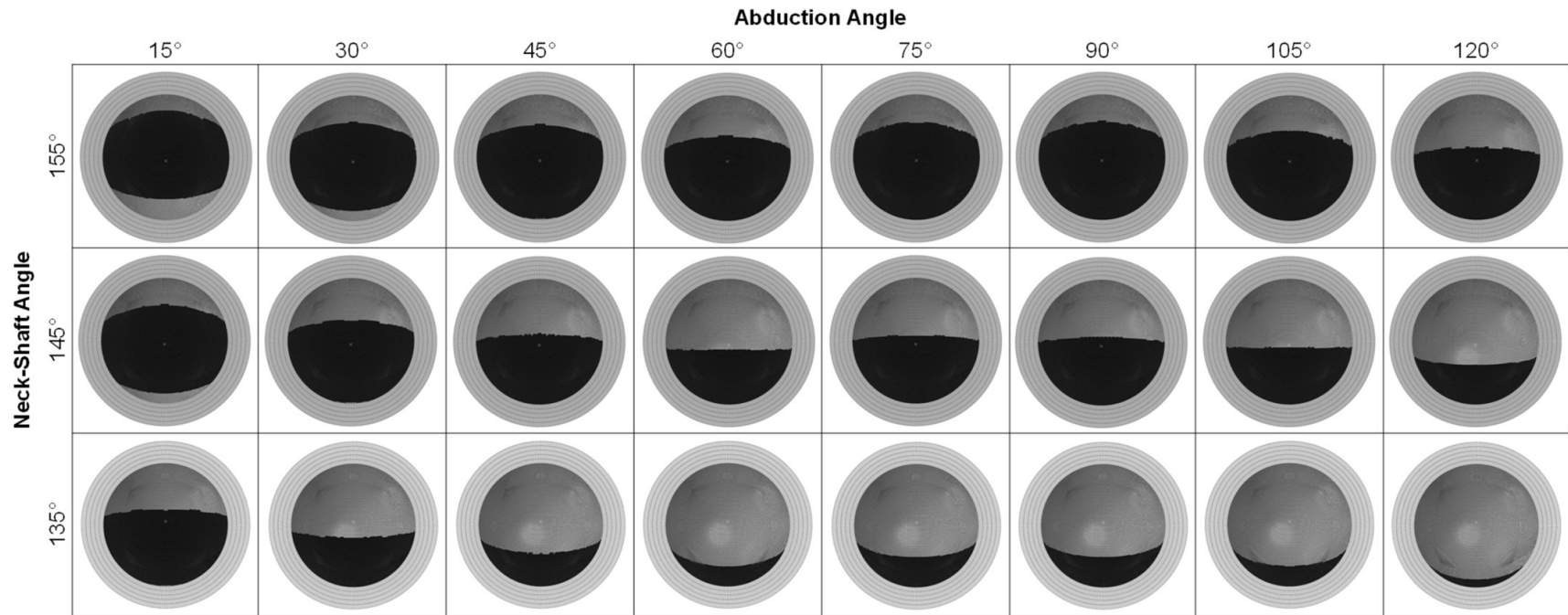
Figure 3-2: Humeral cup contact area maps for humeral N-S angles throughout all abduction angles for the normal cup depth (Black region denotes contact).
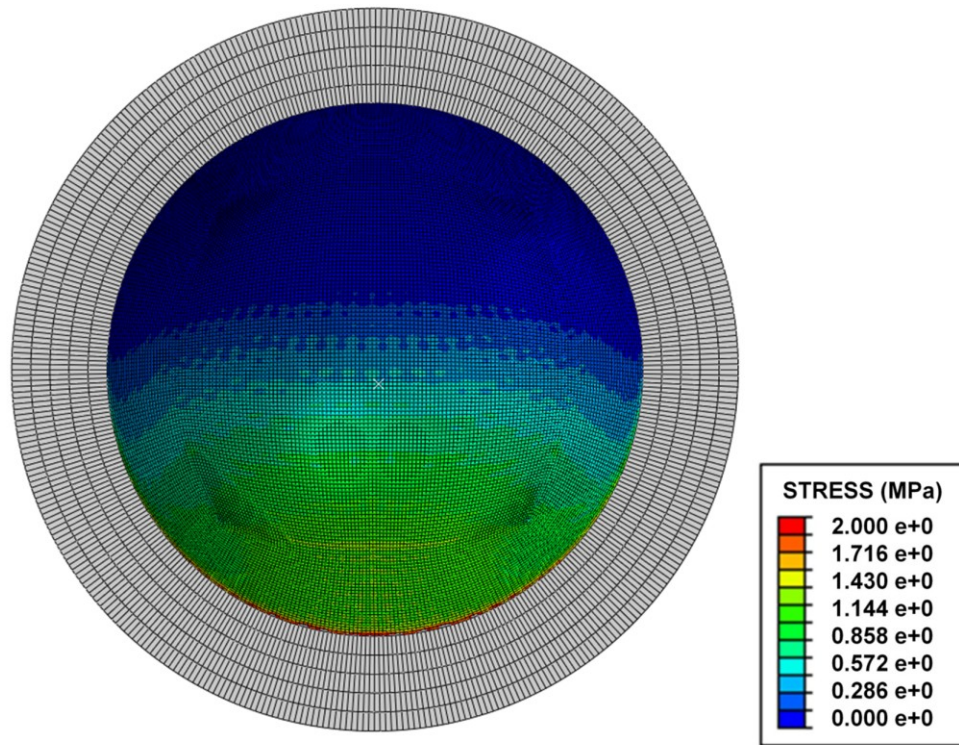
Figure 3-3: Typical humeral cup contact stress distribution showing the location of maximum contact stress at the inferiomedial edge of the cup.

Contact Area (mm²) — left | **Maximum Contact Stress (Mpa)** — right

38 mm Diameter

Study	Abd	CA 155° S	155° N	155° D	145° S	145° N	145° D	135° S	135° N	135° D	Abd	Str 155° S	155° N	155° D	145° S	145° N	145° D	135° S	135° N	135° D
Kwon et al	20°	619	706	768	559	676	752	355	574	712	20°	2.5	2.3	2.3	2.9	2.5	2.3	6	3.3	2.4
Kwon et al	40°	613	777	874	395	622	813	173	371	594	40°	3.1	1.9	1.9	6.8	2.8	1.9	16.2	5.4	3
Kwon et al	60°	521	757	974	289	514	739	116	258	472	60°	3.4	2.4	1.2	7.7	3.7	2.1	19.1	9.4	4.2
Kwon et al	80°	542	781	1011	306	538	766	96	274	498	80°	3.9	2.6	1.5	6.8	4.4	2.5	24.8	9.6	4.4
Kwon et al	100°	631	874	1106	396	637	873	153	371	604	100°	3.6	2	1.3	6.8	2.9	1.8	17.8	5.4	3
Kwon et al	120°	576	818	1038	333	573	812	93	302	531	120°	3.2	2.5	1.4	6.1	3.4	2.2	20.7	6.3	3.5
Ackland et al	15°	642	725	788	604	707	777	446	646	749	15°	2.3	2.3	2.3	2.5	2.4	2.4	4.2	2.6	2.4
Ackland et al	30°	603	706	776	444	643	749	222	427	646	30°	2.3	2.1	2.3	3.9	2.3	2.3	9.3	4.6	2.3
Ackland et al	45°	541	744	859	315	537	757	135	285	502	45°	2.9	1.9	1.8	6.2	3.6	1.8	14.3	7.7	3.8
Ackland et al	60°	431	660	881	203	411	639	106	170	366	60°	4.2	2.7	1.4	9.2	4.3	2.8	19.2	12.3	5.6
Ackland et al	75°	532	768	998	294	523	754	99	259	484	75°	3.3	2.1	1.3	7	3.8	2	20.9	7.7	4.3
Ackland et al	90°	534	744	1004	293	525	762	83	260	487	90°	3.2	2.3	1.4	6.4	3.3	2.4	21.9	8.6	4.2
Ackland et al	105°	454	694	928	209	433	671	49	169	385	105°	4.2	2.4	1.8	9.2	5	2.9	34.3	12.9	5.5
Ackland et al	120°	325	558	799	90	291	523	25	54	235	120°	6.1	3.8	2.3	19.7	7.5	4	44.4	28.6	8.9

42 mm Diameter

Study	Abd	CA 155° S	155° N	155° D	145° S	145° N	145° D	135° S	135° N	135° D	Abd	Str 155° S	155° N	155° D	145° S	145° N	145° D	135° S	135° N	135° D
Kwon et al	20°	741	842	916	661	804	894	405	650	834	20°	2.1	1.9	2	2.4	2.1	1.9	5.5	2.8	2.1
Kwon et al	40°	719	919	1035	454	705	941	190	402	645	40°	2.9	1.7	1.6	6	2.5	1.4	15.1	5	2.8
Kwon et al	60°	607	866	1116	326	571	825	128	267	498	60°	3.7	2.3	1.2	6.6	4.2	2.4	18.4	9.8	4.5
Kwon et al	80°	633	896	1152	347	599	857	104	286	526	80°	2.9	2.1	1.3	5.9	3.7	2	18.6	8.1	4
Kwon et al	100°	739	1009	1274	453	720	983	165	399	652	100°	2.8	2.3	1	5.9	2.6	1.6	16.5	5.1	2.8
Kwon et al	120°	672	942	1191	380	642	907	95	318	567	120°	3.1	2.3	1.4	5.6	3.8	2.3	24.4	8.3	4
Ackland et al	15°	770	867	941	720	840	927	517	753	885	15°	1.9	1.8	1.9	2.3	2	1.8	4	2.1	2
Ackland et al	30°	719	838	926	514	752	885	244	472	715	30°	2	1.8	1.8	3.6	2.1	2	8.6	5.4	2.7
Ackland et al	45°	632	871	1013	356	606	852	148	300	535	45°	2.8	1.7	1.6	5.8	3.7	2.1	15.3	8.5	4.2
Ackland et al	60°	496	751	1003	223	453	698	114	168	373	60°	4.2	2.7	1.6	10.7	5.6	3	22.8	14.9	6.4
Ackland et al	75°	617	879	1133	331	587	842	110	271	509	75°	3.4	2.3	1.3	6	4.3	2.4	20.8	9.4	4.4
Ackland et al	90°	621	886	1141	330	591	847	92	265	511	90°	3	2.3	1.5	6.7	4.2	2.4	17.6	9.4	4.5
Ackland et al	105°	523	787	1050	230	481	736	51	165	391	105°	3.7	2.7	1.7	10	5.5	3	24.2	15	5.9
Ackland et al	120°	365	625	893	91	309	555	29	53	215	120°	5.4	3.8	2.3	25.2	8.4	4.2	28	18.4	11

Table 3-1: Contact Area (left) and Maximum Contact Stress (right) for 38 mm (top) and 42 mm (bottom) Glenosphere Diameters with various Neck-Shaft (N-S) Angles and polyethylene cup depths of Shallow (S), Normal (N), and Deep (D).
Note that the cell gradient was determined by assigning red to the worst (lowest contact area or the highest maximum contact stress), green to the best (highest contact area or lowest contact stress), and interpolating all remaining cells between those values for each outcome.

3.3.3   Humeral Component Neck-Shaft Angle

As implant neck-shaft angle decreased, the mean contact area decreased and the maximum contact stress increased (Figure 3-4). On average for all implant variants investigated, reducing the humeral neck-shaft angle from 155° to 145° decreased joint contact area by 29% (210.9 ± 96.5 mm^2) and increased maximum contact stress by 71% (2.1 ± 2.7 MPa, Figure 3-7). Decreasing the neck-shaft angle from 155° to 135° had an even greater effect; decreasing the average joint contact area by 59% (445.7 ± 161.7 mm^2), and increasing the average maximum contact stress by 286% (8.0 ± 7.6 MPa). Neck-shaft angle also interacted with cup depth for maximum contact stress, where the effect of reducing neck-shaft angle was increased with reduced cup depth (Table 1).

3.3.4   Glenosphere Diameter

As glenosphere diameter increased, the contact area of all implant configurations increased, however maximum contact stress was not as affected (Figure 3-5). Increasing glenosphere diameter from 38 to 42 mm increased the mean contact area by 12% (73.0 ± 49.5 mm^2), while the mean maximum contact stress decreased only by 2% (0.28 ± 2.3 MPa, Figure 3-7) . Also, the positive effect of increasing glenosphere diameter on joint contact area was reduced as both humeral N-S angle was reduced, and as cup depth was increased.

3.3.5   Polyethylene Cup Depth

As cup depth was increased, contact area increased and maximum contact stress decreased for all implant configurations (Figure 3-6). On average, decreasing cup constraint from normal to shallow reduced contact area by 40% (198.3 ± 61.6 mm^2) and increased maximum contact stress by 81% (4.6 ± 4.9 MPa); and increasing constraint from normal to deep increased contact area by 52% (203.3 ± 62.1 mm^2,) and decreased maximum contact stress by 36% (2.2 ± 2.8 MPa, Figure 3-7). The negative effects of reducing cup constraint on contact area and maximum contact stress was increased as humeral neck-shaft angle was reduced (Table 1).
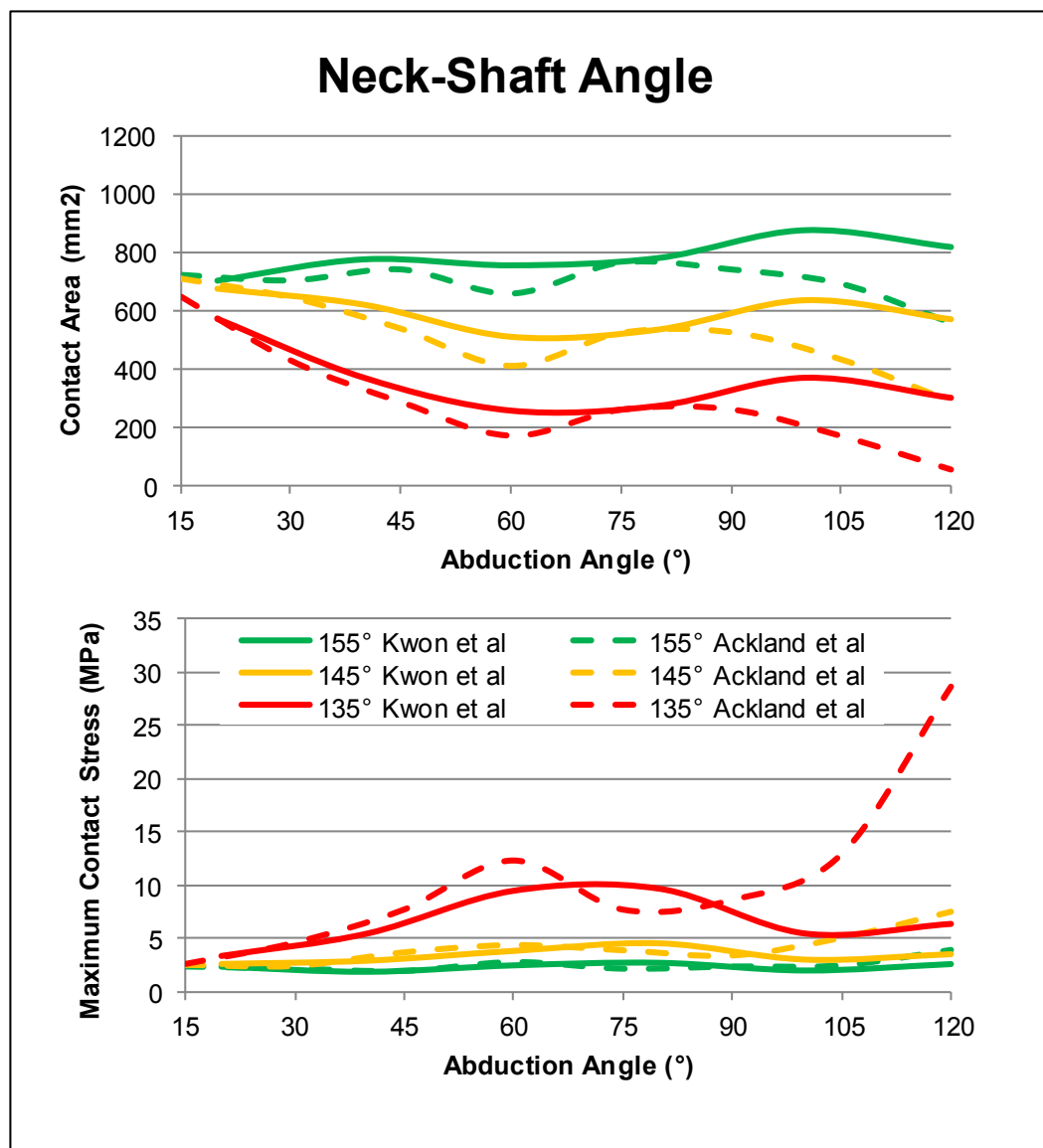
Figure 3-4: Contact area (top) and maximum contact stress (bottom) for varying implant neck-shaft angles (155°, 145°, and 135°) vs. abduction angle for implants having a 38 mm diameter and a normal cup depth.
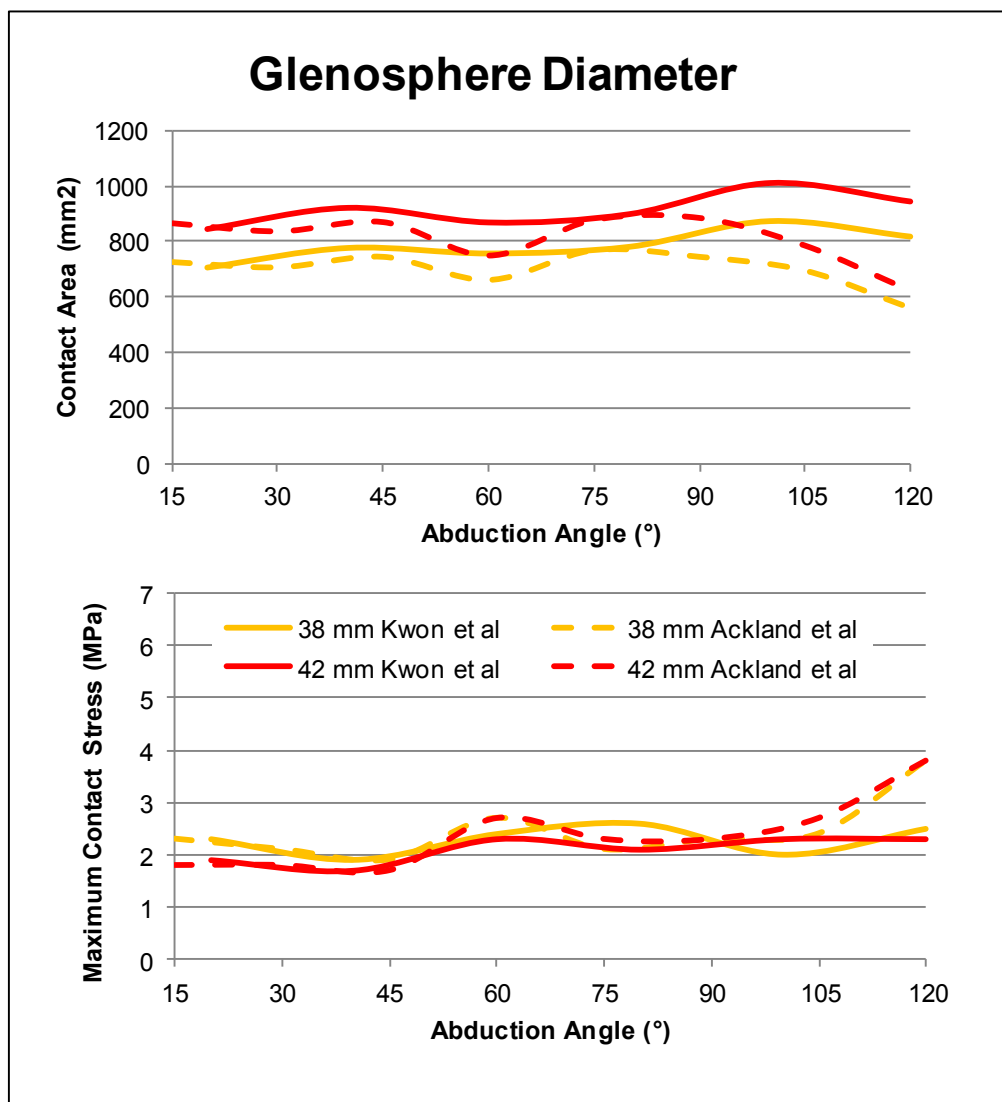
Figure 3-5: Contact area (top) and maximum contact stress (bottom) for varying glenosphere diameters (38 mm, 42 mm) vs. abduction angle for implants having a 155° neck-shaft angle and a normal cup depth.
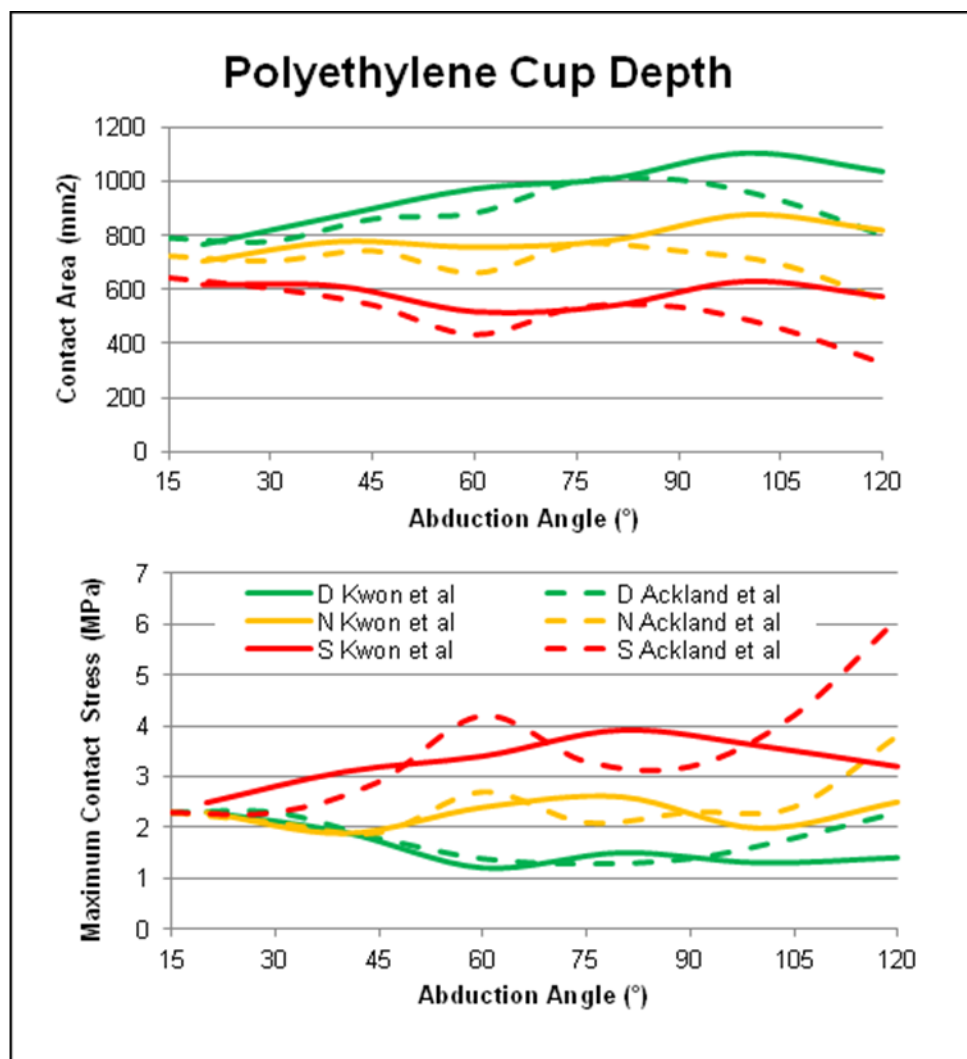
Figure 3-6: Contact area (top) and maximum contact stress (bottom) for varying cup depths (deep (D), normal (N), and shallow (S)) vs. abduction angle for implants having a 155° neck-shaft angle and a 38 mm diameter.
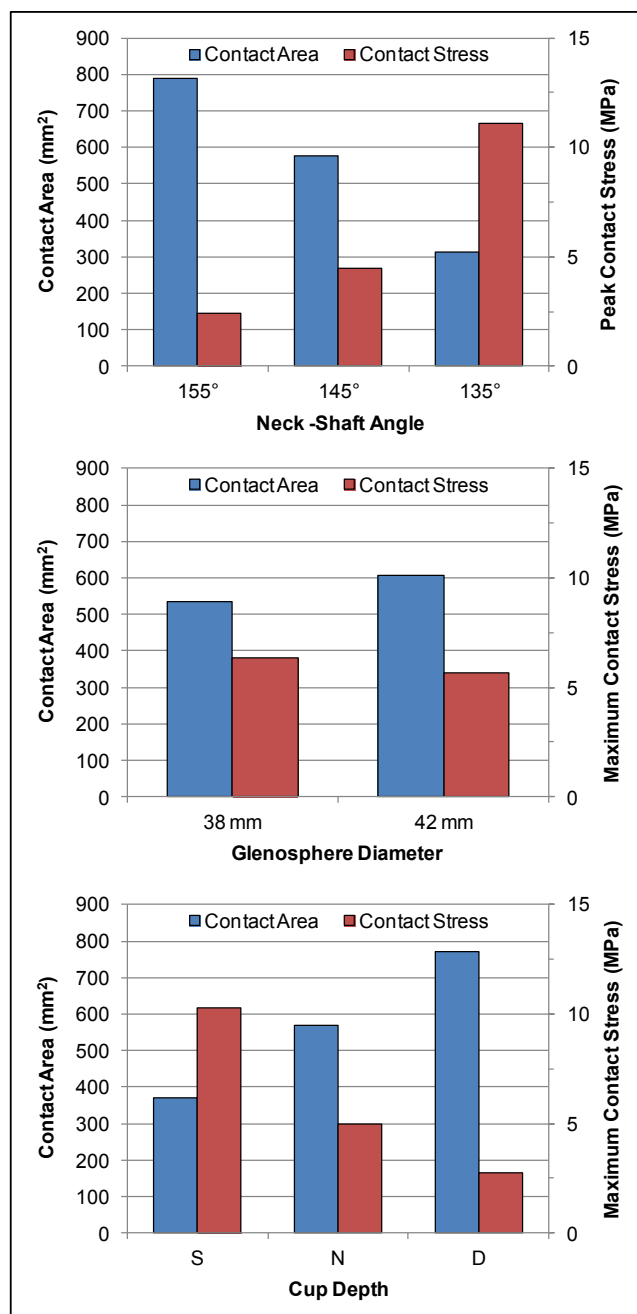
Figure 3-7: Mean contact area (blue) and maximum contact stress (red) for all implants investigated having varying neck shaft angles (155°, 145, 135°, top), glenosphere diameters (38, 42 mm, middle), and cup depths (shallow (S), normal (N) and deep (D), bottom).

3.4   Discussion

Reducing RSA humeral component neck-shaft angle, decreasing cup depth, and increasing glenosphere diameter are relatively well-known techniques used to reduce the probability of scapular impingement and improve RSA range of motion (Berhouet et al., 2014; Chou et al., 2009; de Wilde et al., 2010; Gutiérrez et al., 2009; Gutiérrez et al., 2008; Roche et al., 2009; Virani et al., 2013). However, the present study is, to the authors' best knowledge, the first to investigate the effects of these implant design parameters on RSA articular contact mechanics.

Examination of the humeral cup contact patches showed that contact moved inferiorly as the humeral component neck-shaft angle was decreased (155°→145°→135°). This was a direct result of the humeral cup being rotated in the direction of abduction relative to the humeral shaft as the neck-shaft angle was reduced (Figure 2), which also effectively increased the humeral cup shear load due to the larger angle between the joint load and the central axis of the cup. Reducing neck-shaft angle reduced contact area and increased maximum contact stress for all implant configurations investigated, and had greater effects on joint contact area and maximum contact stress as cup constraint decreased, likely due to the interaction between the resulting increased shear loading and the reduced cup depth.

It is important to note that in the present study, changes in neck-shaft angle were implemented without changing other RSA design parameters such as humeral offset and/or humeral neck length. Some clinical implants which use lower neck-shaft angles also incorporate larger humeral offsets, which attempt to increase joint compressive loading by resulting in a more horizontal deltoid line of action in an effort to reduce edge loading of the humeral cup. While the present study does not implicitly incorporate these nuances of RSA designs in order to isolate the effects of changes in this parameter, it does aid in the illustration of the need for such accommodations in RSA implant design.

Increasing glenosphere diameter increased joint contact area, likely as a result of the larger contact surface available for articulation. As neck-shaft angle was reduced,

increasing glenosphere diameter had less of an effect on contact area, which is thought to be due to the increased shear at lower neck-shaft angles and the resulting edge-centric contact patches, which were similar in size and morphology even for the larger diameter articulations. Glenosphere diameter seemed to not have a significant effect on maximum contact stress during abduction. This was unanticipated, as it was postulated that the larger glenosphere and deeper mating humeral cup would be able to resist shear loading more effectively. It is thought that since the maximum contact stress was typically located at the inferior edge of the cup, simply scaling the geometry of the cup, rather than actually increasing cup coverage, did not affect the load transfer at the periphery of the cup required to resist the applied shear force. This result also agreed with Gutiérrez et al. (Gutiérrez, Keller, et al., 2008) who found similar changes in glenosphere diameter had little effect on RSA dislocation force.

Decreasing cup depth, and effectively cup constraint, can increase RSA range of motion (Gutiérrez et al., 2009), however, the results of our study also show that this can also reduce joint contact area and increase maximum articular contact stress. Increasing cup depth has the ability to increase RSA stability and the force required to dislocate the joint (Gutiérrez, Keller, et al., 2008), and was shown to increase joint contact area and reduce maximum contact stress. Therefore, this suggests that increasing cup depth can improve RSA contact mechanics and reducing cup depth can negatively impact contact area and maximum contact stress. This is a similar trend as found by Gutiérrez et al. (Gutiérrez, Keller, et al., 2008) who reported that increased cup depths resulted in increased forces required for dislocation, likely due to the increased ability of the cup to resist shear, as seen in the present study by reduced maximum contact stresses. Moreover, it was found that decreasing humeral cup depth resulted in greater changes to maximum contact stress than increasing constraint, particularly at lower neck-shaft angles. This suggests caution when using lower depth cups in accompaniment with reduced neck-shaft angle implants.

It must also be noted that both the contact patch and the location of maximum contact stress on the humeral cup was typically located inferomedially, which agrees with the results of a finite element study performed by Terrier et al (Terrier et al., 2009). The

inferior cup quadrant has also been reported as the location where cup damage is most commonly visualized on RSA retrieval implants (Nam et al., 2010). This is of importance since inferior humeral cup damage is most often associated with damage due to scapular impingement, although this type of damage is sometimes found without the presence of scapular notching (Nam et al., 2010). Increased contact stress can increase polyethylene wear, and therefore the results of the present study may explain why inferior cup damage can occur independently of scapular impingement. Furthermore, the present study shows the importance of the inferior cup edge in preventing translation, and as such, damage to the inferior of the cup due to impingement may interact with the elevated contact stresses at this location as any removal of articular surface area would place a higher demand on the remaining material, which may further accelerate inferior cup wear, damage, and particle generation.

3.5   Conclusions

The current study yields new insight regarding the impact of changes in common RSA implant parameters on joint contact area and maximum contact stress, both of which may affect long term wear performance. Reducing neck-shaft angle reduced joint contact area by up to one-half and more than doubled maximum contact stress. Increasing glenosphere diameter was found to have a positive effect on joint contact area. Reducing cup constraint reduced contact area and increased maximum contact stress, particularly at lower neck-shaft angles, while increasing cup constraint improved joint contact area and reduced maximum contact stress. This implies that the use of low constraint cups should be limited to RSA prostheses with higher N-S angles, while high constraint cups can improve the contact mechanics of all RSA configurations. Finally, the similarities between the inferior location of the maximum contact stress of the polyethylene cup and the observation of wear in clinical retrievals yields insight into potential reasons why inferior cup damage is not always coincident with scapular notching. This may also help explain the progression of inferior cup damage due to scapular impingement, since damage to this section of the cup due to scapular contact may further facilitate high

contact stresses at the edge of the cup and accelerate the tribological wear processes of the articulation.

3.6 References

Ackland, D. C., Roshan-Zamir, S., Richardson, M., & Pandy, M. G. (2011). Muscle and joint-contact loading at the glenohumeral joint after reverse total shoulder arthroplasty. Journal of Orthopaedic Research, 29(12), 1850–1858. http://doi.org/10.1002/jor.21437

Berhouet, J., Garaud, P., & Favard, L. (2014). Evaluation of the role of glenosphere design and humeral component retroversion in avoiding scapular notching during reverse shoulder arthroplasty. Journal of Shoulder and Elbow Surgery, 23(2), 151–158. http://doi.org/10.1016/j.jse.2013.05.009

Castagna, A., Delcogliano, M., de Caro, F., Ziveri, G., Borroni, M., Gumina, S., … De Biase, C. F. (2013). Conversion of shoulder arthroplasty to reverse implants: clinical and radiological results using a modular system. International Orthopaedics, 37(7), 1297–1305. http://doi.org/10.1007/s00264-013-1907-4

Chou, J., Malak, S. F., Anderson, I. A., Astley, T., & Poon, P. C. (2009). Biomechanical evaluation of different designs of glenospheres in the SMR reverse total shoulder prosthesis: range of motion and risk of scapular notching. Journal of Shoulder and Elbow Surgery, 18(3), 354–359. http://doi.org/10.1016/j.jse.2009.01.015

Day, J. S., MacDonald, D. W., Olsen, M., Getz, C., Williams, G. R., & Kurtz, S. M. (2012). Polyethylene wear in retrieved reverse total shoulder components. Journal of Shoulder and Elbow Surgery, 21(5), 667–674. http://dx.doi.org/10.1016/j.jse.2011.03.012

De Wilde, L. F., Poncet, D., Middernacht, B., & Ekelund, A. (2010). Prosthetic overhang is the most effective way to prevent scapular conflict in a reverse total shoulder prosthesis. Acta Orthopaedica, 81(6), 719–726. http://doi.org/10.3109/17453674.2010.538354

Drake, G. N., OConnor, D., Edwards, T. B., O'Connor, D. P., & Edwards, T. B. (2010). Indications for Reverse Total Shoulder Arthroplasty in Rotator Cuff Disease. Clinical Orthopaedics and Related Research, 468(6), 1526–1533. http://doi.org/10.1007/s11999-009-1188-9

Ek, E. T., Neukom, L., Catanzaro, S., & Gerber, C. (2013). Reverse total shoulder arthroplasty for massive irreparable rotator cuff tears in patients younger than 65 years old: results after five to fifteen years. Journal of Shoulder and Elbow Surgery, 22(9), 1199–1208. http://doi.org/10.1016/j.jse.2012.11.016

Flury, M. P., Frey, P., Goldhahn, J., Schwyzer, H. K., & Simmen, B. R. (2011). Reverse shoulder arthroplasty as a salvage procedure for failed conventional shoulder replacement due to cuff failure--midterm results. International Orthopaedics, 35(1), 53–60. http://doi.org/10.1007/s00264-010-0990-z

Gutiérrez, S., Comiskey, C. a, Luo, Z.-P., Pupello, D. R., Frankle, M.A. (2008). Range of impingement-free abduction and adduction deficit after reverse shoulder arthroplasty. Hierarchy of surgical and implant-design-related factors. The Journal of Bone and Joint Surgery. American Volume, 90(12), 2606–2615. http://doi.org/10.2106/JBJS.H.00012

Gutiérrez, S., Keller, T. S., Levy, J. C., Lee III, W., Luo, Z.-P. P. (2008). Hierarchy of stability factors in reverse shoulder arthroplasty. Clinical Orthopaedics and Related Research, 466(3), 670–676. http://doi.org/10.1007/s11999-007-0096-0

Gutiérrez, S., Levy, J. C., Frankle, M. a., Cuff, D., Keller, T. S., Pupello, D. R., … Lee, W. E. (2008). Evaluation of abduction range of motion and avoidance of inferior scapular impingement in a reverse shoulder model. Journal of Shoulder and Elbow Surgery, 17(4), 608. http://dx.doi.org/10.1016/j.jse.2007.11.010

Gutiérrez, S., Luo, Z.-P. P., Levy, J., Frankle, M. A. (2009). Arc of motion and socket depth in reverse shoulder implants. Clinical Biomechanics, 24(6), 473–479. http://doi.org/10.1016/j.clinbiomech.2009.02.008

Haider, H., Sperling, J., & Throckmorton, T. (2013). A method for wear testing of reverse shoulder arthroplasty systems. Bone Joint J.

Hua, X., Li, J., Wang, L., Jin, Z., Wilcox, R., & Fisher, J. (2014). Contact mechanics of modular metal-on-polyethylene total hip replacement under adverse edge loading conditions. Journal of Biomechanics, 47(13), 3303–3309. http://dx.doi.org/10.1016/j.jbiomech.2014.08.015

Kwon, Y. W., Forman, R. E., Walker, P. S., & Zuckerman, J. D. (2010). Analysis of reverse total shoulder joint forces and glenoid fixation. Bulletin of the NYU Hospital for Joint Diseases, 68(4), 273–280.

Langohr, G. D. G., Giles, J. W., Athwal, G. S., & Johnson, J. A. (2015). The effect of glenosphere diameter in reverse shoulder arthroplasty on muscle force, joint load, and range of motion. Journal of Shoulder and Elbow Surgery, 24(6), 972–979. http://doi.org/10.1016/j.jse.2014.10.018

Leung, B., Horodyski, M., Struk, A. M., & Wright, T. W. (2012). Functional outcome of hemiarthroplasty compared with reverse total shoulder arthroplasty in the treatment of rotator cuff tear arthropathy. Journal of Shoulder and Elbow Surgery, 21(3), 319. http://dx.doi.org/10.1016/j.jse.2011.05.023

Nam, D., Kepler, C. K., Nho, S. J., Craig, E. V., Warren, R. F., & Wright, T. M. (2010). Observations on retrieved humeral polyethylene components from reverse total shoulder arthroplasty. Journal of Shoulder and Elbow Surgery, 19(7), 1003. http://dx.doi.org/10.1016/j.jse.2010.05.014"

Nicholson, G. P., Strauss, E. J., & Sherman, S. L. (2011). Scapular Notching: Recognition and Strategies to Minimize Clinical Impact. Clinical Orthopaedics and Related Research, 469(9), 2521–2530. http://doi.org/10.1007/s11999-010-1720-y

Nolan, B. M., Ankerson, E., & Wiater, J. M. (2011). Reverse total shoulder arthroplasty improves function in cuff tear arthropathy. Clinical Orthopaedics and Related Research, 469(9), 2476–2482. http://doi.org/10.1007/s11999-010-1683-z

Oh, J. H., Shin, S.-J. J., McGarry, M. H., Scott, J. H., Heckmann, N., & Lee, T. Q. (2014). Biomechanical effects of humeral neck-shaft angle and subscapularis integrity in reverse total shoulder arthroplasty. Journal of Shoulder and Elbow Surgery, 23(0), http://dx.doi.org/10.1016/j.jse.2013.11.003

Ortmaier, R., Resch, H., Matis, N., Blocher, M., Auffarth, A., Mayer, M., … Tauber, M. (2013). Reverse shoulder arthroplasty in revision of failed shoulder arthroplasty-outcome and follow-up. International Orthopaedics, 37(1), 67–75. http://doi.org/10.1007/s00264-012-1742-z

Peers, S., Moravek Jr., J. E., Budge, M. D., Newton, M. D., Kurdziel, M. D., Baker, K. C., … Wiater, J. M. (2015). Wear rates of highly cross-linked polyethylene humeral liners subjected to alternating cycles of glenohumeral flexion and abduction. Journal of Shoulder and Elbow Surgery, 24(1), 143–149. http://dx.doi.org/10.1016/j.jse.2014.05.001

Pruitt, L. A. (2005). Deformation, yielding, fracture and fatigue behavior of conventional and highly cross-linked ultra high molecular weight polyethylene. Biomaterials, 26(8), 905–915. http://dx.doi.org/10.1016/j.biomaterials.2004.03.022

Roche, C., Flurin, P.-H., Wright, T., Crosby, L. A., Mauldin, M., & Zuckerman, J. D. (2009). An evaluation of the relationships between reverse shoulder design parameters and range of motion, impingement, and stability. Journal of Shoulder and Elbow Surgery, 18(5), 734. http://dx.doi.org/10.1016/j.jse.2008.12.008

Terrier, A., Merlini, F., Pioletti, D. P., & Farron, A. (2009). Comparison of polyethylene wear in anatomical and reversed shoulder prostheses. The Journal of Bone and Joint surgery.British Volume, 91(7), 977–982. http://doi.org/10.1302/0301-620X.91B7.21999

Vaupel, Z. M., Baker, K. C., Kurdziel, M. D., & Wiater, J. M. (2012). Wear simulation of reverse total shoulder arthroplasty systems: effect of glenosphere design. Journal of Shoulder and Elbow Surgery, 21(10), 1422–1429. http://dx.doi.org/10.1016/j.jse.2011.10.024

Virani, N. A., Cabezas, A., Gutiérrez, S., Santoni, B. G., Otto, R., & Frankle, M. (2013). Reverse shoulder arthroplasty components and surgical techniques that restore glenohumeral motion. Journal of Shoulder and Elbow Surgery, 22(2), 179–187. http://doi.org/10.1016/j.jse.2012.02.004

Werner, B. S., Boehm, D., & Gohlke, F. (2013). Revision to reverse shoulder arthroplasty with retention of the humeral component. Acta Orthopaedica, 84(5), 473–478. http://doi.org/10.3109/17453674.2013.842433

Willing, R., & Kim, I. Y. (2009). A holistic numerical model to predict strain hardening and damage of UHMWPE under multiple total knee replacement kinematics and experimental validation. Journal of Biomechanics, 42(15), 2520–2527. http://doi.org/10.1016/j.jbiomech.2009.07.008

Chapter 4

4 The Development of a Wear Simulation Strategy for Reverse Shoulder Arthroplasty Implants

OVERVIEW

This chapter reviews the current state of literature regarding the wear simulator testing of reverse total shoulder arthroplasty (RTSA) implants, develops a wear simulator protocol for RTSA, and then tests it by completing a pilot study. The review of wear simulator testing in the literature revealed considerable variation in protocols. A combination of our own cadaveric testing and those of other research groups helped in determining the magnitude and direction of joint loading for the development of the present protocol. A MATCO orbital bearing simulator was adapted using custom fixtures to simulate a circumduction motion of the shoulder under mildly adverse conditions and a pilot study gave wear rates within the wide range found in the literature. Arguments were presented in support of the currently developed protocol but it was also suggested that, rather than rely on one protocol, a series of simulator wear protocols should be developed to fully test the implant wear performance in RTSA. [3]

4.1   Introduction

Reverse total shoulder arthroplasty (RTSA) is a clinically accepted treatment for rotator cuff tear arthropathy, fracture, and revision of failed shoulder arthroplasty (Castagna et al., 2013; Drake, OConnor, Edwards, O'Connor, & Edwards, 2010; Ek, Neukom, Catanzaro, & Gerber, 2013; Flury, Frey, Goldhahn, Schwyzer, & Simmen, 2011; Leung, Horodyski, Struk, & Wright, 2012; Nolan, Ankerson, & Wiater, 2011; Ortmaier et al., 2013; Werner, Boehm, & Gohlke, 2013). RTSA reverses the natural glenohumeral anatomy by replacing the concave glenoid with a convex hemispherical "glenosphere" and the convex humeral head with a concave polyethylene cup (Figure 4-1). In order to provide the large range of motion required at the shoulder joint, the polyethylene cup on the humeral component is relatively shallow compared to ball-in-socket type articulations used in other total joint arthroplasty implants, resulting in low "coverage" of the hemispherical glenosphere.

Examination of retrieved RTSA polyethylene inserts by Day et al (Day et al., 2012) and Nam et al (Nam et al., 2010) demonstrated that typically the greatest amount of wear was in the inferior quadrant. This was generally attributed to scapular impingement (contact of the inferiomedial edge of the cup with the scapula), which results in notching of the scapula. The resulting rim damage and the subsequent wear from scapular impingement seemed to predominate over wear of the intended articular surfaces (Day et al., 2012). However, sometimes the rim damage propagated into the intended articular surface (Kohut, Dallmann, & Irlenbusch, 2012) and it was postulated that scapular notching itself was made worse by the presence of wear debris, some of which might come from the intended articular surfaces (Vaupel, Baker, Kurdziel, & Wiater, 2012). A finite element study of RTSA implants showed that, even in the absence of scapular notching, the largest contact stresses were estimated at the inferiomedial edge of the polyethylene insert (Terrier, Merlini, Pioletti, & Farron, 2009). All of the aforementioned should be considered in the development of wear simulator strategies.
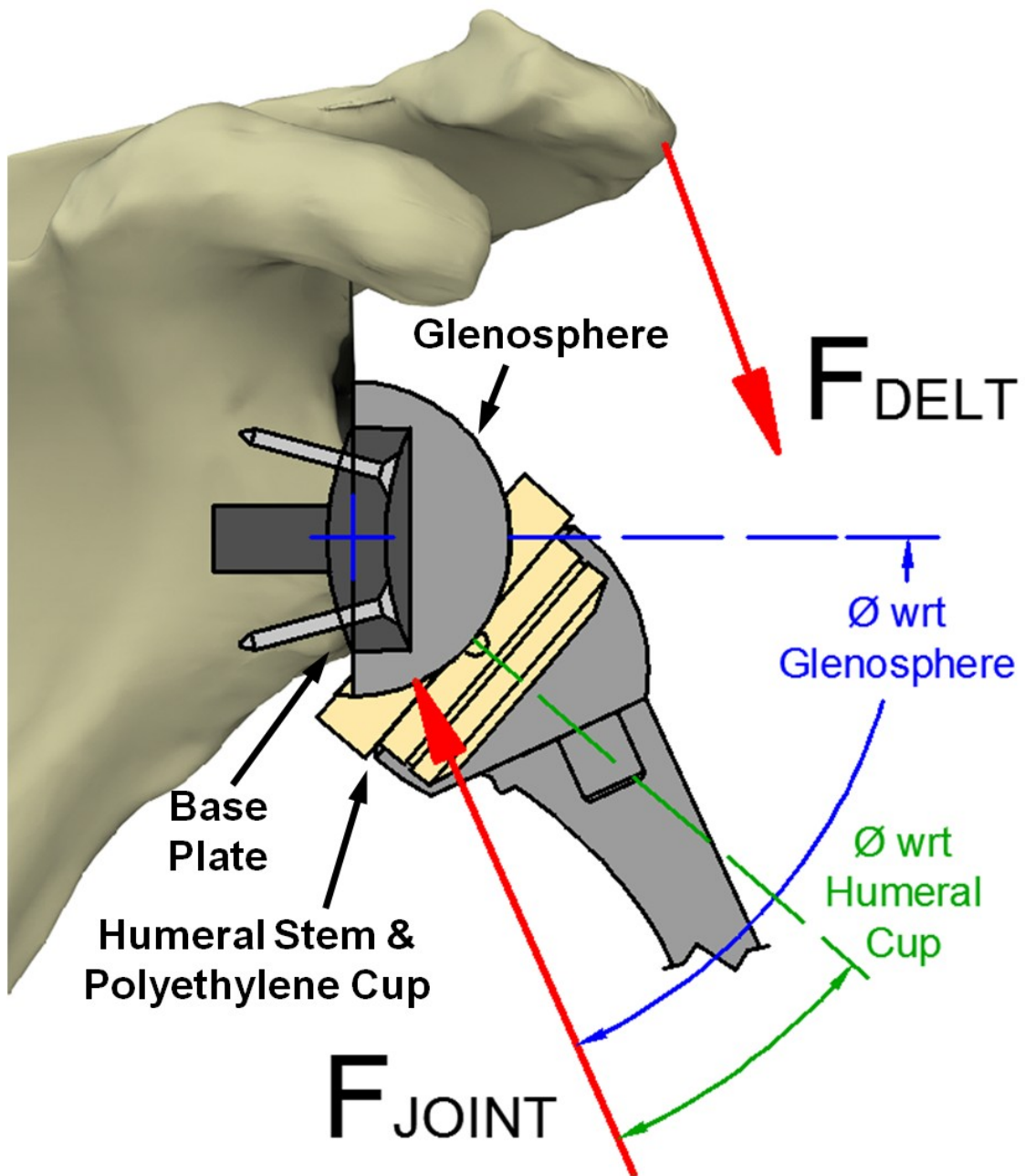
Figure 4-1: RTSA implant showing the force of the deltoid muscle acting on the scapula, the joint load acting on the glenosphere through the articulation, and the load angle with respect to both the glenosphere and the polyethylene cup.

The work of Ackland et al (Ackland, Roshan-Zamir, Richardson, & Pandy, 2011) and Kwon et al (Kwon, Forman, Walker, & Zuckerman, 2010) had inferred RTSA joint loads by measuring the forces imparted to the scapula during static positioning of the humerus throughout abduction, and have both reported loads ranging from approximately 10 to 40% body weight (BW) during unloaded abduction (Ackland et al., 2010; Kwon et al., 2010). A finite element study by Terrier et al (Terrier, Reist, Merlini, & Farron, 2008) showed similar results, estimating RTSA joints loads ranging from 110 to 310 N during unloaded abduction. Langohr et al (Langohr, Giles, Athwal, & Johnson, 2014) directly measured glenosphere loading in RTSA reconstructed cadaveric shoulders in an active shoulder joint simulator and reported joint loads ranging from 250 to 340 N for unloaded active glenohumeral abduction. When these RTSA joint loads were compared with loads reported by Bergmann et al (Bergmann et al., 2007), measured in-vivo through the use of instrumented primary TSA implants (not RTSA), they were about one-half of the maximum in-vivo load of 88% BW (647 N) for unloaded abduction. The differences in magnitude of loading of RTSA compared with TSA could be attributed to various aspects of the joints biomechanics, in particular the larger deltoid moment arm provided by RTSA due to the medial offset of the joint centre of rotation, thereby reducing the deltoid force required for abduction. It was important to note that not only were the reported RTSA loads lower than those measured for TSA, the resultant joint load angles were also markedly different. In TSA, the load was generally more centrally oriented through the articulation whereas in RTSA the load was more obliquely directed with a greater shear component, due to its constrained centre of rotation (Terrier et al., 2008).

Previous RTSA wear studies were performed, typically through the modification of a hip wear simulator by using custom fixtures, and the incorporation of joint loads drawn from the studies of Bergmann et al (Bergmann et al., 2007, 2011) who actually used instrumented in-vivo primary TSA (but not RTSA) implants. Vaupel et al (Vaupel et al., 2012) took this approach and investigated whether the placement of the hole in the centre of the glenosphere (used for fixation) affected RTSA wear performance. They used an "orbital bearing" type hip simulator (MTS Bionix, MTS, Eden Prairie, MN, USA) with a biaxial rocking motion of $\pm23^{o}$ and alternated between representations of dominant

abduction-adduction and dominant flexion-extension motions every 0.25 million cycles (Mc) by changing both the custom mounting fixtures and the input load profile. In the abduction-adduction motion, the load ranged from 20 N to 617 N (90% BW) and was applied centrally to the cup. In the flexion-extension motion, the load ranged from 20 N to 927 N (135% BW) and was applied obliquely to the cup thus bringing the contact zone to the cup edge. However, due to the orbital bearing kinematics, the dominant abduction-adduction motion included some symmetric flexion-extension motion. With their sinusoidal loading profile, it was likely that only very low loads were applied during the part of the cycle corresponding to flexion-extension. The same sort of low load synchronization might have occurred for the dominant flexion-extension motion. If so, this meant that the polyethylene cup would have to be positioned carefully in rotation as well as inclination when going from one dominant motion condition to the other.

Vaupel et al (Vaupel et al., 2012) tested eight implant pairs with central holes in the glenosphere and eight without the central holes. They did not detect significant differences in wear between the RTSA implants with and without holes. The same group performed another study (Peers et al., 2015) with the same wear test protocol comparing non crosslinked and highly crosslinked polyethylene cups, and found the wear rate of the highly crosslinked polyethylene cups to be approximately one-half that of the non crosslinked cups. It is important to note that both of these studies applied the concept of a "duty cycle" that sequentially applied 0.25 Mc simulations of first abduction-adduction dominant and then flexion-extension dominant motions. However, they did not try to account for any effect of scapular notching damage on the wear rates.

Haider et al (Haider, Sperling, & Throckmorton, 2013) described a wear study (using an adapted AMTI hip simulator) of Vitamin E doped highly crosslinked polyethylene cups compared with moderately crosslinked polyethylene cups that did not contain Vitamin E. They imparted 38°-79° forward elevation in two separate planes (15° and 45°) while ranging over 57° giving abduction-adduction motion along with internal-external rotation (no mention of flexion-extension motion), under a sinusoidal load ranging from 50-1700 N. A detailed description of the application of these conditions was not provided.

However, for six implant pairs in each group, they found on average that the highly crosslinked polyethylene cups exhibited approximately 80% less wear than the moderately crosslinked versions. They did not account for any effects of scapular notching damage on the wear rates.

Simulator wear tests were also performed by Kohut et al (Kohut et al., 2012) that involved comparing the wear of custom-made non crosslinked polyethylene humeral cups in RTSA with the wear of custom-made RTSA implants with a non crosslinked polyethylene glenosphere articulating with a metal humeral cup. Their "E-sim" hip simulators subjected the components to "shoulder conditions" of load (250 – 1000 N) and motion. In particular, they had a 43° range in flexion-extension, an 11° range in abduction-adduction and a 13° range of internal-external rotation. However, later on in their paper they said that their testing did not simulate eccentric wear and thus the oblique load angles of RTSA were not applied. Unlike the other simulator studies mentioned above, Kohut et al attempted to estimate the volume (or mass) loss due to abrasive wear/damage at the rim of the polyethylene humeral cups by observing a number of RTSA retrievals. This abrasive wear/damage was attributed to scapular notching, and was much greater than the wear they found at the glenosphere-cup articulation in their simulator wear tests. This observation was supported by the previously mentioned retrieval analysis of Day et al. Also, Kohut et al found that the wear at the glenosphere-cup articulation was not markedly influenced by which component (head or cup) was made of the non crosslinked polyethylene.

RTSA implant configuration and articular loading are clearly unique relative to other total joint arthroplasty devices. As such, investigations of the tribological performance of these implants using wear/damage simulation strategies must incorporate methodologies that best represent the in-vivo conditions acting on the RTSA implants. It is not clear what these methodologies should be. The purpose of the present work was to review the current literature on RTSA wear simulator testing, to develop a wear simulator protocol for RTSA implants, and to perform a pilot study to test the protocol. This included the determination of input loading and variation of load angles using data obtained from our

own cadaveric testing of RTSA implants and data from the testing of other research groups.

4.2 Materials & Methods

4.2.1 Instrumented In-Vitro Cadaveric Shoulder Simulator Testing

To explore the loads acting on RTSA implants in vivo (Figure 4-2), the previous work of Langohr et al (Langohr et al., 2014) was extended to include 9 more specimens and the joint load angles with respect to the humeral cup axis and glenosphere were recorded for the total number of 15 RTSA reconstructed cadaveric shoulders (68 ± 16 yrs). A clinically available implant (Delta XTEND, DePuy, Warsaw, IN) was used that had a size of 38 mm, a neck-shaft angle or 155°, with the glenoid base plate located at the inferior rim of the glenoid and the glenosphere centre of rotation positioned approximately at the native glenoid articular surface. Joint load was measured using a six degrees-of-freedom load cell (NANO25, ATI, Apex, NC) that was inserted between the glenosphere and the base plate, which was buried into the glenoid vault to accommodate the added height of the load sensor.

RTSA was performed on each specimen as previously described (Langohr et al., 2014), and attached to a shoulder motion testing apparatus by "potting" the scapula and attaching the three heads of the deltoid, the subscapularis, and the infraspinatus/teres minor by cables to actuators that applied loads acting along their physiological lines of action. The shoulder motion testing apparatus then generated active motion through independent muscle loading controlled by a multi-PID control system (Giles, Ferreira, Athwal, & Johnson, 2013) that provided accurate and repeatable glenohumeral and scapular motion. Using this control system, abduction was input from 0° to 90° of abduction at 1°/sec which was slow enough to avoid any substantial dynamic effects on the resultant load magnitude. At the same time, scapular rotation (which was known to occur in vivo) was applied in the same direction at one-third the value of the abduction angle following Inman et al (Inman, Saunders, & Abbott, 1996). This scapular rotation reduced relative rotation of the humeral cup over the glenosphere in the simulation.

Throughout motion simulation, the resultant joint load and its angle were recorded along with the position of the humerus and the scapula to provide orientation data. This allowed the load angles with respect to the humeral cup and the glenosphere axes to be determined. Statistical analysis was performed using a one-way (abduction angle) repeated measures ANOVA.

4.2.2   RTSA Wear Simulation Strategy

The unique functional characteristics of RTSA implants dictated the use of a specialized wear and damage simulating strategy, which took into account the load, motion and likely damage modification to the cup that these implants experienced in-vivo.

Following Vaupel et al (Vaupel et al., 2012), an orbital bearing hip wear simulator was selected to form the basis of the present RTSA wear simulation. The chosen MATCO simulator (model MMED EW08, originally manufactured by MATCO in La Canada, CA, USA) had previously been used to study the wear performance of total hip implants (McKellop & Clarke, 1984; J. B. Medley, Chan, Krygier, & Bobyn, 1996), and was the subject of a kinematic analysis in which the motion of points on the contact zone of total hip implants were mapped (J B Medley et al., 1997).

The simulator (J B Medley et al., 1997) had eight wear test stations, each configured (Figure 4-2) to provide a total of 45° of biaxial rocking motion using a driving block that was inclined at 22.5° to the horizontal and rotated at a speed of 1.134 Hz (68 rev/min). The motion of each drive block was synchronized mechanically by a horizontal chain drive and a vertical load was applied to each station by a small hydraulic cylinder that was supplied with pressurized oil from a central chamber.

The lower chambers were mounted with their central axes perpendicular to the block faces using pivot bearings and each chamber was connected to the chamber of an adjacent station using a pinned link rod that underwent curvilinear translation and prevented the chambers from rotating with the drive blocks (J B Medley et al., 1997). Furthermore, one of the link rod pins had a single degree of freedom and this imposed a constraint that prevented the chambers from rotating about their central axes. Thus, the

simulator represented a circumduction motion of the shoulder without internal-external rotation.

A digital load versus time curve was input into the simulator controller, which converted it to a proportional pressure curve. A servo-hydraulic valve controlled the flow from the central pressurized chamber and a sensor on the chamber wall provided pressure feedback so that the proportional input pressure signal could be reproduced in the central chamber. The pressure acted on the hydraulic cylinders of the stations to produce the desired input load versus time curve which was monitored in real time through a closed feedback loop. The simulator accommodated attachment of wear test specimens to the upper vertical shafts of the hydraulic cylinders through a self-aligning rod coupler to allow small adjustments in alignment that were needed because the implant specimens could not be perfectly oriented. The relative motion provided by the simulator between glenosphere and humeral cup was fixed by the drive block angle such that a constant biaxial rocking motion of 22.5° amplitude was applied. However, the orientation of the wear couples was modified with the use of custom fixtures such that the direction of the compressive force with respect to the implant specimen was altered. Therefore, the scope of the present study included the selection of both the wear test specimen orientation (with required custom fixtures) and the time varying load profile for use in the wear testing of RTSA implants using the simulator.
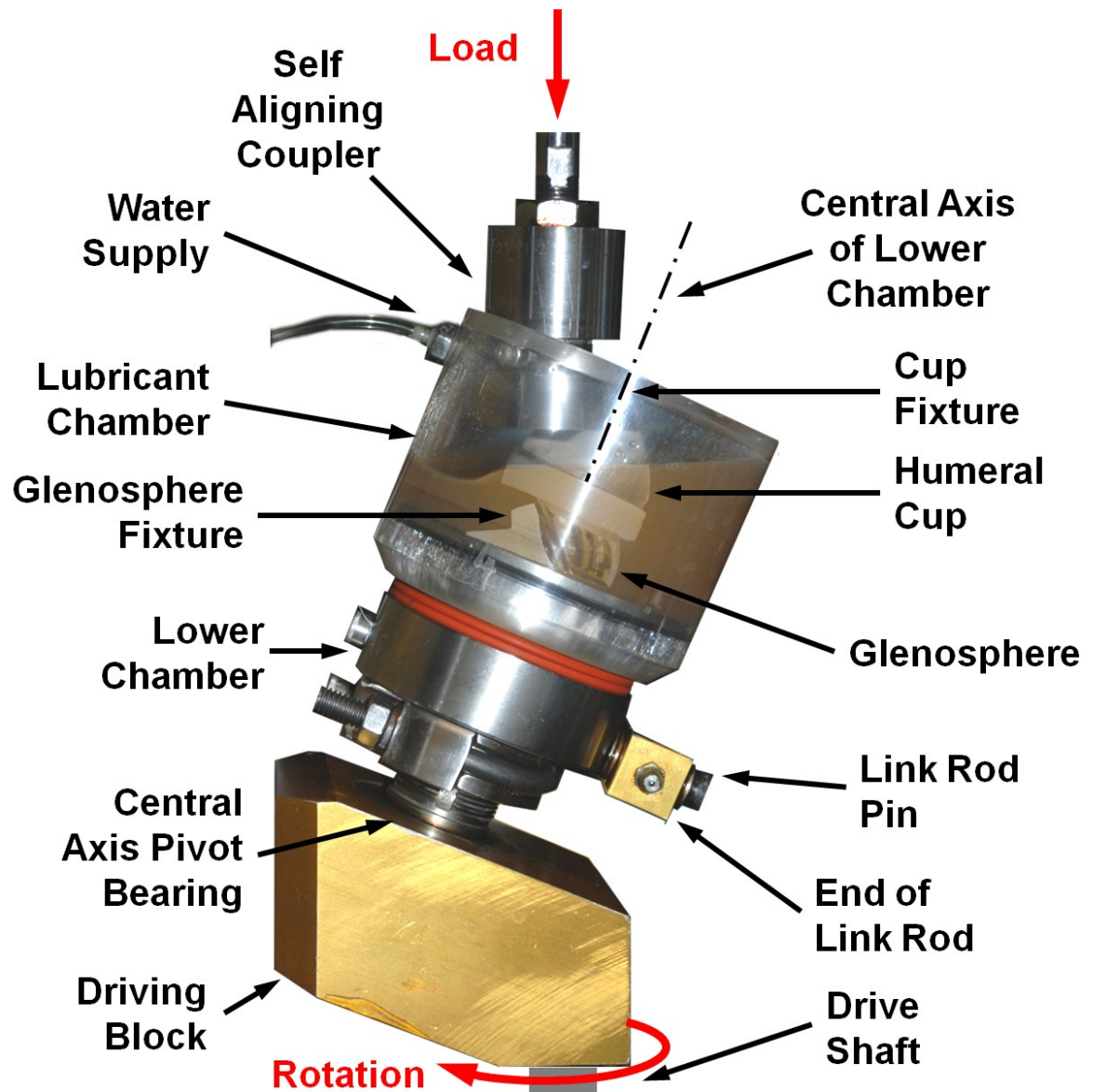
Figure 4-2: Single station of the MATCO simulator configured for RTSA wear testing

4.2.3   Simulation Protocols

To provide insight into the appropriateness of the selected RTSA wear and damage simulation strategy, a wear simulation and analysis with a single implant pair was performed for 2 Mc using the simulator and the associated custom fixtures and time-varying load from the previously mentioned cadaver simulator study. After 1 Mc, a small region of the inferior quadrant of the cup was removed using a 3D milling machining process to simulate the presence of moderate scapular impingement damage, and the wear test was continued for another 1 Mc. A commercially available RTSA implant (Delta XTEND, DePuy, Warsaw, IN, US) with a standard depth non crosslinked polyethylene cup (size: 42mm) mated to a standard glenosphere (size: 42mm) was chosen for this pilot study.

The lubricant used in the present study was alpha calf fraction serum without iron (Fisher Scientific Canada, Whitby, Ontario) diluted with phosphate buffer solution (PBS, VWR International, ON, Canada) to a protein concentration of 30 g/L. Research grade sodium hyaluronate (HA) was then added at a concentration of 1.5 g/L, and stirred for 12 hours at 37° C to ensure it was fully dissolved. Bacteria growth was suppressed with the addition of 5 mL of antimycotic antibiotic (Invitrogen Inc., ON, Canada) per 500 mL of lubricant. Brandt et al (J. M. Brandt, Mahmoud, Koval, MacDonald, & Medley, 2013) argued that this lubricant formulation provided a superior analogue for synovial fluid during wear simulator testing of knee implants in terms of both lubricant biochemistry, and in terms of wear rate magnitudes. During wear testing, the lubricant was maintained at approximately 37° C. The contact surface temperatures were likely to be a little above 37°C due to frictional heating. Evaporation was significantly reduced via sealing the interior volume from the external environment, and water volume loss due to evaporation during testing was replaced using an extremely slow, controlled flow rate of deionized water to each individual chamber.

Every 0.25 Mc, the polyethylene humeral cup was removed from the wear simulator, cleaned and weighed (Table 4-1) using a Mettler Toledo AX205 Analytical Balance (Columbus, OH) with a precision of 0.01 mg. The mass of the cup was measured three

times and the average of these values was compared with the initial average mass to determine mass loss. The specimen was then reinstalled and the test chamber was reassembled and filled with fresh lubricant for the next test interval.

No load-soak controls were included, however the cup tested had been pre-soaked for several months and was probably close to saturation and based on Brandt et al (J M Brandt, Charron, MacDonald, & Medley, 2011) the amount of fluid uptake was expected to be small. Additionally, the purpose of this pilot study was to investigate the wear processes and consider the feasibility of the main protocols. So, any loss in precision due to changes in fluid absorption during testing did not have significant impact on the overall objectives. Subsequent studies will implement load-soak controls.

After assessing the mass loss of the specimen due to wear in mg, it was converted to volumetric wear (V) in mm^3 by dividing by the polyethylene density of 0.935 mg/mm^3, and then plotted against test duration in Mc to describe its wear performance. The wear rate was then calculated by curve fitting the wear versus test duration (excluding the origin) and finding the slope following ISO 14242-2.

In addition to this gravimetric wear measurement, micro-CT was also used to visualize wear (Teeter, Langohr, Medley, & Holdsworth, 2014). The polyethylene cup was scanned before wear testing and again after the completion of 1 Mc. The specimen was scanned using a laboratory micro-CT scanner (eXplore Vision 120, GE Healthcare) at 50 μm isotropic voxel spacing, with an x-ray tube voltage of 90 kVp and current of 40 mA. For each scan, 1200 views were obtained in 0.3° increments, and 10 frames were averaged per view, at an exposure time of 16 ms per frame. The cup geometries, measured before and after wear, were then co-aligned and the three-dimensional deviations mapped. Differences due to wear were calculated in three dimensions and then mapped for wear visualization.

Table 4-1: Protocols for mass measurement of load-soak and wear test specimens

Step	Description
1.	Rinse with de-ionized water to remove loose contaminants.
2.	Scrub with a soft brush and rinse with de-ionized water.
3.	Clean in an ultrasonic cleaner in individual containers in a solution of 2% Liqui-NOX® detergent (Alconox, Inc., White Plains, NY, U.S.A.) for 10 min.
4.	Rinse with de-ionized water.
5.	Clean in an ultrasonic cleaner in individual containers in de-ionized water for 5 min.
6.	Soak in isopropyl alcohol for 5 min. to remove residual surface water and then dry in a stream of nitrogen gas.
7.	Allow to air dry and acclimatize next to the balance for 10 min.
8.	Calibrate the balance using the automatic calibration feature and set its zero value.
9.	Measure the mass of to manual calibration "weights" (20g and 100g).
10.	Successively measure the masses of each specimen once.
11.	Repeat the preceding protocol item twice more to obtain three measurements for each*.
12.	Average the three mass measurements for each specimen. If all three measured values of a particular specimen were not in the range of 0.2 mg, repeat steps 8 – 12.
13.	Measure the mass of the manual calibration "weights" to ensure that it is within 0.2 mg of the value determined in step 9.

*Note that the mass values showed no tendency to change with time and some were measured some 45 minutes after drying without showing any significant decrease (or increase) in mass. This suggested that the fluid content of the specimens was not changing.

Results

4.2.4   Specified Simulator Conditions

During active abduction, both the load angle with respect to the glenosphere and the load angle with respect to the humeral cup were affected by abduction angle (p<0.01, Figure 4-3). When the results of the present study were curve fit and then averaged with the curve fits of a number of previous studies[16–18], the mean glenosphere load angle ranged from about 52°-22° and the mean humeral cup load angle ranged from about 12°-20° throughout 30° – 94° of abduction (Figure 4-3). It was noted that the humeral cup load angle showed less variation than the glenosphere load angle.

Resultant load was also sensitive to abduction angle (p<0.01), slightly increasing from early abduction to mid-abduction, and then slightly decreasing as 90° of abduction was approached. When averaged with previously published data, the mean resultant load ranged from 210-315 N for an unloaded arm (Figure 4-3).

Reproducing something close to the RTSA load angles with respect to both the glenosphere and the humeral cup in the simulator needed custom mounting fixtures. The simulator subjected the superiorly mounted component to a constant, vertically oriented load angle which did not change throughout the cycle. Thus, it was appropriate to mount the humeral cup superiorly because it experienced the lower variation in load angle. Vaupel et al[14] also had the cup in the superior position in their orbital bearing wear simulator.

As shown in Figure 4-3, the mean humeral cup load angle ranged from about 12°-20° and it was directed towards the inferior quadrant of the cup for the majority of the abduction cycle, which was also the most common location of damage on retrievals[11–13,18]. Therefore, in order to produce an inferiorly oriented humeral cup angle, as well as apply a slightly more severe shear load to the cup, a constant 25° humeral cup load angle was chosen (Figure 4-4).
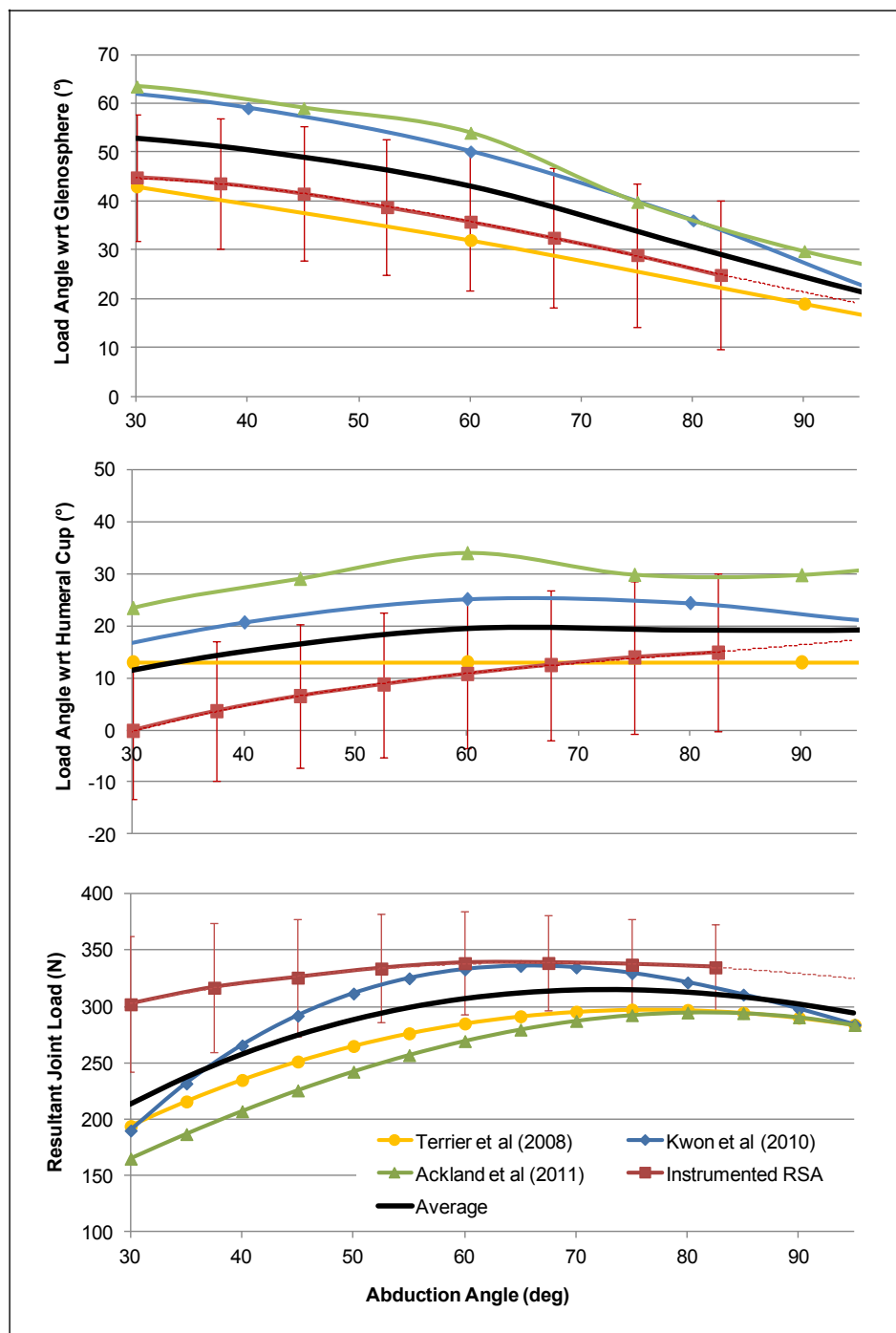
Figure 4-3: Load angle with respect to the glenosphere, with respect to the humeral cup, and the resultant joint load throughout abduction for the present study compared to previously published data.

The glenosphere mean load angle ranged through 30° from about 52°-22° during abduction (Figure 4-3). The simulator with its existing angled drive blocks applied a range of 45° to the load angle with respect to the glenosphere. However, it was considered important to simulate the contact of the edge of the glenosphere (which was actually a spherical cone not a full sphere) with the edge of the humeral cup (Figure 4-4) as it moved over the cup bearing surface because this often occurred in adduction. In order to best replicate the glenosphere load angles obtained in our testing, as well as generate the edge-related contact issues, a glenosphere orientation which produced glenosphere load angles range (of 45°) from 25°-70° was selected (Figure 4-4). In vivo, this corresponded to an abduction angle range of 67.5° due to the influence of scapular rotation in the coronal plane[25].

However, the simulator motion also caused implant flexion/extension through a range of 45° and this directly translated to the in vivo range of flexion-extension. Thus, as previously mentioned, the simulator represented a circumduction motion of the shoulder which is a symmetric combination of abduction-adduction and flexion-extension.
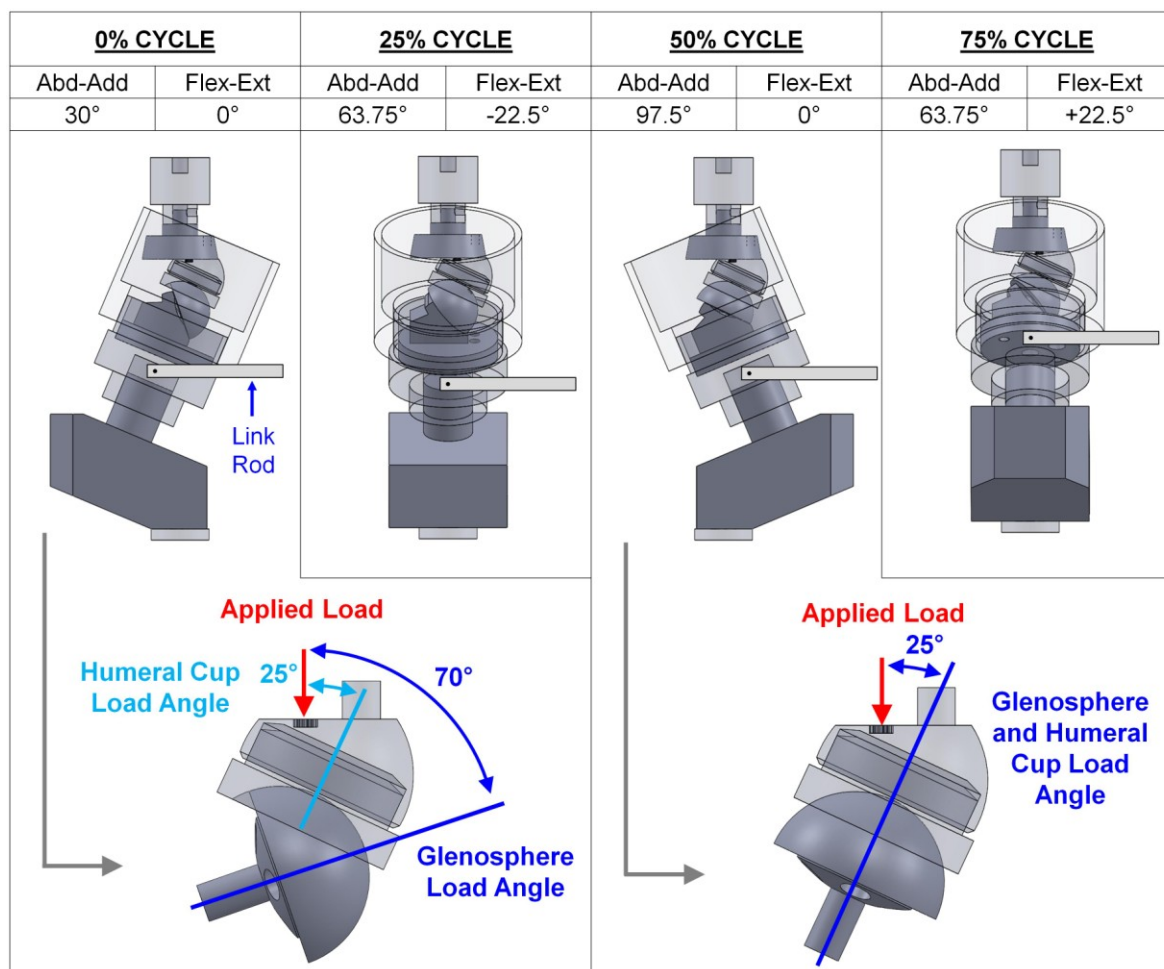
Figure 4-4: Abduction and flexion/extension angles imparted by the RTSA wear simulator (top) and the resulting humeral cup angles and glenosphere load angles applied at the end limits of abduction corresponding to 0% and 50% of the total circumduction cycle.

The mean resultant load via a combination of the present cadaveric study and previously published results ranged from 213-314 N, all of which were obtained from unloaded arms. The average load curve in the range of abduction generated by the selected RTSA implant fixtures was used to convert the resultant load curves to a percentage (%) of the circumduction cycle that was applied by the simulator. This conversion involved the following assumptions:

1. The loads during the adduction angles were considered to be the same as the loads during the abduction angles. Thus, the load profile has symmetry about a vertical line drawn at 50 percent of the cycle. This assumption neglects any dynamic effects involved in the motion.

2. The load profile representing abduction-adduction could be applied during the circumduction motion that occurred in the orbital bearing simulator. Thus, both abduction-adduction and flexion-extension were applied with the same load profile.

In order to subject the RTSA to higher loads during wear simulation studies and thus moving towards mildly adverse conditions for the simulation strategy, the mean resultant load was scaled such that several load curves of varying peak values could be attained (Figure 4-5). The 314 N peak load curve represented an unloaded hand, the 614 N and 914 N peak load curves represented the low and high values expected for a hand loaded to 0.5 kg according to Masjedi and Johnson[32]. It was also interesting to note that for a RTSA implant in a flexion-extension type of motion under low hand loading (answering the telephone), Masjedi and Johnson predicted a fairly constant 350 N peak load thus suggesting that flexion-extension loading was not so different from abduction-adduction loading. Finally, the 1714 N peak curve was selected to represent a high loading scenario. For the present pilot study, the 914 N peak load was chosen.
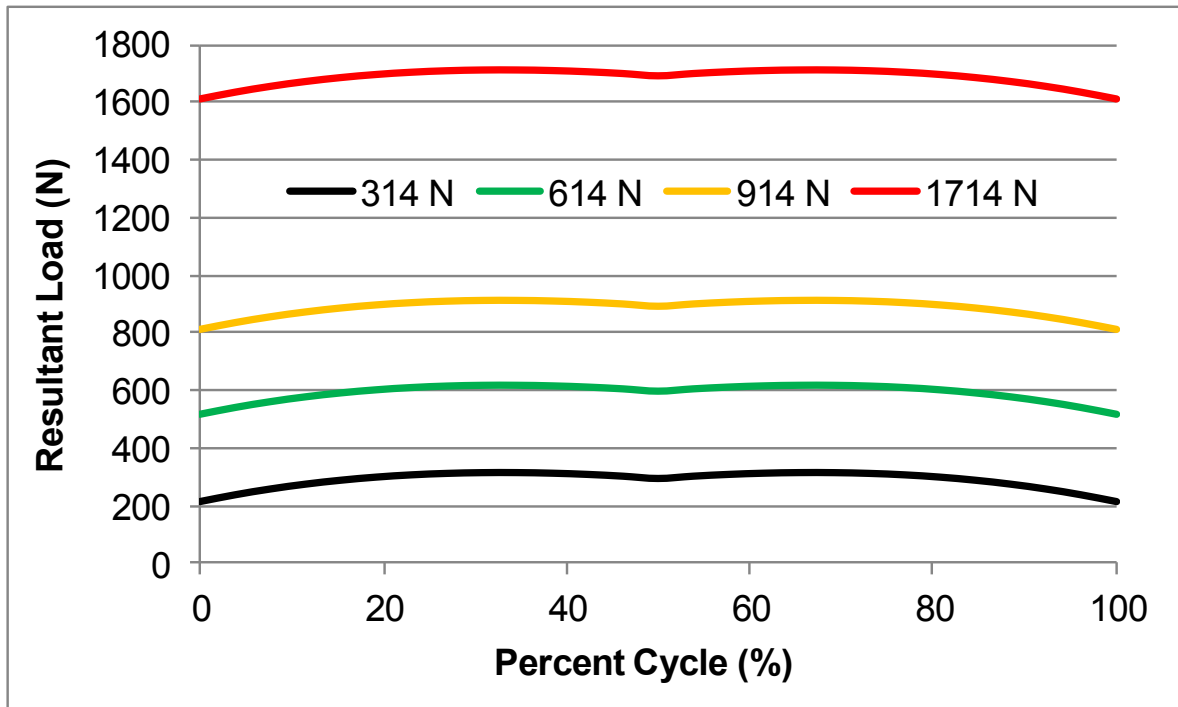
Figure 4-5: Resultant load as a function of percentage of cycle for unloaded hand (314 N peak), moderately loaded hand (614 N and 914 N peak), and high loaded hand (1714 N peak).

4.2.5   Pilot Study

The humeral cup showed signs of polishing in the inferior half of articulation which were first observed after 0.25 Mc and persisted until the end of the test. The micro-CT wear analysis showed material loss similarly in the inferior quadrant, with the largest area of deviation (or material removal) centered in the polished region (Figure 4-6).

The wear of the humeral cup was fairly consistent throughout the first Mc of the test (Figure 4-7), during which the mean wear rate of the humeral cup was 42.0 mm^3/Mc. During the second Mc of testing, after the introduction of simulated scapular impingement damage, the wear rate was 38.8 mm^3/Mc. This wear rate was surprisingly a little lower than when the cup was in the un-notched state.
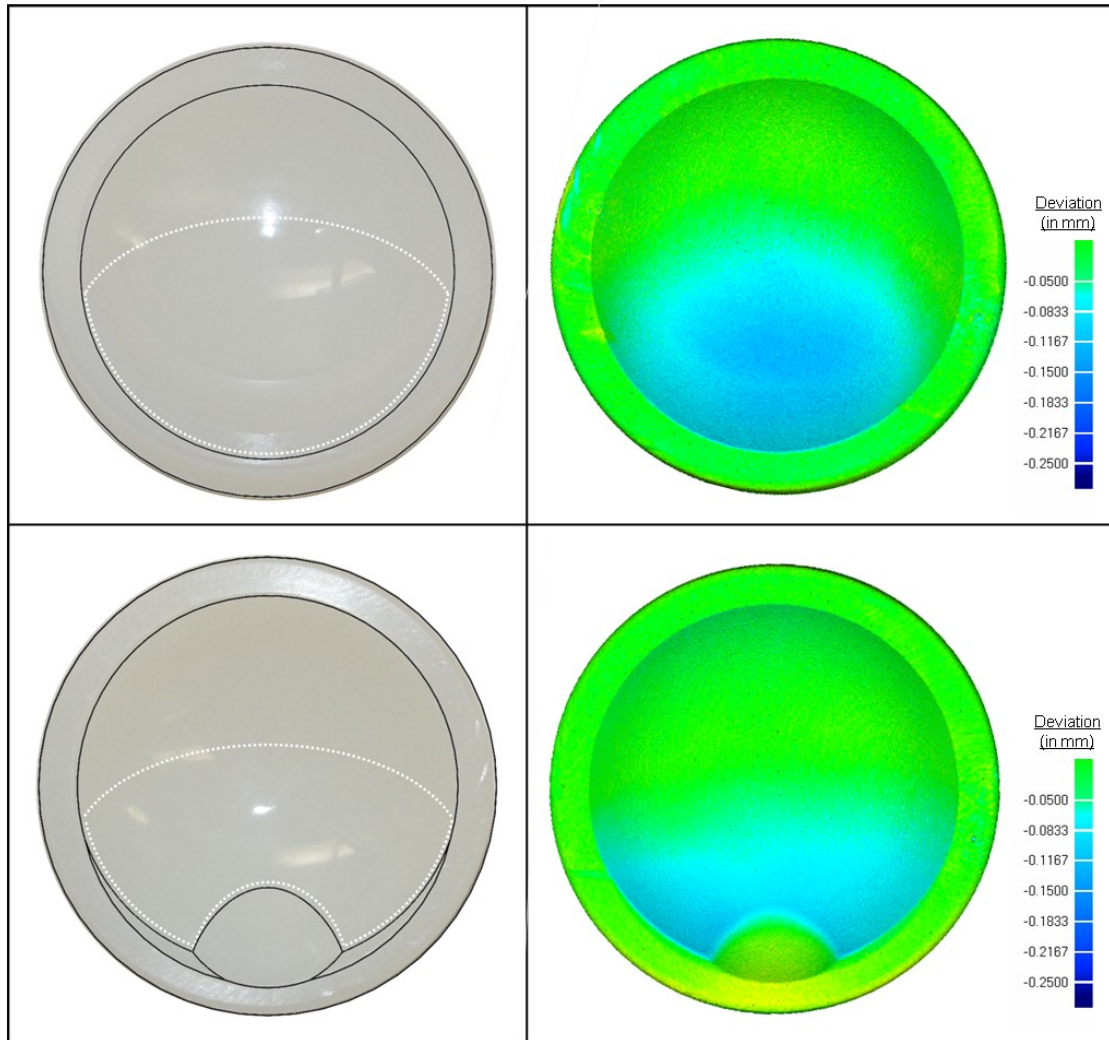
Figure 4-6: Humeral cup after 1 Mc (top) with polished region outlined in black (left) and Micro-CT deviation map showing wear morphology during first Mc (right) and humeral cup after 2 Mc (bottom) with simulated scapular notching outlined (left) and Micro-CT deviation map showing wear during second Mc (right).
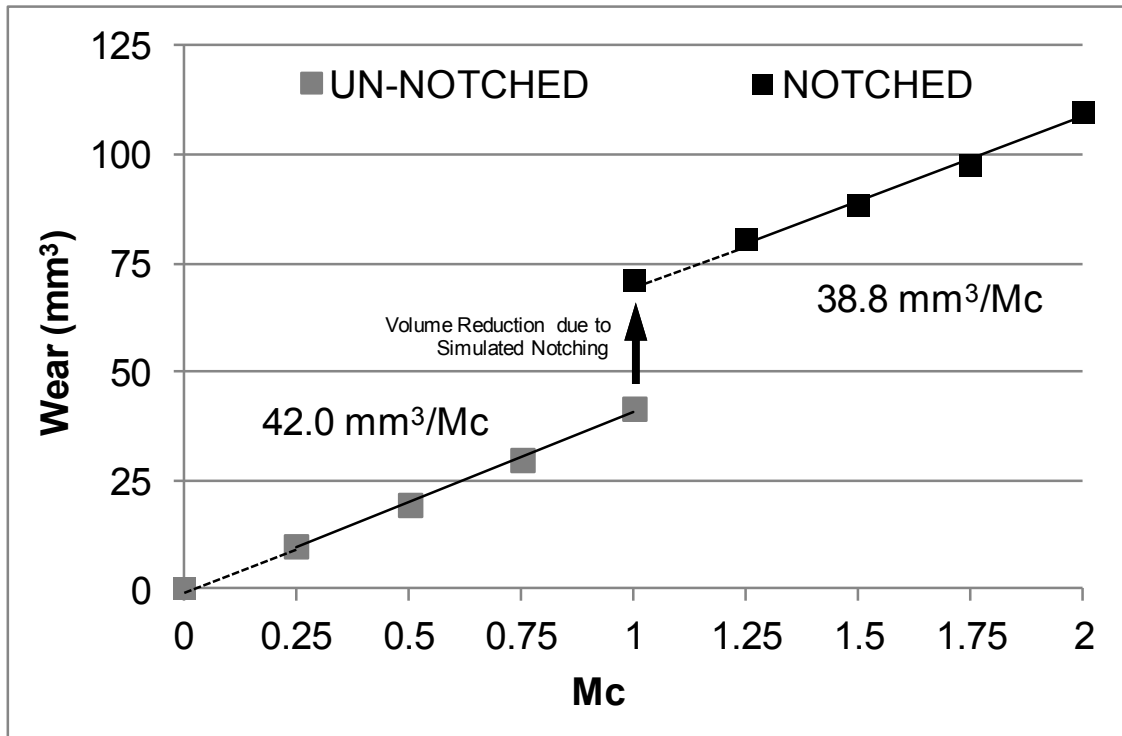
Figure 4-7: Wear of the Humeral cup before and after being notched. The linear curve fits to find the wear rates omit the first point (as suggested by ISO 14242-2).

4.3 Discussion

In the present study, decisions on the protocol were based, to some extent, on data (of other research groups and generated as part of the present study) but also on arguments supporting simplicity of the simulator device while imposing mildly adverse conditions. For example, the selection of the MATCO hip simulator with drive blocks oriented at 22.5^o from the horizontal was made because the device was available and simple. It was driven by one continuous rotation motion yet caused crossing-path motion at the articulating surfaces. The simulation represented a circumduction motion of the shoulder. It was considered likely that flexion-extension combined with a smaller amount of abduction-adduction might be a more common shoulder motion. However, the symmetric circumduction motion might provide a somewhat more adverse condition for wear and this might be desirable to more rigorously test an implant.

The stationary humeral cup with a 25° humeral cup load angle was another example of an argument for both a simple yet mildly adverse condition while still maintaining some link to the data for abduction-adduction motion. The chosen $25^o - 70^o$ range in glenosphere load angle was a little less than the in vivo limits but was easily implemented using the current simulator, and was probably closer to more common in vivo activities.

 As described above, resultant load was chosen based on in-house and other research group data. It should be noted that the RTSA resultant load curve during abduction does not vary as much as the hip load curve during walking. In RTSA, soft tissue tension and active musculature maintain fairly constant high compressive forces which helped stabilize the shoulder joint, and as a result the fluctuation in joint loads during arm abduction was relatively low.

The idea that the time varying abduction load could be extended to cover adduction and then applied to a circumduction cycle was another example of simplicity. The actual loading for a circumduction cycle of an RTSA implant had apparently not been measured by anyone. Vaupel et al[14] chose a higher peak load (927 N) for their flexion-extension

motion than the peak load (628 N) for their abduction-adduction motion based on estimates of predicted shoulder hemiarthroplasty implant loading. This suggested that a circumduction peak load for an RTSA implant might be higher than for just abduction-adduction. However, as previously mentioned, for an RTSA in a flexion-extension type of motion under low hand loading (answering the telephone), Masjedi and Johnson[32] predicted a fairly constant 350 N peak load thus suggesting that flexion-extension loading was not so different from abduction-adduction loading. The 914 N peak load of the present pilot study was between the two peak loads of Vaupel et al loads but close to the higher value. Thus, the approach of simplicity and mildly adverse conditions was maintained.

Another guiding principle for the simulator design involved the production of wear zones that were similar in location to those seen in retrievals. The inferior location of the humeral cup wear that was found in the present pilot study was also the region which Nam et al[12] reported as having the highest damage score in retrievals.

The wear rates of the pilot wear study could be compared with those from the academic literature (Table 4-2). When only the non crosslinked polyethylene results were considered, the wear rates ranged from 17.4 to 125 mm^3/Mc with those of the present study (42.0 and 38.8 mm^3/Mc) falling within the range. Even the crosslinked polyethylene (50 kGy) had wear rates from 17.4 to 36.5 mm^3/Mc. In the pilot study, an unconventional lubricant was used following Brandt et al. The role this played in the wear rate was not determined but Brandt et al did find somewhat higher wear for this lubricant compared with bovine serum diluted with distilled water and no hyaluronate. So, there were differences in the strategies and conditions for the previous simulator wear studies (as discussed in the Introduction section), the large variation in wear rates warranted attention.

Table 4-2: Comparison of wear rates of the previous studies and the present pilot study

Group	Motion Range (^{o})	Load Range (N)	Lubricant	Cup Material	**Wear rate (mm^3/Mc)**
Vaupel et al[14]	abd-add 46 flex-ext 46	20 – 618 20 – 927	calf serum + DW (21 g/L protein)	PE	125 $\pm$ 32
Peers et al[22]	abd-add 46 flex-ext 46	20 – 618 20 – 927	calf serum + DW (21 g/L protein)	PE	83.6 $\pm$ 20.6
	abd-add 46 flex-ext 46	20 – 618 20 - 927	calf serum + jDW (21 g/L protein)	XPE (50 kGy)	36.5 $\pm$ 10.0
Kohut et al[13]	abd-add 11 flex-ext 43 int-ext 13	250 – 1000	bovine serum (30 g/L protein)	PE	*17.4 $\pm$ 6.1
Haider et al[23]	abd-add 41 int-ext 57	50 – 1700	not specified	XPE (50 kGy)	†19.1 $\pm$ 0.9
	abd-add 41 int-ext 57	50 - 1700	not specified	HXPE (100 kGy)	†3.7 $\pm$ 0.2
Present Pilot Study (n = 1)	abd-add 45 flex-ext 45	813 - 914	alpha calf serum + PBS (30 g/L protein + 1.5 g/L hyaluronate)	PE	42.0
	abd-add 45 flex-ext 45	813 - 914	alpha calf serum + PBS (30 g/L protein + 1.5 g/L hyaluronate)	PE notched	38.8

PE = non crosslinked polyethylene   XPE = crosslinked polyethylene
HXPE = highly crosslinked polyethylene
DI = deionized water   PBS = phosphate buffer solution
abd = abduction   add = adduction   flex = flexion   ext = extension
int = internal rotation   ext = external rotation

*to simplify used last recorded wear value divided by Mc
†assuming density of PE was 0.935 mg/mm^3

There is no general consensus regarding simulator test conditions. Even the lowest wear rate of 17.4 mm^3/Mc for non crosslinked polyethylene is quite high and may in combination with scapular notching damage cause wear particle induced osteolysis. In addition, some individual patients may have very high shoulder activity levels and thus, in our opinion, there is an urgent need to explore wear of RTSA.

The Standard Specification for Shoulder Prostheses (ASTM F1378-12) states that wear testing is not necessary because *it is felt that at this time wear is not a major issue in existing or potential implant designs…*, except to ensure that new materials are not introduced with wear rates that exceed those found for CoCrMo alloy against ultra high molecular weight polyethylene under "physiological conditions". This approach suggests that wear is considered, by the ASTM, to be a material property and not related to device specific conditions. Furthermore, the so-called "physiological conditions" are difficult to specify for all patients with RTSA. In any case, it is the present authors' opinion that no single wear simulator test protocol is sufficient to predict wear performance under the wide variety of conditions found in RTSA patients and to ensure the safety of RTSA in clinical practice. A series of wear simulator tests with different protocols including some that are device specific are needed to address the long term efficacy of RTSA with regards to wear. The present pilot study provides most of the details of a single protocol that includes the idea of having material removed to simulate scapular notching. It is our attempt to initiate one of these protocols, although in this pilot study no substantial difference was shown for the effect of scapular notching and thus this detail might eventually be removed.

4.4 Conclusions

The present study described the development of RTSA wear simulation strategies that incorporated loading and load directions from cadaveric testing and previously published data. Fairly constant and quite high loads were selected to represent mildly adverse load conditions. A fairly realistic circumduction motion was applied using an orbital bearing simulator in which symmetric adduction-abduction and flexion-extension actions were applied to provide a representation of typical daily shoulder motion.

The pilot wear test produced wear that was coincident with the most common location of retrieval wear. The wear rates were within the wide range of published simulator wear results for RTSA. The developed wear simulation protocol and the strategic considerations expressed provide a useful first step in developing a series of wear simulator protocols for RTSA.

4.5 References

Ackland, D. C., Roshan-Zamir, S., Richardson, M., & Pandy, M. G. (2010). Moment arms of the shoulder musculature after reverse total shoulder arthroplasty. The Journal of Bone and Joint surgery. American Volume, 92(5), 1221–1230. http://doi.org/10.2106/JBJS.I.00001

Ackland, D. C., Roshan-Zamir, S., Richardson, M., & Pandy, M. G. (2011). Muscle and joint-contact loading at the glenohumeral joint after reverse total shoulder arthroplasty. Journal of Orthopaedic Research, 29(12), 1850–1858. http://doi.org/10.1002/jor.21437

Bergmann, G., Graichen, F., Bender, A., Kaab, M., Rohlmann, A., & Westerhoff, P. (2007). In vivo glenohumeral contact forcesâ€"Measurements in the first patient 7 months postoperatively. Journal of Biomechanics, 40(10), 2139–2149. http://dx.doi.org/10.1016/j.jbiomech.2006.10.037

Bergmann, G., Graichen, F., Bender, A., Rohlmann, A., Halder, A., Beier, A., & Westerhoff, P. (2011). In vivo gleno-humeral joint loads during forward flexion and abduction. Journal of Biomechanics, 44(8), 1543–1552. http://dx.doi.org/10.1016/j.jbiomech.2011.02.142

Brandt, J. M., Charron, K. D. J., MacDonald, S. J., & Medley, J. B. (2011). Mass gain behaviour of tibial polyethylene inserts during soak testing. Proceedings of the Institution of Mechanical Engineers. Part H, Journal of Engineering in Medicine, 225(3), 324–331. http://doi.org/10.1177/2041303310392629

Brandt, J. M., Mahmoud, K. K., Koval, S. F., MacDonald, S. J., & Medley, J. B. (2013). Antimicrobial agents and low-molecular weight polypeptides affect polyethylene wear in knee simulator testing. Tribology International, 65, 97–104. http://doi.org/10.1016/j.triboint.2013.02.019

Castagna, A., Delcogliano, M., de Caro, F., Ziveri, G., Borroni, M., Gumina, S., … De Biase, C. F. (2013). Conversion of shoulder arthroplasty to reverse implants: clinical and radiological results using a modular system. International Orthopaedics, 37(7), 1297–1305. http://doi.org/10.1007/s00264-013-1907-4;

Day, J. S., MacDonald, D. W., Olsen, M., Getz, C., Williams, G. R., & Kurtz, S. M. (2012). Polyethylene wear in retrieved reverse total shoulder components. Journal of Shoulder and Elbow Surgery, 21(5), 667–674. http://dx.doi.org/10.1016/j.jse.2011.03.012

Drake, G. N., OConnor, D., Edwards, T. B., O'Connor, D. P., & Edwards, T. B. (2010). Indications for Reverse Total Shoulder Arthroplasty in Rotator Cuff Disease. Clinical Orthopaedics and Related Research, 468(6), 1526–1533. http://doi.org/10.1007/s11999-009-1188-9

Ek, E. T., Neukom, L., Catanzaro, S., & Gerber, C. (2013). Reverse total shoulder arthroplasty for massive irreparable rotator cuff tears in patients younger than 65 years old: results after five to fifteen years. Journal of Shoulder and Elbow Surgery, 22(9), 1199–1208. http://doi.org/10.1016/j.jse.2012.11.016

Flury, M. P., Frey, P., Goldhahn, J., Schwyzer, H. K., & Simmen, B. R. (2011). Reverse shoulder arthroplasty as a salvage procedure for failed conventional shoulder replacement due to cuff failure--midterm results. International Orthopaedics, 35(1), 53–60. http://doi.org/10.1007/s00264-010-0990-z

Giles, J. W., Ferreira, L. M., Athwal, G. S., & Johnson, J. A. (2013). Validation of a Novel In-Vitro Simulator for Real-Time Control of Active Shoulder Movements in Various Planes of Motion ASME 2013 Summer Bioengineering Conference (Vol. Volume 1B:, p. pp. V01BT31A001). http://doi.org/doi:10.1115/SBC2013-14067

Haider, H., Sperling, J., & Throckmorton, T. (2013). A method for wear testing of reverse shoulder arthroplasty systems. Bone Joint J., Vol. 95-B, SUPP 34 (607).

Hua, X., Li, J., Wang, L., Jin, Z., Wilcox, R., & Fisher, J. (2014). Contact mechanics of modular metal-on-polyethylene total hip replacement under adverse edge loading conditions. Journal of Biomechanics, 47(13), 3303–3309. http://dx.doi.org/10.1016/j.jbiomech.2014.08.015

Inman, V. T., Saunders, J. B., & Abbott, L. C. (1996). Observations of the function of the shoulder joint. 1944. Clinical Orthopaedics and Related Research, (330), 3–12.

Kohut, G., Dallmann, F., & Irlenbusch, U. (2012). Wear-induced loss of mass in reversed total shoulder arthroplasty with conventional and inverted bearing materials. Journal of Biomechanics, 45(3), 469–473. http://doi.org/10.1016/j.jbiomech.2011.11.055

Kwon, Y. W., Forman, R. E., Walker, P. S., & Zuckerman, J. D. (2010). Analysis of reverse total shoulder joint forces and glenoid fixation. Bulletin of the NYU Hospital for Joint Diseases, 68(4), 273–280.

Langohr, G. D. G., Giles, J. W., Athwal, G. S., & Johnson, J. A. (2014). The effect of glenosphere diameter in reverse shoulder arthroplasty on muscle force, joint load, and range of motion. Journal of Shoulder and Elbow Surgery. http://dx.doi.org/10.1016/j.jse.2014.10.018

Leung, B., Horodyski, M., Struk, A. M., & Wright, T. W. (2012). Functional outcome of hemiarthroplasty compared with reverse total shoulder arthroplasty in the treatment of rotator cuff tear arthropathy. Journal of Shoulder and Elbow Surgery, 21(3), 319. http://dx.doi.org/10.1016/j.jse.2011.05.023

McKellop, H. A., & Clarke, I. C. (1984). Evolution and evaluation of meaterials-screening machines and joint simulators in predicting in vivo wear phenomena. In Functional Behavior of Orthopedic Biomaterials, Volume II: Applications (pp. 51–85). Baco Raton: CRC Press.

Medley, J. B., Chan, F. W., Krygier, J. J., & Bobyn, J. D. (1996). Comparison of Alloys and Designs in a Hip Simulator Study of Metal on Metal Implants. Clinical Orthopaedics and Related Research, 329(S), 148–159.

Medley, J. B., Krygier, J. J., Bobyn, J. D., Chan, F. W., Lippincott, a, & Tanzer, M. (1997). Kinematics of the MATCO hip simulator and issues related to wear testing of metal-metal implants. Proceedings of the Institution of Mechanical Engineers. Part H, Journal of Engineering in Medicine, 211(1), 89–99. http://doi.org/10.1243/0954411971534719

Nam, D., Kepler, C. K., Nho, S. J., Craig, E. V., Warren, R. F., & Wright, T. M. (2010). Observations on retrieved humeral polyethylene components from reverse total shoulder arthroplasty. Journal of Shoulder and Elbow Surgery, 19(7), 1003. http://dx.doi.org/10.1016/j.jse.2010.05.014"

Nolan, B. M., Ankerson, E., & Wiater, J. M. (2011). Reverse total shoulder arthroplasty improves function in cuff tear arthropathy. Clinical Orthopaedics and Related Research, 469(9), 2476–2482. http://doi.org/10.1007/s11999-010-1683-z

Ortmaier, R., Resch, H., Matis, N., Blocher, M., Auffarth, A., Mayer, M., … Tauber, M. (2013). Reverse shoulder arthroplasty in revision of failed shoulder arthroplasty-outcome and follow-up. International Orthopaedics, 37(1), 67–75. http://doi.org/10.1007/s00264-012-1742-z

Peers, S., Moravek Jr., J. E., Budge, M. D., Newton, M. D., Kurdziel, M. D., Baker, K. C., … Wiater, J. M. (2015). Wear rates of highly cross-linked polyethylene humeral liners subjected to alternating cycles of glenohumeral flexion and abduction. Journal of Shoulder and Elbow Surgery, 24(1), 143–149. http://dx.doi.org/10.1016/j.jse.2014.05.001

Teeter, M. G., Langohr, G. D. G., Medley, J. B., & Holdsworth, D. W. (2014). Nondestructive microimaging during preclinical pin-on-plate testing of novel materials for arthroplasty. Proceedings of the Institution of Mechanical Engineers, Part H: Journal of Engineering in Medicine}, 228(2), 159–164. http://doi.org/10.1177/0954411914522615

Terrier, A., Merlini, F., Pioletti, D. P., & Farron, A. (2009). Comparison of polyethylene wear in anatomical and reversed shoulder prostheses. The Journal of Bone and Joint surgery.British Volume, 91(7), 977–982. http://doi.org/10.1302/0301-620X.91B7.21999

Terrier, A., Reist, A., Merlini, F., & Farron, A. (2008). Simulated joint and muscle forces in reversed and anatomic shoulder prostheses. The Journal of Bone and Joint surgery.British Volume, 90(6), 751–756. http://doi.org/10.1302/0301-620X.90B6.19708

Vaupel, Z. M., Baker, K. C., Kurdziel, M. D., & Wiater, J. M. (2012). Wear simulation of reverse total shoulder arthroplasty systems: effect of glenosphere design. Journal of

Shoulder and Elbow Surgery, 21(10), 1422–1429. http://dx.doi.org/10.1016/j.jse.2011.10.024

Werner, B. S., Boehm, D., & Gohlke, F. (2013). Revision to reverse shoulder arthroplasty with retention of the humeral component. Acta Orthopaedica, 84(5), 473–478. http://doi.org/10.3109/17453674.2013.842433

Chapter 5

5   In-Vitro Wear Simulation of Reverse Total Shoulder Arthroplasty Implants

OVERVIEW

This chapter discusses the in-vitro wear simulation of reverse total shoulder arthroplasty implants using the wear simulation strategy described in the previous chapter. Eight clinically available RTSA implants having a diameter of 38 mm with a normal cup depth (DELTA Xtend, DePuy) were tested in an RTSA wear simulator apparatus: 5 implants were wear couples and the remaining 3 served as load soak specimens to account for fluid absorption. The location of wear on the humeral cups was described, as was the occurrence of inferior cup edge wear; a location which was identified in Chapter 3 as important to load transfer from the humeral cup. The wear rate of the present study was higher than that of the pilot study of Chapter 4 but this difference might have arisen because a different base serum was used. Further wear testing with identical base serum was suggested to provide further insight on this observed difference in wear rate.

5.1 Introduction

As previously described, reverse total shoulder arthroplasty (RTSA) replaces the native glenohumeral joint with an implant that reverses the native anatomy by placing a convex glenosphere on the concave glenoid and replaces the convex humeral head with a concave humeral cup (Figure 5-1). RTSA employs a ball-in-socket articular geometry, although the humeral cup is relatively shallow which results in a joint that is not very constrained.

Retrieved RTSA polyethylene cups have typically exhibited the greatest amount of wear in the inferior quadrant of the cup, which was generally attributed to follow from the damage of scapular impingement that occurs when the inferiomedial edge of the cup contacts the scapula (Day et al., 2012; Nam et al., 2010). In the present work, a distinction is made between damage that occurs rapidly due to unintended surface contact and wear that is more gradual and within the intended articulating region. This inferiomedial cup damage was found to extend into the wear zone of the intended articular surface of the humeral cup. As a result, the presence of scapular impingement damage and its associated damage debris may accelerate the progression of wear and the presence of wear debris may in turn accelerate the progression of scapular notching (Kohut, Dallmann, & Irlenbusch, 2012; Vaupel, Baker, Kurdziel, & Wiater, 2012). In the absence of scapular notching, the inferiomedial edge of the cup has also been shown to be the location of peak contact stress in a finite element model (Terrier, Merlini, Pioletti, & Farron, 2009). Thus it is difficult to determine the in vivo wear of RTSA implants using in vitro simulators and most in vitro studies have not included a representation of scapular notching damage.

Recent interest in the wear performance of RTSA implants has been generated by the increasing prevalence of these devices for the treatment of rotator cuff arthropathy, fracture, and revision of primary total shoulder arthroplasty (Castagna et al., 2013; Flury, Frey, Goldhahn, Schwyzer, & Simmen, 2011; Frankle et al., 2006).
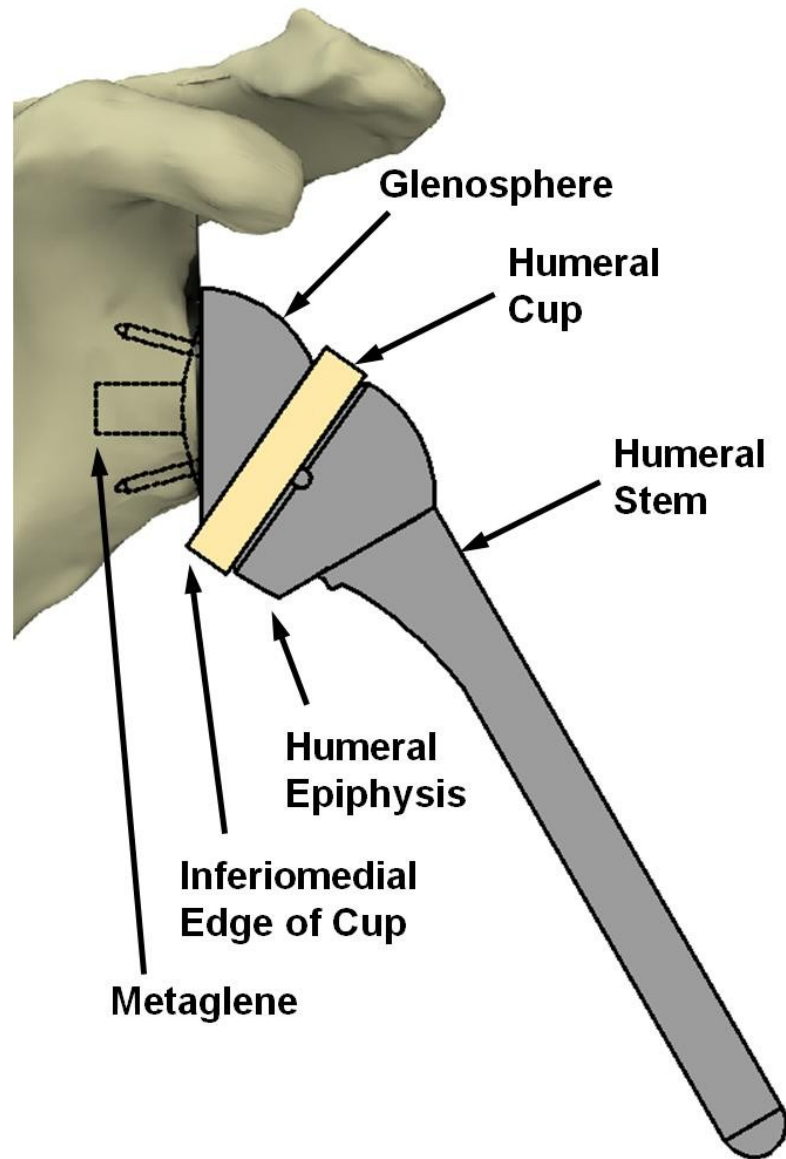
Figure 5-1: Reverse total shoulder arthroplasty (RTSA) implant

Vaupel et al (2012) did not detect significant differences in wear between the RTSA implants with and without holes in the glenosphere (used for fixation) using an "orbital bearing" hip simulator alternating between representations of dominant abduction-adduction and dominant flexion-extension motions every 0.25 million cycles (Mc). They reported a mean wear rate of 125 ± 32 mm^3/Mc for all RTSA implants investigated (Vaupel et al., 2012).

Peers et al (2015) compared non-crosslinked and highly crosslinked polyethylene cups using the same wear simulator strategy as Vaupel et al (2012), and reported wear rates of 84 ± 21 mm^3/Mc for non-crosslinked and 37 ± 10 mm^3/Mc for crosslinked cups. Crosslinking was found to significantly reduce wear (Peers et al., 2015).

Haider et al (2013) performed a wear study comparing Vitamin E doped highly crosslinked polyethylene cups compared with moderately crosslinked polyethylene cups, and found on average that the highly crosslinked polyethylene cups had much less wear than the moderately crosslinked versions. They reported mean wear rates of 4 ± 0.2 mm^3/Mc for Vitamin E doped and 19 ± 1 mm^3/Mc for non-doped versions.

Simulator wear tests were also performed by Kohut et al (2012) comparing the wear of custom-made non-crosslinked polyethylene humeral cups in RTSA with the wear of custom-made RTSA implants with a non-crosslinked polyethylene glenosphere articulating with a metal humeral cup. Interestingly, the reversal of bearing materials did not significantly alter the wear rate compared to the standard configuration. They reported a mean wear rate of 17 ± 6 mm^3/Mc for their non-crosslinked polyethylene cups (Kohut et al., 2012). To put their wear rate into context, they attempted to estimate the volume loss due to scapular notching damage at the rim of the polyethylene humeral cups by studying a number of RTSA retrievals. This abrasive damage was much greater than the wear they found at the glenosphere-cup articulation in their simulator wear tests, which supports the retrieval analysis of Day et al.

In the previous chapter, the wear of a single 42 mm diameter non-crosslinked polyethylene cup was reported to be 42 mm^3/Mc in the as received state, and 39 mm^3/Mc after simulated notching was applied to the inferiomedial edge of the cup.

These above-mentioned RTSA wear simulation studies make use of varying test conditions including lubricant constituents and concentration, applied load ranges, relative motion, and load angle with respect to both the glenosphere and humeral cup. The current wear simulation study employed the wear simulation strategy described in the previous chapter which was developed based on a combination of instrumented in-vitro cadaveric testing of RTSA reconstructed shoulders and previously published data regarding RTSA loading characteristics. This testing protocol was considered to be a simplistic representation of circumduction (combination of both adduction-abduction and flexion-extension) motion at loads and load angles representative of what could occur in-vivo.

As mentioned in the previous chapter, there is no ASTM standard for simulator testing of RTSA implants. In the opinion of the present author, a series of wear simulator test protocols, including some that are patient and device specific, are needed to address the long term efficacy of RTSA with regards to wear. The ASTM standard may not be able to specify such tests but given the rather high wear rates that have been reported from simulator testing in the academic literature, they are needed to further address the clinical safety of RTSA implants.

Therefore, the purpose of the present study was to more fully assess the wear of standard configured clinically available RTSA implants using the wear simulation strategy developed in the preceding chapter. We hypothesized that due to the inferiorly oriented joint load that occurs in vivo, the majority of wear would occur in the inferior quadrant of the polyethylene cup, and that the wear rate of the polyethylene cups would fall within the relatively wide range of previously reported RTSA wear rates.

5.2 Materials & Methods

5.2.1 RTSA Wear Simulation Strategy

The modified orbital bearing hip wear simulator (model MMED EW08, originally manufactured by MATCO in La Canada, CA, USA; as described in Chapter 4) with five wear test stations and three load soak stations was used to perform the wear testing (Figure 5-2). The simulator was capable of providing a total of 45° of biaxial rocking motion at a speed of 1.134 Hz (68 rev/min). Each individual station was prevented from rotating with its drive block by a link arm which connected it to an adjacent station. The biaxial rocking motion corresponded to a range of flexion-extension of ±22.5° and a range of adduction-abduction of 30° to 97.5° (as described in Chapter 4) which combined to produce a circumduction motion that was repeated once per cycle (Figure 5-3).

A transient load profile with a peak value of 900 N as selected in Chapter 4 (Figure 5-4) was applied to the wear couples via the simulator controller, which converted a digital loading profile to a proportional pressure curve which was input to a servo-hydraulic valve which controlled the pressure to the hydraulic cylinder of each stations to produce the desired input load versus time curve.

Humeral cup wear test specimens were held in place by custom fixtures that were attached to the upper vertical shafts of the hydraulic cylinders through a self-aligning rod coupler. Glenosphere specimens were held in the lower chamber using their own custom fixtures. The orientation of the wear couples was controlled such that the direction of the compressive force with respect to the implant specimen was similar to those observed in in-vitro testing of RTSA reconstructed cadaveric shoulders (Chapter 4), applying the load at angles ranging from 25°-70° relative to the central axis of the glenosphere and at a constant 25° with respect to the central axis of the humeral cup (Figure 5-4).
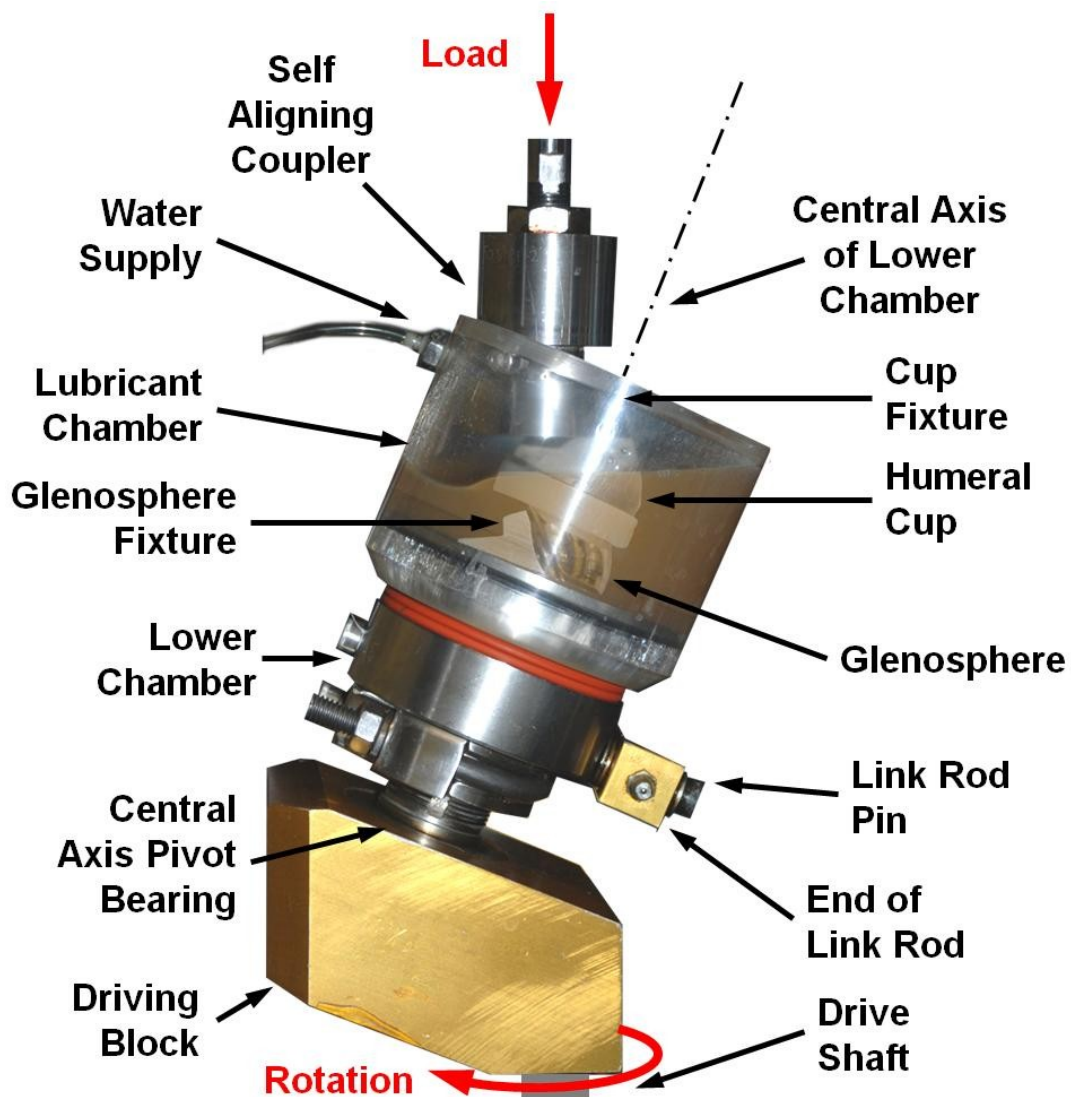
Figure 5-2: Single station of the RTSA wear simulator
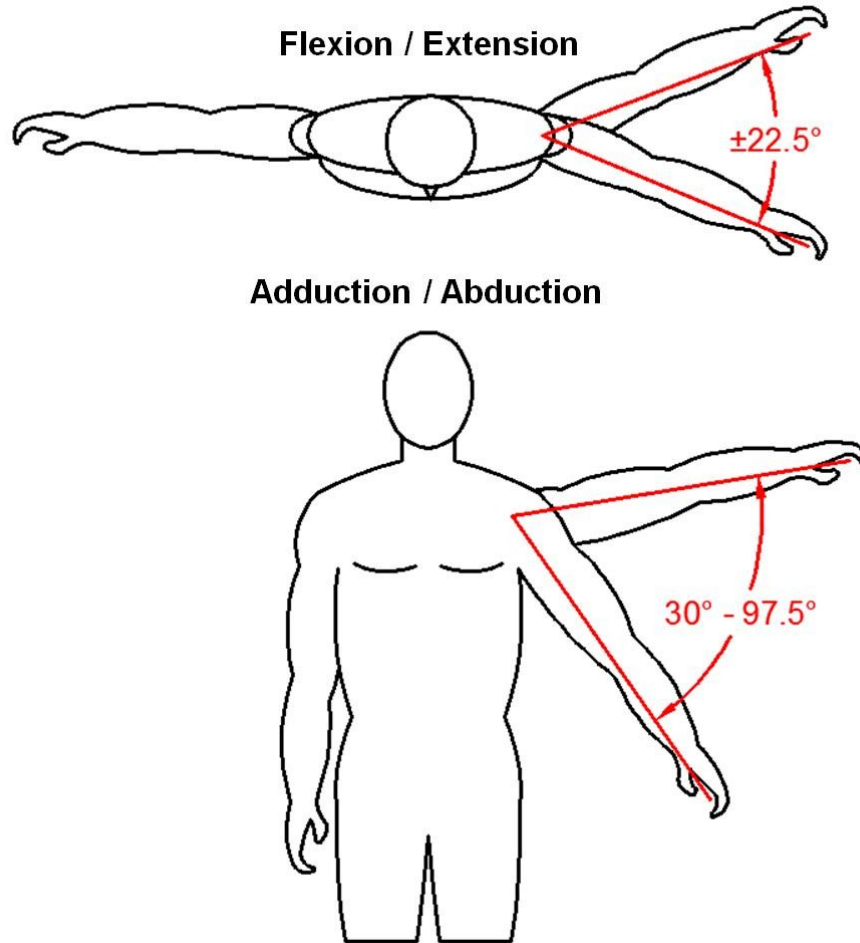
Figure 5-3: Range of motion imparted to RTSA implants in the wear simulator
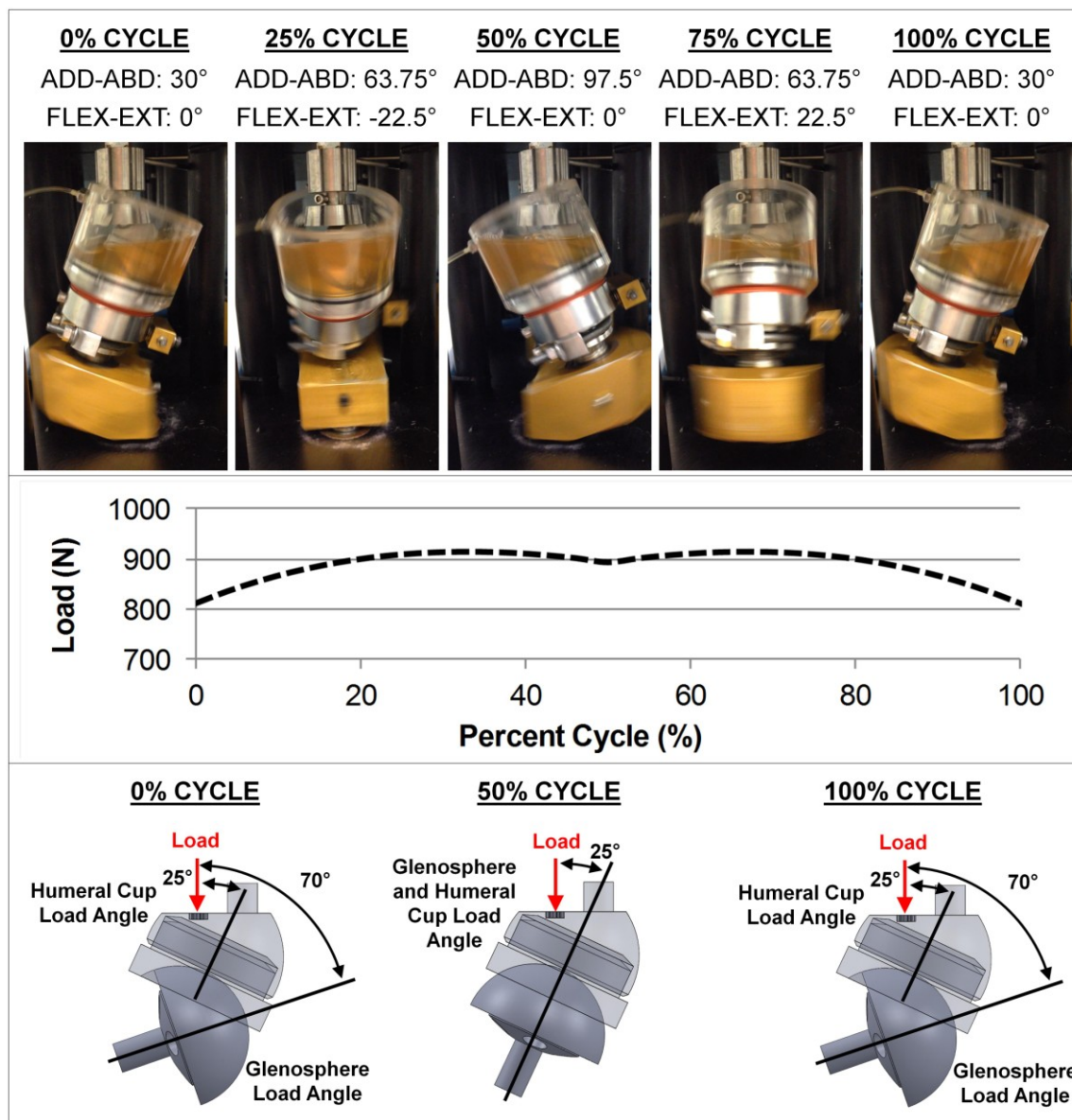
Figure 5-4: Resultant load applied by RTSA wear simulator as a function of % cycle

5.2.2   Simulation Protocols

Wear testing of five wear couples was performed for 1.44 Mc using the simulator and the associated custom fixtures and time-varying load from the previous as described in the previous section. (The target number of cycles had been 2 Mc but one of the anti-rotation rod suffered a catastrophic failure causing enough damage to the machine to delay further testing. The rod failure was instantaneous and therefore it is not likely to have impacted the wear test results prior to breakdown.) The simulator wear testing was conducted on eight commercially available RTSA implants (Delta XTEND, DePuy, Warsaw, IN, US) with standard depth non crosslinked polyethylene cups (size: 38 mm) and matching standard glenospheres (size: 38 mm).

The lubricant used in the present study was bovine calf serum (Fisher Scientific Canada, Whitby, Ontario) diluted with phosphate buffer solution (PBS, VWR International, ON, Canada) to a protein concentration of 30 g/L. Research grade sodium hyaluronate (HA) was then added at a concentration of 1.5 g/L, and stirred for 12 hours at 37° C to ensure it was fully dissolved. Bacteria growth was suppressed with the addition of 5 mL of antimycotic antibiotic (Invitrogen Inc., ON, Canada) per 500 mL of lubricant. Bovine calf serum was used in the lubricant rather than the alpha calf serum that had been used in the pilot study described in the previous chapter due to serum supply issues. Bovine calf serum with HA had also been used by (DesJardins et al., 2006) in their attempt to better represent the biochemistry and rheology of synovial fluid.

During wear testing, the lubricant was maintained at approximately 37° C. Evaporation was minimized via sealing the interior volume from the external environment, and water volume loss due to evaporation during testing was replaced using an extremely slow, controlled flow rate of deionized water to each individual chamber.

Every 0.25 Mc, the polyethylene humeral cups were removed from the wear simulator, cleaned and weighed (Appendix A) using a Mettler Toledo AX205 Analytical Balance (Columbus, OH) with a precision of 0.01 mg. The mass of the cup was measured three times and the average of these values was compared with the initial average mass to

determine mass loss. The specimen was then reinstalled and the test chamber was reassembled and filled with fresh lubricant for the next test interval.

Three load-soak controls were included, and were subjected to identical test conditions as the wear couples. These conditions included similar temperature, the same lubricant bath, and the same loading profiles. However, the load soak specimens were not subjected to any relative motion and therefore any mass change in this subgroup was due to changes in fluid content rather than material removal. In addition, all cups used for wear and load-soak control had been pre-soaked for six months and were likely close to saturation and based on Brandt et al (J M Brandt, Charron, MacDonald, & Medley, 2011). Thus, the amount of fluid absorption (uptake) was expected to be small compared with the mass loss due to wear.

The mass loss of each specimen due to wear was determined by weighing each specimen and subtracting its starting mass to determine its apparent net change in mass from the start of the test. The effect of fluid absorption was then accommodated by adding the mean increase in mass of the load soak specimens. This assumed that all specimens in the wear study would have the same change in fluid content. The "real" change in mass of each specimen was then converted to volumetric wear (V) in mm^3 by dividing by the polyethylene density of 0.935 mg/mm^3, and then plotted against test duration in Mc to describe its wear performance. The wear rate of each specimen was then calculated by curve fitting the wear versus test duration (excluding the origin) and finding the slope following ISO 14242-2.

In addition to this gravimetric wear measurement, micro-CT was also used to visualize wear (Teeter, Langohr, Medley, & Holdsworth, 2014). The polyethylene cups were scanned before wear testing and again after the completion of 1.44 Mc. The specimens were scanned using a laboratory micro-CT scanner (eXplore Vision 120, GE Healthcare) at 50 µm isotropic voxel spacing, with an x-ray tube voltage of 90 kVp and current of 40 mA. For each scan, 1200 views were obtained in 0.3° increments, and 10 frames were averaged per view, at an exposure time of 16 ms per frame. The cup geometries, measured before and after wear, were then co-aligned and the three-dimensional

deviations mapped. Differences due to wear were calculated in three dimensions and then mapped for wear visualization.

5.3   Results

All of the humeral cups showed signs of wear of the articulation after the first 0.25 Mc, and continued throughout the duration of testing. Although it was difficult to see in photographs, wear was apparent using the naked eye when the cups were tilted slightly to "catch the light". The wear zones were estimated and shown visually in Figure 5-5. Specimen 1 exhibited a large wear scar with a flat and/or scuffed appearance covering the entire intended articular surface, with only a small region at the superior-most aspect of the cup remaining in the as new condition. The remaining specimens (Figure 5-5, white dashed lines), were similar except for the presence of a part line near the superior margin of the wear scar which divided the inferiorly positioned flat and/or scuffed wear scar and a thinner region showing signs of polishing (Figure 5-5, thin black lines). All humeral cups showed signs of inferior cup edge wear which presented as a thinning of the thickness of the flat ring around the intended articular surface (Figure 5-5, red lines).

The glenospheres all exhibited some light surface scratching throughout the contact zone, which was located in the inferior quadrant (Figure 5-5). Upon removal of the glenospheres after every 0.25 Mc, there was some surface staining present also within the contact zone (Figure 5-6), which was removed during ultrasonic cleaning of the components.

The wear rates of the humeral cups were quite variable, with a range of 114.7 to 344.5 mm^3/Mc, and a mean wear rate of 201.1 ± 86.5 mm^3/Mc (Figure 5-7).
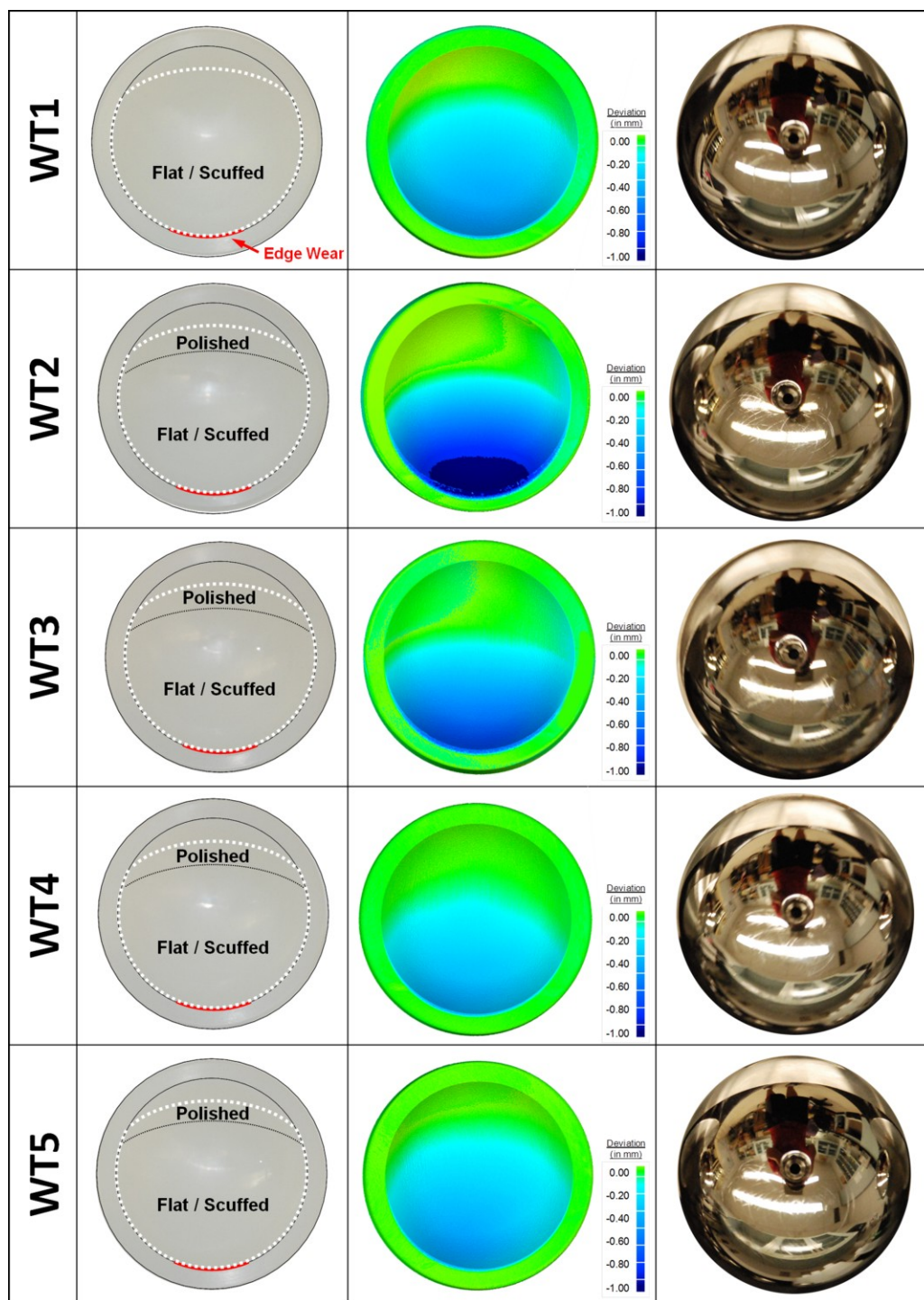
Figure 5-5: Appearance of the worn humeral cups (left) and glenospheres (right) of all wear test specimens. Dashed white lines denote wear scar region, dashed black lines denote part lines in the wear scars, and red lines show edge wear. The specimens are oriented such that superior is towards the top.
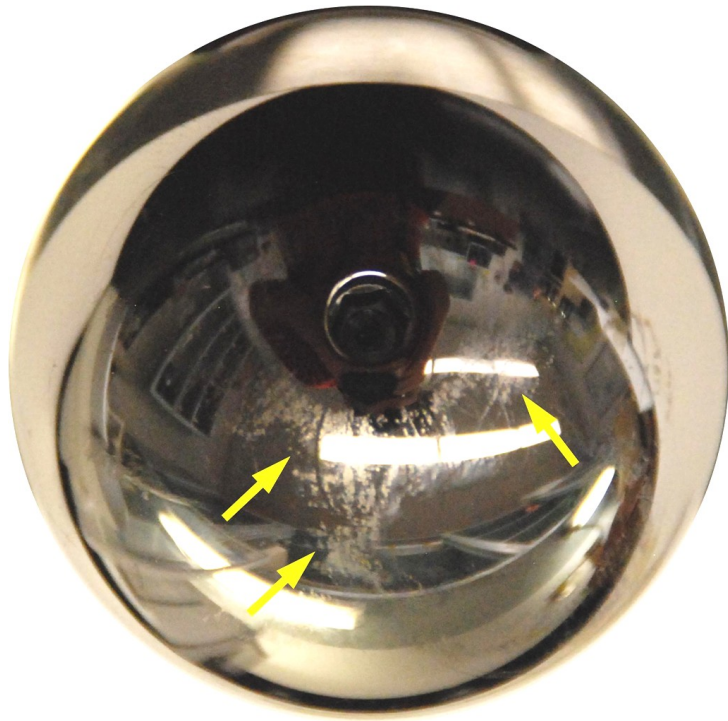
Figure 5-6: Typical glenosphere surface staining present after each 0.25 Mc
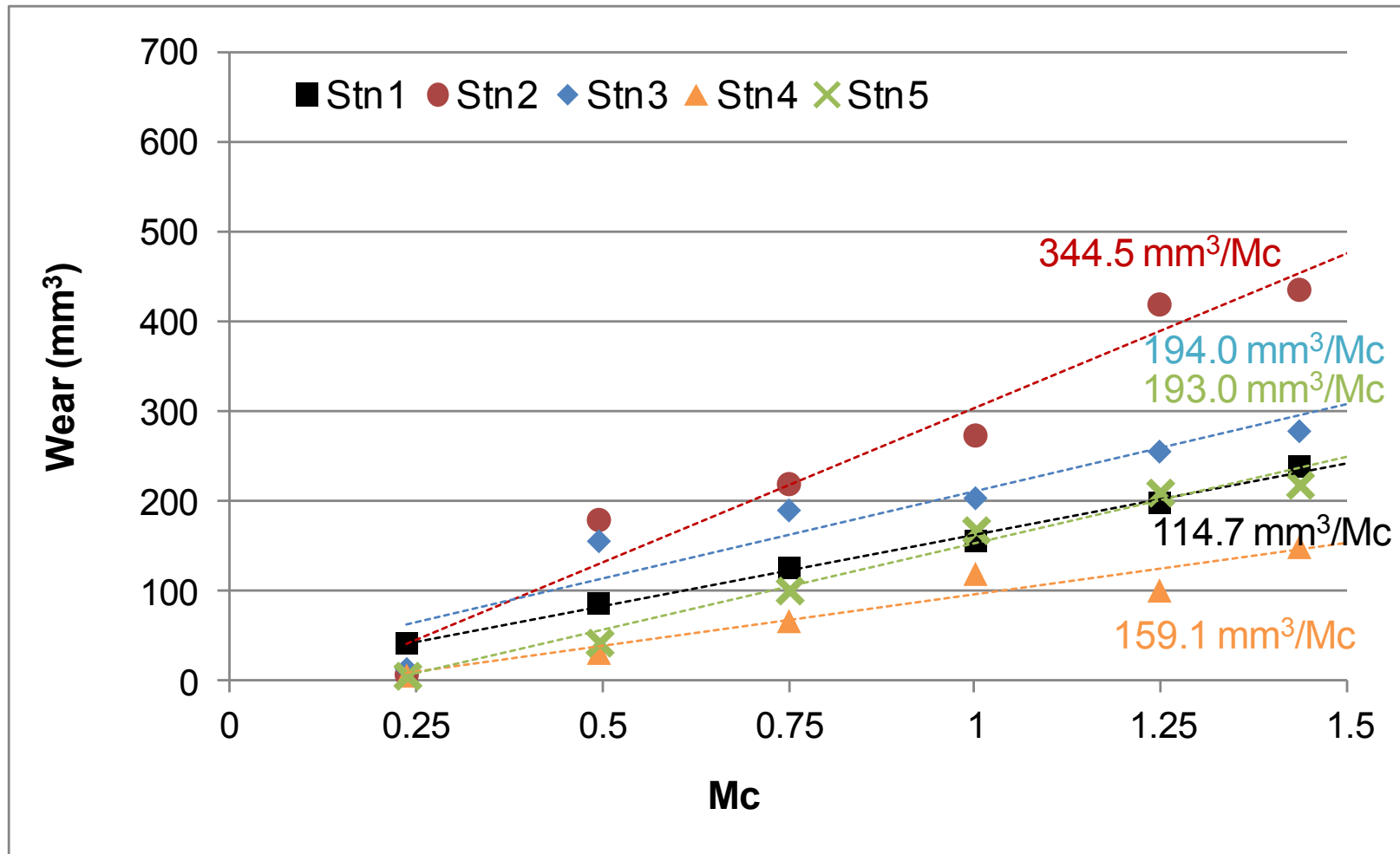
Figure 5-7: Wear rates of the humeral cup in each of stations with their linear least squares curve fits

5.4 Discussion

The present study employed the same wear simulation protocol as described in the previous chapter, albeit with i) a smaller implant (38 mm vs. 42 mm diameter) and ii) a different lubricant composition (identical protein and HA concentration but bovine calf serum instead of alpha calf serum). The humeral cups in the present study wore on average approximately four times more than the single humeral cup in the pilot study. These wear rates were in the range of the highest levels of wear of 125 ± 32 mm^3/Mc found by Vaupel et al (2012) in the current published RTSA wear studies. Vaupel et al used a similar base serum but with a lower net protein concentration (21 g/L vs. 30 g/L) and no added HA. They also had a different motion (alternating between abduction-adduction and flexion-extension) and tested for 5 Mc in total. In a later study, the same research group (Peers et al, 2015) reported an overall wear rate of a lower magnitude of 83.6 ± 20.6 mm^3/Mc for the same specimens and test conditions. Peers et al did not comment on the lower wear rate found in this second study.

In testing without HA, Brandt et al (2013) showed that bovine calf serum produced significantly higher wear rates (up to 10 times) in the wear testing of total knee replacements than alpha calf serum having similar protein concentration (J. M. Brandt, Mahmoud, Koval, MacDonald, & Medley, 2013). This may be an explanation for the larger wear rate found by the present study compared the pilot wear test.

The pilot wear test also used a larger 42 mm diameter implant compared to the present study that included 38 mm diameter implants, which may have resulted in changes in articular contact mechanics. The previously described finite element analysis that compared the effect of glenosphere size on contact area and maximum contact stress showed that the larger implants did indeed have larger contact areas than the smaller 38 mm implants, although maximum contact stress was not much higher for smaller sizes. This may strengthen the argument that the increased wear rate of the present study was due mostly in part to the change in lubricant composition as suggested above.

When compared to all other published RTSA wear rates, the current study reports the highest mean wear rate, but it is important to note that all studies employed widely varying load and motion profiles, lubricant composition, and humeral cup material properties (Haider, Sperling, & Throckmorton, 2013; Kohut et al., 2012; Peers et al., 2015; Vaupel et al., 2012). None of the other studies incorporated HA in their lubricant composition, which Brandt et al (2013) also showed increased the wear rate of total knee replacements by approximately two times and Desjardins et al (2006) showed increased the wear rates by approximately seven times. The lubricant of Desjardins et al (2006) had bovine serum and HA in it which was similar to the lubricant of the present study, although their protein content was about double that of the present study.

The presence of wear on the inferiomedial edge of the cup is also of interest, as this location has been described in previous chapters to be important in terms of both load transfer across the articulation as it resists vertical translation of the humeral cup (and thus the arm) under the typically vertically oriented joint reaction forces. The inferior most edge of the cup was also found to be the location of maximum contact stress in finite element studies under representative loading, and as such, and appreciable material removal from this region of the cup is likely to have a detrimental effect on both contact mechanics and potentially the stability of the reconstructed joint.

The inferior aspect of the cup is also the location where wear and damage to the cup is most often reported for clinically retrieved RTSA implants. The humeral cups in the present study also exhibited the majority of wear and damage in the inferior quadrant of the cup, which may be in part due to the wear simulation strategy used in the present study that was specifically developed for the wear testing of RTSA implants and included load and motion profiles based on those measured in cadaveric testing of RTSA reconstructed shoulders. None of the other simulator wear studies referenced in the present thesis reported the appearance or locations of the wear zones and hence comparisons with other studies are not possible.

This study has limitations. First, the applied loading and relative motion represent only one combined motion which includes both adduction-abduction and flexion-extension.

While this motion is likely to be observed in-vivo, there will also be cases where each motion will occur individually, and the present wear simulation strategy does not include that possibility. Second, as with any in-vitro wear study there exists differences in both the rheology and biochemistry of the lubricant used in place of the natural synovial fluid. This is likely to have an impact on the net wear rates observed in these studies compared to in-vivo, although the results of the present study fell within previously published data and produced wear in the region most commonly found on clinically retrieved RTSA implants.

5.5   Conclusions

The present study describes the first full-scale wear test performed using the RTSA wear simulation strategy developed and described in the previous chapter. The mean wear rate was several times greater than that of the pilot wear test performed with a different base serum and larger sized implant. The wear rate was also higher than that of Vaupel etl al (2012) which was the highest of all the simulator wear tests of RTSA implant found in the literature.

It is expected that the difference compared to the pilot study is mainly due to the use of bovine calf serum rather than alpha calf serum. Regarding the higher wear rate compared to Vaupel et al (2012), bovine serum with HA has been shown to increase wear by about 7 times in knee simulator testing compared with just bovine serum (DesJardins et al, 2007). This massive increase suggested that bovine serum with HA may promote wear. Whether the HA in synovial fluid would promote wear of RTSA implants in-vivo is not known.

The location of the wear of the humeral cups in the present study agrees with wear observed on clinically retrieved RTSA implants. This suggests that the wear simulation strategy used in the current study subjects the wear couples to both loading and motion profiles which may be fairly representative of those occurring in-vivo for some patients. Further wear testing, particularly with alpha calf serum identical to the pilot wear study, should provide further insight into the differences in wear rates found in the present studies.

5.6 References

Brandt, J. M., Charron, K. D. J., MacDonald, S. J., & Medley, J. B. (2011). Mass gain behaviour of tibial polyethylene inserts during soak testing. Proceedings of the Institution of Mechanical Engineers. Part H, Journal of Engineering in Medicine, 225(3), 324–331. http://doi.org/10.1177/2041303310392629

Brandt, J. M., Mahmoud, K. K., Koval, S. F., MacDonald, S. J., & Medley, J. B. (2013). Antimicrobial agents and low-molecular weight polypeptides affect polyethylene wear in knee simulator testing. Tribology International, 65, 97–104. http://doi.org/10.1016/j.triboint.2013.02.019

Castagna, A., Delcogliano, M., de Caro, F., Ziveri, G., Borroni, M., Gumina, S., … De Biase, C. F. (2013). Conversion of shoulder arthroplasty to reverse implants: clinical and radiological results using a modular system. International Orthopaedics, 37(7), 1297–1305. http://doi.org/10.1007/s00264-013-1907-4

Day, J. S., MacDonald, D. W., Olsen, M., Getz, C., Williams, G. R., & Kurtz, S. M. (2012). Polyethylene wear in retrieved reverse total shoulder components. Journal of Shoulder and Elbow Surgery, 21(5), 667–674. http://dx.doi.org/10.1016/j.jse.2011.03.012

DesJardins, J., Aurora, a, Tanner, S. L., Pace, T. B., Acampora, K. B., & Laberge, M. (2006). Increased total knee arthroplasty ultra-high molecular weight polyethylene wear using a clinically relevant hyaluronic acid simulator lubricant. Proceedings of the Institution of Mechanical Engineers. Part H, Journal of Engineering in Medicine, 220(5), 609–623. http://doi.org/10.1243/09544119JEIM30

Flury, M. P., Frey, P., Goldhahn, J., Schwyzer, H. K., & Simmen, B. R. (2011). Reverse shoulder arthroplasty as a salvage procedure for failed conventional shoulder replacement due to cuff failure--midterm results. International Orthopaedics, 35(1), 53–60. http://doi.org/10.1007/s00264-010-0990-z

Frankle, M., Levy, J. C., Pupello, D., Siegal, S., Saleem, A., Mighell, M., & Vasey, M. (2006). The reverse shoulder prosthesis for glenohumeral arthritis associated with severe rotator cuff deficiency. a minimum two-year follow-up study of sixty patients surgical technique. The Journal of Bone and Joint Surgery. American Volume, 88 Suppl 1(July 2015), 178–190. http://doi.org/10.2106/JBJS.D.02813

Haider, H., Sperling, J., & Throckmorton, T. (2013). A method for wear testing of reverse shoulder arthroplasty systems. Bone Joint J., Vol. 95-B, SUPP 34 (607).

Kohut, G., Dallmann, F., & Irlenbusch, U. (2012). Wear-induced loss of mass in reversed total shoulder arthroplasty with conventional and inverted bearing materials. Journal of Biomechanics, 45(3), 469–473. http://doi.org/10.1016/j.jbiomech.2011.11.055

Nam, D., Kepler, C. K., Nho, S. J., Craig, E. V., Warren, R. F., & Wright, T. M. (2010). Observations on retrieved humeral polyethylene components from reverse total shoulder arthroplasty. Journal of Shoulder and Elbow Surgery, 19(7), 1003. http://doi.org/http://dx.doi.org/10.1016/j.jse.2010.05.014

Peers, S., Moravek Jr., J. E., Budge, M. D., Newton, M. D., Kurdziel, M. D., Baker, K. C., … Wiater, J. M. (2015). Wear rates of highly cross-linked polyethylene humeral liners subjected to alternating cycles of glenohumeral flexion and abduction. Journal of Shoulder and Elbow Surgery, 24(1), 143–149. http://doi.org/http://dx.doi.org/10.1016/j.jse.2014.05.001

Teeter, M. G., Langohr, G. D. G., Medley, J. B., & Holdsworth, D. W. (2014). Nondestructive microimaging during preclinical pin-on-plate testing of novel materials for arthroplasty. Proceedings of the Institution of Mechanical Engineers, Part H: Journal of Engineering in Medicine, 228(2), 159–164. http://doi.org/10.1177/0954411914522615

Terrier, A., Merlini, F., Pioletti, D. P., & Farron, A. (2009). Comparison of polyethylene wear in anatomical and reversed shoulder prostheses. The Journal of Bone and Joint surgery. British Volume, 91(7), 977–982. http://doi.org/10.1302/0301-620X.91B7.21999

Vaupel, Z. M., Baker, K. C., Kurdziel, M. D., & Wiater, J. M. (2012). Wear simulation of reverse total shoulder arthroplasty systems: effect of glenosphere design. Journal of Shoulder and Elbow Surgery, 21(10), 1422–1429. http://doi.org/http://dx.doi.org/10.1016/j.jse.2011.10.024

Chapter 6

6   Thesis Closure

OVERVIEW

This concluding chapter summarizes the objectives and hypotheses outlined in the introductory chapter, and discusses the studies performed to accomplish these objectives, as well as the findings of these works. The strengths and limitations of the present works are explored and the future research directions regarding the wear simulation strategy are proposed.

6.1   Summary and Conclusions

In order to further understand the functional characteristics of RTSA performance and in particular implant wear, it is essential to study both the biomechanics and the tribology of these implant systems, as well as the relationships between these two aspects of RTSA performance. An effective means by which to evaluate RTSA biomechanics is to use in-vitro cadaveric simulator testing, a method that the current thesis used in conjunction with a custom instrumented RTSA implant device that allowed for the direct measurement of joint loading. RTSA tribology was investigated using a combination of finite element methods to study articular contact area and stress, as well as simulator wear testing where load and relative motion are imparted to RTSA implants and the resulting wear is measured and characterized.

The first objective of this research was to develop a means by which to investigate RTSA joint loading characteristics using an in-vitro shoulder joint motion simulator (Objective 1), and then to evaluate the effect changes in implant parameters (Objectives 1a through 1c). Objectives 1a through 1c were achieved by making an instrumented implant system that permitted the measurement of joint forces, which was modular in that the key implant geometry parameters such as neck-shaft angle, cup depth, and glenosphere diameter could be easily modified so as to allow for the repeated testing with varying implant parameters.

The results of this study as described in Chapter 2 gave the first major conclusion: decreasing neck-shaft angle did not affect joint load or muscle forces but did increase adduction range of motion. This confirmed Hypothesis 1a although there was no difference detected between the 145° and 135° neck-shaft angle. The second major conclusion was also established: decreasing cup depth was also found to not alter joint load, muscle force or range of motion. This agreed with Hypothesis 1b(i), but the lack of effect on range of motion contradicted Hypothesis 1b(ii). This lack of effect on range of motion may have been due to the inferior position of the glenosphere used in the present study, which could have reduced the chance of inferior impingement enough that cup depth effects were not found for the present study population. The third major conclusion was: increasing glenosphere diameter increased the range of motion, particularly in

adduction and the joint load increased for the 42 mm diameter compared with the smaller 38 mm diameter. This contradicted Hypothesis 1c, although it was also found that the larger 42 mm implant used in the present study resulted in a small increase in the distance between the centre of rotation to the backside of the humeral cup (ie. an increase in apparent cup thickness), which was thought to be the cause of this increase as it resulted in a reduction in deltoid mechanical advantage.

The second objective of the present thesis was to investigate the contact mechanics of RTSA implants in terms of the magnitudes and locations of both contact area and contact stress, and ascertain the effects of changes in implant configuration (neck-shaft angle, cup depth, and glenosphere diameter). The results of this study are outlined in Chapter 3, and gave the fourth major conclusion: the location of both the contact patch and the peak contact stress was typically found in the inferior quadrant of the humeral cup. This was in agreement with Hypothesis 2a and was coincident with the most common location of damage found on RTSA clinical retrievals.

The results also gave the fifth major conclusion: the implant configurations which were best for RTSA contact mechanics were those having higher neck-shaft angles, deeper cup depths, and larger glenosphere diameters. This was in agreement with Hypothesis 2b. While reducing neck-shaft angle can improve adduction range of motion, as shown in Chapter 2, it was also found that reducing neck-shaft angle also results in large reductions in contact area and increases in peak contact stress, which could negatively affect wear performance. Decreasing cup depth has been shown in the literature to increase range of motion, although this was not found in the results of Chapter 2. However, the results of Chapter 3 showed that decreased cup depth results in reduced contact area and increased peak contact stress, which might have negative effects on long term implant performance. Increasing glenosphere diameter can increase adduction range of motion (Chapter 2), and the results of Chapter 3 show that this comes at no cost in terms of contact mechanics for quasi-static abduction motions, with the larger glenosphere providing increased contact area, with similar values for peak contact stress.

The third objective of this research was to develop a means by which to perform in-vitro wear simulator studies of RTSA implants in a manner that was representative of the in-vivo state (Chapter 4). This chapter showed that, in agreement with Hypothesis 3a, the load angles with respect to the glenosphere were typically superiorly oriented and with respect to the humeral cup were typically inferiorly oriented during abduction. The resulting wear simulation strategy developed using load magnitude and angle data obtained from the agglomeration of the instrumented RTSA reconstructed cadaveric shoulders investigated in Chapter 2 gave the sixth major conclusion: wear zones and cup damage in the inferior quadrant during the pilot wear test agreed with the location of wear and damage on clinically retrieved humeral cups. This conclusion agreed with Hypothesis 3b and gave confidence that the developed wear simulation strategy represented loads and motions which could be reasonable expected to occur in-vivo. This study also initiated the investigation as to whether damage due to scapular notching and wear of the intended articular surface interacted, and found that for relatively minor cup damage. The seventh major conclusion followed: a large difference in wear rate was not found for the single cup subjected to simulated scapular notch damage in the pilot wear study. However, this conclusion might change for larger degree of cup damage or with the testing of more implants.

The fourth objective was to perform a full scale, multi-specimen wear study with the wear simulation strategy developed in Chapter 4. The results of Chapter 5 describe the wear study of the standard 38 mm RTSA implants and gave the eighth major conclusion: a mean wear rate of 201.1 ± 86.5 mm^3/Mc occurred. This was considerably larger than the highest wear rate reported in previously published wear simulator testing using a variety of different load and motion profiles and thus contradicted Hypothesis 4. This might have been a consequence of using HA in the lubricant, a condition that was known to occur in vivo but was not included in any other simulator wear test protocol for RTSA implants. The wear scar and majority of wear occurred in the inferior aspect of the cup, which again agreed with the location of wear most commonly noted on clinical retrievals. However, clinical retrievals often had both wear and scapular notching damage whereas the present study only had wear. Thus, comparisons with clinical retrievals were difficult to make. In any case, this finding of high wear rates was very disconcerting and

suggested that clinical problems related to wear for RTSA might become more apparent in the future.

An additional, and final objective (that was summarized in Appendix B) was to estimate the average motion of an RTSA reconstructed shoulder in an effort to link the number of 'cycles' tested during in-vitro wear simulation to the number of years in-vivo. The results of this study showed that the number of 'cycles' per year are heavily dependent on what elevation angle is selected as a threshold as to what defines a cycle. However the ninth major conclusion could be made: for an elevation threshold of 80°, the extrapolated number of cycles per year was approximately 330,000, however for an elevation threshold of 60° the extrapolated number of cycles becomes approximately 1.5 million. Because the upper extremities are not used for human locomotion, there is no way of defining a 'gait cycle' which represents one step as is done in the lower extremity. Instead we are left defining the number of cycles to different humeral elevations. The humeral elevation thresholds of 60° and 80° are two reasonable limits that could be selected to represent motions which are significant enough to denote a unique and desired motion of the shoulder while ignoring small changes in humeral elevation during such activities as walking or sitting still which are unlikely to constitute a shoulder 'cycle'. Based on the numbers of cycles per year at these two humeral elevation thresholds, it appears that the shoulder is cycled at similar orders of magnitude as the lower extremities, although for higher elevation thresholds they may be used comparatively less.

The present work represents advancement in the current state of knowledge regarding RTSA biomechanics and tribology, and in particular, the effect of changes in implant configuration on the articular contact mechanics of the device. It is interesting to note the specific tradeoffs in terms of range of motion and contact mechanics that was observed for the reduction of both neck-shaft angle and cup depth, whereby increases in range of motion came at the cost of reduced contact area and increased peak contact stress. Increasing glenosphere diameter was found to increase range of motion without any negative consequences in terms of contact mechanics, and as such this clinical practice can be performed without sacrificing potential long term implant performance.

6.2 Strengths and Limitations

The incorporation of articular joint loading characteristics into the development and implementation of an RTSA wear simulation strategy represents a step forward for the in-vitro wear testing of RTSA implants. The measurement of RTSA joint loading in an actively controlled shoulder simulator yielded important insight which was used in the development of the load for wear simulation. Because joint loading was directly measured through the insertion of a load sensing device directly using a custom implant, as well as obtaining data from a population of cadaveric shoulders, the data obtained was well representative of what could reasonably be expected to be imparted to implants in-vivo.

However, the loads measured in the present thesis were used in an averaging procedure to obtain the proposed load conditions for wear simulator testing. Then, the load magnitudes were increased to obtain a more severe loading condition. Alternatively, the loads obtained in the present thesis could have been used alone to directly define the load conditions. The sensitivity of wear to the load conditions were not explored in the present thesis but this should be done in the future. The present wear simulation strategy produced damage coincident with where it is most commonly observed on clinical retrievals but wear rates that were higher than previously published wear studies.

The investigation of RTSA contact mechanics using a finite element model allowed for the measurement and visualization of the distribution of contact stress across the articular surface, something which is not physically possible using laboratory methods without the insertion of a pressure transducer film which alters the articular contact mechanics. This also allowed for each abduction level to be repeatedly investigated using all possible combinations of RTSA implant configurations and compared. This provided insight into the effect of these changes on RTSA contact mechanics throughout abduction.

There were also some limitations of the present work. First, the RTSA joint loading data were obtained using cadaveric shoulders mounted to a shoulder joint simulator which introduced some error into the measured joint load and joint load angles due to the assumptions made with respect to the apportioning of the applied muscle group.

However, it was not considered unreasonable to assume that the muscle ratios used during the shoulder joint simulator testing were indicative of what could be observed in a subset of reconstructed shoulders in-vivo. Second, the finite element model made several assumptions regarding the contact between the glenosphere and the humeral cup. The overall influence of these assumptions was expected to be reasonably small as justified by acceptably small error found when finite element model predictions were compared with those of the theoretical Hertzian contact model for both contact area and peak contact stress. Third, the wear simulation strategy used a motion profile which combined flexion-extension and adduction-abduction motion to produce a circumduction motion profile. This was done because the wear testing frame produced biaxial rocking which inherently required the linking of these two physiologic motions. While the shoulder joint could certainly achieve these motions independently, the current wear simulation strategy did not allow for the independent investigation of motion. While this may be viewed as a limitation, it is important to note that the shoulder is subjected to a variety of different motions, some of which are surely independent, and some of which are surely combined. Therefore the combination of motions in the described wear simulation strategy was thought to effectively represent the wide range and variety of motion that the shoulder would be required to perform.

6.3 Future Directions

The current wear simulation strategy has achieved the specific objectives outlined at the beginning of this thesis, however there still exists the opportunity to further investigate the tribology of RTSA implants.

First, the present work describes a pilot wear study and a full scale study of standard cups configured for a standard neck-shaft angle (155°), cup depth, and glenosphere size. There still exists the need to perform wear testing for RTSA variants investigated in Chapters 2 & 3 of the current work. This includes reductions in neck-shaft angle (145° & 135°), changes in cup depth (shallow and deep), and a full scale test of larger glenosphere diameters (42 mm). This could easily be accommodated by simply inserting implants of

varying cup depths and sizes, and alterations of the humeral cup fixtures for different neck-shaft angles.

Second, through the use of micro-CT techniques to obtain wear morphology, the 3D geometry of each humeral cup is easily obtainable, the worn geometry of which could then by imported into a finite element model to allow for the investigation of contact area and contact stress distributions as wear progresses during testing. This could yield insight into how the contact mechanics of the humeral cup change as wear and implantation length increases. Furthermore, this could be extended to investigate the potential relationships between inferiomedial cup damage and wear of the intended articular surface in a similar fashion where damaged cup geometry is imported into the computational model.

Finally, after the completion of wear testing of all RTSA implant variants, as well as the finite element modeling of the progression of articular contact mechanics during the wear process, an optimization process could be performed to identify the optimal RTSA implant parameters to produce the best contact mechanics and lower wear rates. Furthermore, the actual articular geometry could also be optimized to produce the optimal contact mechanics using finite element modeling to provide guidance, and then prototype humeral cups could then be investigated using the wear simulation strategy.

6.4   Significance

As the prevalence of RTSA reconstruction continues to increase, a greater understanding of the effects of changes in implant configuration, some of which can be selected at the time of implantation, are of paramount interest as they can affect long term implant performance. The present work shows the importance of taking into consideration the potential consequences of implant parameter selection on contact mechanics in addition to the benefits of such selections on shoulder range of motion. Furthermore, understanding the effects of current implant parameter selection may aid in the development of improved articular geometry in future RTSA implant design iterations.

The ability to assess the wear of joint replacement implants in-vitro is also important to implant design as process can yield insight into both the expected life of the implant in-vivo, as well as help improve the current state of implant technology by allowing the wear of different materials and articular geometries to be assessed. This will result in an overall improvement in RTSA implant technology, as well as a greater understanding of the pending clinical performance of implants currently in use.

Appendix A - Index of Terminology

Abduction: To draw away from the median plane, specifically, in the plane of the scapula.

Adduction: To draw towards the median plane, specifically, in the plane of the scapula.

Acromion: The lateral extension of the spine of the scapula, forming the highest point of the shoulder. Adj. acromio-

Analysis of Variance (ANOVA): A statistical method for making simultaneous comparisons between two or more means; a statistical method that yields values that can be tested to determine whether a significant relation exists between variables.

Anterior: Situated at or directed toward the front; opposite of posterior. Adj. antero-

Arthroplasty: Repair of a joint by implanting an artificial component.

Articular: Pertaining to a joint.

Articular cartilage: A specialized, fibrous connective tissue present in adults lining the articular surface of synovial joints.

Articulation: A joint; the place of union or junction between two or more bones of the skeleton.

Axial plane: See 'Transverse plane'.

Biomechanics: The study of the mechanical laws relating to the movement or structure of living organisms.

Cadaveric: Pertaining to a human body preserved for anatomical study.

Cancellous: Of or denoting bone tissue with a mesh-like structure containing many pores, typical of the interior of mature bones.

Cartilage: A specialized, fibrous connective tissue present in adults, and forming the temporary skeleton in the embryo, providing a model in which the bones develop, and constituting a part of the organisms joint mechanism.

Contact mechanics: The study of the deformation of solids that touch each other at one or more points.

Coronal plane: A vertical plane, at right angles to a sagittal plane, dividing the body into anterior and posterior portions.

Degree of freedom (DOF): In kinematic and kinetic analysis, a manner in which a motion or force can occur. For two DOF to be independent, they must be defined about two perpendicular axes.

Deltoid: Muscle which abducts, flexes or extends the arm.

Elevation: To move away from the body.

Extension: The movement by which the two ends of any jointed part are drawn away from each other; the bringing of the members of a limb into or toward a straight condition. [Motion in the vertical plane perpendicular to the plane of the scapula (Wuelker et al., 1998)]

External rotation: Rotation about the longitudinal axis of the humerus laterally.

Finite element analysis (FEA): A method which discretizes a continuous object into many small 'finite' pieces that can then be analyzed individually using traditional mechanics equations to determine the overall load and displacement of the object.

Flexion: Elevation in the sagittal plane of the body.

Glenohumeral: Pertaining to the glenoid and humerus.

Glenoid: A fossa located on the lateral scapula resembling a pit or socket. Adj. gleno-

Glenosphere: The hemispherical ball placed on the glenoid to reverse the anatomy of the shoulder during Reverse Total Shoulder Arthroplasty.

Humerothoracic: Relating to the humerus and thorax.

Humerus: Long bone of upper arm. Adj. humero-

Impingement: When two bones contact each other in a pathological manner.

Inferior: Situated below, or directed downward; in anatomy, used in reference to the lower surface of a structure, or to the lower of two (or more) similar structures. Adj. infra- or infero-

Inferiorization: In Reverse Total Shoulder Arthroplasty, movement of the center of rotation of the shoulder joint in the inferior direction.

Infraspinatus: Muscle originating on the posterior scapula which rotates the arm laterally.

Instability: A pathologic condition in which there is an inability to maintain the normal relationship of the humeral head on the glenoid fossa.

Internal rotation: Rotation about the longitudinal axis of the humerus medially.

***In-silico*:** Performed on computer or via computer simulation

***In-vitro*:** In an artificial environment.

***In-vivo*:** Within the living body.

Kinematics: Description of an objects motion without consideration for the forces causing it.

Lateral: Denoting a position farther from the median plane or midline of the body or a structure.

Lateralization: In Reverse Total Shoulder Arthroplasty, movement of the center of rotation

of the shoulder joint or the humeral head in the lateral direction.

Ligament: A band of fibrous tissue connecting bones or cartilages, serving to support and strengthen joints. Adj. ligamentous.

Mechanical Advantage: Increasing the effectiveness of a force by applying it at a distance.

Medial: Situated toward the midline of the body or a structure. Adj. medio222

Medialization: In Reverse Total Shoulder Arthroplasty, movement of the center of rotationof the shoulder joint in the medial direction.

Moment: The tendency of a force to rotate an object about an axis when that forces is applied at a distance (also known as Torque).

Moment arm: The perpendicular distance between a force and the axis it is causing a moment about.

Muscle: An organ which by contraction produces movement of an animal organism. Adj.

muscular and musculo-.

Orthopaedics: That branch of surgery dealing with the preservation and restoration of the function of the skeletal system, its articulations, and associated structures.

Physiological: Normal, not pathologic.

Plane of elevation: A rotation degree of freedom which defines the plane in which the arm will elevate in.

Posterior: Directed towards, or situated at the back; opposite of anterior. Adj. postero-

Proximal: Nearest to the point of reference, as to a center or median line or to the point of attachment or origin.

Quasi-static: A condition in which a body is moving but at a rate for which the effects of

acceleration and inertia can be neglected.

Range of motion: The arc of motion that a joint possess.

Retroversion: Tipping backward.

Rigid body: An idealization of a solid body in which deformation is neglected

Rotator cuff: Group of muscles surrounding the glenohumeral joint, consisting of the supraspinatus, subscapularis, infraspinatus and teres minor muscles.

Sagittal plane: A longitudinal vertical plane that divides the body into left and right segments.

Scapula: Wide, thin, triangular bone (shoulder blade) opposite second to seventh ribs in upper part of back. Adj. scapular or scapulo-

Scapulohumeral: Pertaining to the scapula and humerus.

Scapulothoracic: Pertaining to the scapula and thorax.

Shear: A motion or force parallel to the face of an object.

Subscapularis: Muscle which rotates the arm medially.

Superior: Situated above, or directed upward. Adj. supra225

Supraspinatus: Muscle which originates at the supraspinatus fossa and abducts the arm.

Synovial joint: An articulation permitting more of less free motion, the union of the bony elements being surrounded by an articular capsule enclosing a cavity lined by synovial membrane.

Tendon: A fibrous cord of connective tissue continuous with the fibres of a muscle and attaching the muscle to bone or cartilage. Adj. tendinous

Teres minor: Muscle which originates on lateral border of the scapular and rotates the arm laterally.**Thorax:** The chest.

Torso: See Thorax.

Transverse: Extending from side to side; at right angles to the long axis.

Version: In scapular motion, the rotation about a superoinferior axis which causes the

glenoid to face anterior (ante-) or posterior (retro-).

Appendix B - Daily Motion of Arthroplasty Reconstructed Shoulders

OVERVIEW

This appendix describes the development and implementation of a wearable shoulder motion measurement apparatus that was worn by human subjects after total shoulder arthroplasty (both primary and reverse). The magnitude of shoulder motion was determined for both the operated and non-operated side and compared. The motion of the operated side was extrapolated to provide insight into how many cycles a shoulder arthroplasty implant is subjected to during the average year.

B.1   Introduction

Shoulder arthroplasty, both primary (TSA) and reverse (RTSA), are common interventions for arthritis and cuff tear arthropathy. The daily magnitude of total shoulder motion, and furthermore the effect of shoulder arthroplasty on shoulder motion is of particular interest in assessing the effectiveness of the procedure and the development and biomechanical testing of implants. A comparison of the arthroplasty shoulder to that of the non-operated contralateral shoulder may also provide insight into how well the reconstruction has restored natural shoulder motion. A greater understanding of shoulder motion during normal daily activity would assist in the design and testing of shoulder prostheses, providing insight into how many 'cycles' an 'average' shoulder experiences. The purpose of this study was to ascertain i) the shoulder motion of patients who have undergone shoulder arthroplasty, ii) to compare the motion of the reconstructed shoulder to that of the contralateral natural joint, and iii) to estimate the number of 'cycles' an 'avearge' reconstructed shoulder performs each year. We hypothesized that the operated shoulder would perform less motion than the non-operated side, and similar to the lower extremities, the estimated average number of shoulder cycles per year will range between 1-2 Mc.

B.2   Materials & Methods

A wearable shoulder motion tracking apparatus was developed which incorporated five sensors; one located on the torso and one on each humerus and one on each forearm (Figure B-1), each using a tri-axial accelerometer, gyroscope, and compass to measure its orientation in space. Sensors were held securely using pockets sewn into a compression shirt which ensured that the sensors moved with the extremities as effectively as possible without imparting excessive discomfort to the user. The data from the forearm trackers were not used in the present study, but were used in studies regarding elbow motion.

The 3D orientation of each humerus sensor was first synchronized by 'zeroing' the sensors to all have the same reference vectors. The orientations were then transformed with respect to the torso to allow for the calculation of humeral elevation and plane of elevation angles. Joint angles for each subject were then discretized by identifying the peaks and valleys of humeral elevation using custom written software, and the resulting shoulder motion was then determined. The position and motion of operated and non-operated shoulders were then compared.

Eleven human subjects (70±9yrs) who had undergone shoulder arthroplasty (5 TSA;6 RTSA) wore a custom instrumented shirt measuring shoulder position for the waking hours of one day.

Figure B-1 Custom instrumented wearable shoulder motion tracking apparatus
Showing modified compression shirt with motion sensors inserted at the torso, humeri, and forearms.

B.3　　　　Results

The majority of both the arthroplasty and control shoulder elevation motions took place below 80° of elevation, totaling on average 1910±373 and 1887±312 motions per hour, respectively. Conversely, elevations greater than 80° were significantly less occurring totaling only 55±31 and 78±41 motions per hour for the arthroplasty and control shoulders, respectively ($p < 0.01$, Figure B-2).

Both the arthroplasty and control shoulder were at elevations below 80°for 98±26% and 97±20% of the day, respectively. When the total motion of the arthroplasty and non-operative control shoulders were compared, no statistically significant difference was detected ($p = 0.788$), although the non-operated side exhibited marginally more motion than the operated side, an effect which was larger at higher elevation angles ($p = 0.309$, Figure B-2).

The most common range of humeral elevation was 0°-60° for both the left and right shoulder ($p < 0.05$, Figure B-3), which represented on average 88±26% and 88±19% of the total day, respectively. The most frequent humeral plane of elevation range was -10° to 70° for both the left and right shoulder (Figure B-4), which was observed for 71±23 % and 72±31% of the day respectively. No significant difference was detected between dominant and non-dominant hands ($p = 0.9$).

When the daily shoulder motions were discretized, humeral elevations in the 0°-20° and 20°-40° range represented the majority of shoulder motions ($p < 0.05$,Figure B-2). The number of elevation events that were greater than 80° were significantly lower than the elevation events which occurred below 80° ($p < 0.01$). On average, the left and right shoulders were only elevated to angles greater than 100° 17±5 and 24±10 times per hour.

Figure B-2: Mean (± 1 stdev) number of humeral elevation motions per hour discretized by level of elevation for the operated (left) and non-operated side (right)
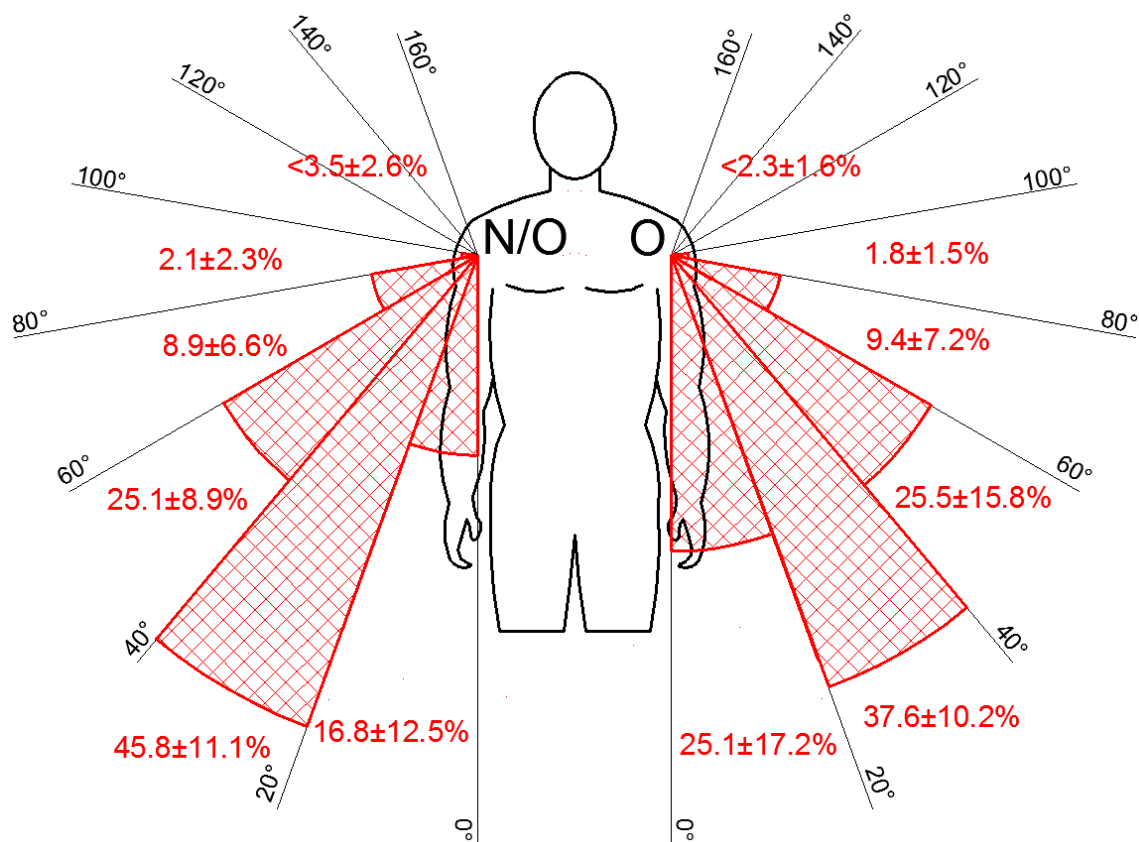
Figure B-3: Mean (± 1 stdev) percentage of total day spent at each abduction
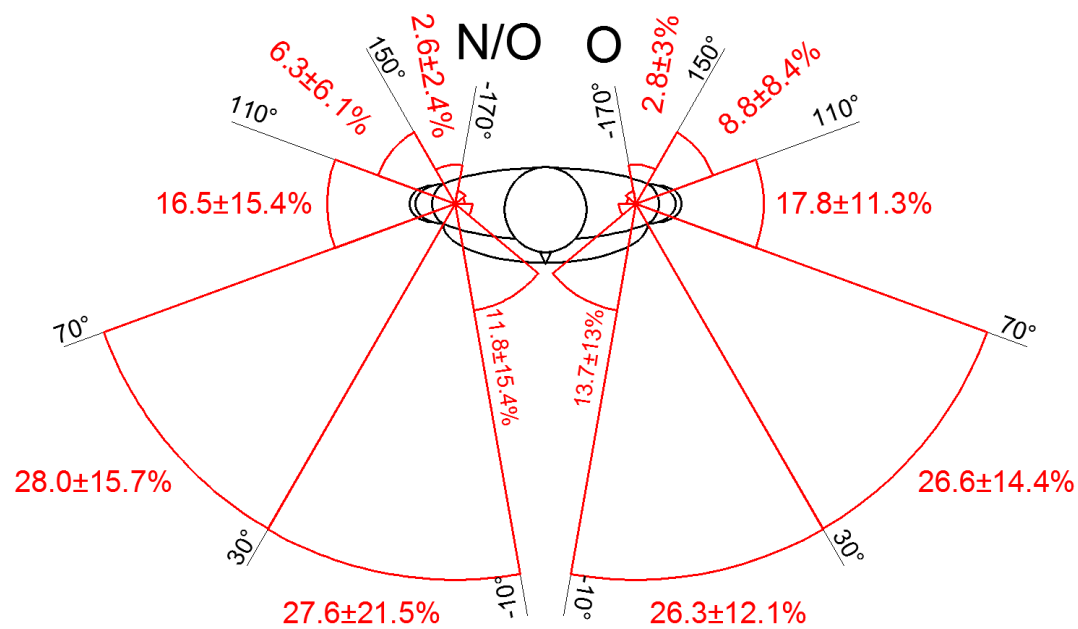
Figure B-4: Mean (± 1 stdev) percentage of total day spent at each plane of elevation

B.4   Discussion

This study provides insight into the effects of shoulder arthroplasty on thoraco-humeral motion and compares it to the non-operative side. Interestingly, there were no significant differences measured between the arthroplasty and the control side, which may demonstrate the effectiveness of reconstruction on restoring natural shoulder motion. It is interesting to note that on average, each shoulder arthroplasty elevated above 80° approximately 55 times per hour, corresponding to just under 330,000 motions per year. Similarly, when elevations greater than 60° are extrapolated, the resulting yearly motions total approximately 1.5 million cycles (Mc), which suggests that the 'duty cycle' of the shoulder is similar to the hip, approximated to be between 1-2 Mc per year.

Arthroplasty wear simulators should be calibrated to simulate these patterns of motion, and component design may be improved by understanding the kinematics of actual shoulder motion.

B.5   Conclusions

Novel insight into the duty cycle of a healthy shoulder is described. This will help in the assessment of ergonomic design, recreational tasks and occupational demands. Additionally, this information may assist design and testing for shoulder arthroplasty prostheses, enabling testing in more realistic patterns of motion for wear and durability testing. Mean shoulder motion after arthroplasty is not significantly different than the contralateral normal side. The number of shoulder arthroplasty elevations greater than 60° approach 1.5 Mc per year.

CURRICULUM VITAE
G. DANIEL LANGOHR MASc

Vanier Canada Graduate Scholar
CIHR Graduate Research Fellow
The Hand and Upper Limb Clinic
Lawson Health Research Institute, St. Josephs Hospital

PhD Candidate
Biomedical Engineering Graduate Program
The University of Western Ontario

EDUCATION

2011 - Candidate for PhD (Biomedical Engineering), *Vanier Scholar, CIHR Graduate Fellow in Musculoskeletal Research: Shoulder Implant Wear and Design*
The University of Western Ontario, London Canada

2009 – 2011 MASc (Mechanical Engineering) 2011
Design of a Cervical Total Level Arthroplasty System with all-polymer PEEK Articulations
University of Waterloo, Waterloo Canada

2003 – 2008 BASc (Mechanical Engineering, Management Sciences Option) 2008
Graduated with Distinction and Dean's Honors List Designation
University of Waterloo, Waterloo Canada

POSITIONS

2011 – **The University of Western Ontario**
Research Assistant to Dr. Jim A. Johnson PhD
Department of Biomedical Engineering
The Hand and Upper Limb Clinic, Lawson Health Research Institute

2011 – **The University of Western Ontario**
Teaching Assistant (Thermodynamics, Engineering Design Studio, Engineering Biomechanics, Component Design, Advanced Design)
Department of Mechanical and Materials Engineering

2013 – **Department of Biomedical Engineering**
Chair, BME Student Committee
Faculty of Engineering, The University of Western Ontario

2013 – 2014	**The University of Western Ontario Summer Academy** *Organizer/Manager for Biomedical Engineering Program / Lecturer* Summer Engineering Academy, Biomedical Engineering Outreach Program, Western Engineering
2011 – 2012	**The University of Western Ontario Summer Academy** *Lecturer / Lab Instructor* Summer Engineering Academy, Biomedical Engineering Outreach Program, Western Engineering
2008 –	**University of Waterloo** *Research Assistant to Dr. John B. Medley PhD (Wear & Design of Orthopaedic Implants)* Department of Mechanical and Mechatronics Engineering
2008 – 2010	**University of Waterloo** *Teaching Assistant (Mechanics, Dynamics, Biomechanics)* Department of Mechanical and Mechatronics Engineering
2007 – 2010	**General Motors of Canada Ltd.** St. Catharines ON Canada *Weekend Maintenance/Production Group Leader and Mechanical Engineer* High Feature V6 Engine Machining and Assembly
2008 – 2008	**General Motors of Canada Ltd.** St. Catharines ON Canada *Industrial Engineer* GEN IV V8 Engine Machining and Assembly
2006 – 2007	**General Motors of Canada Ltd.** St. Catharines ON Canada *Mechanical Engineering Co-op (Three Four-Month Terms)*
2004 – 2005	**Abibiti Consolidated Paper Division** Thorold ON Canada *Predictive Maintenance Mechanical Engineering Co-op (Three Four-Month Terms)*

HONOURS and AWARDS

2012 – 2015	**NSERC Vanier Canada Graduate Scholarship ($150,000)** National Scholarship (1 of 53 awarded), The University of Western Ontario
2012 – 2015	**NSERC Alexander Graham Bell Canada Graduate Scholarship (Declined) ($105,000)** National Scholarship, The University of Western Ontario
2014	**Residents Research Day Best Podium Presenter Award ($500)** Institutional Research Day Award, London Health Sciences, London, Ontario
2012 - 2013	**Ontario Graduate Scholarship (Declined) ($15,000)** Provincial Scholarship, The University of Western Ontario
2012	**AMTI Force and Motion Foundation Travel Award ($500)** Industry Foundation Travel Grant, AMTI, Force and Motion Foundation

2011 – 2014	**CIHR Graduate Research Fellowship in Musculoskeletal Research ($23,000)** The University of Western Ontario
2011 – 2012	**Ontario Graduate Scholarship ($15,000)** Provincial Scholarship, The University of Western Ontario
2011	**Margaret Moffat Research Day Best Paper Award ($500)** Schulich School of Medicine and Dentistry Research Award
2010 – 2011	**Ontario Graduate Scholarship ($15,000)** Provincial Scholarship, University of Waterloo and The University of Western Ontario
2010 – 2011	**President's Graduate Scholarship ($10,000)** University of Waterloo Academic Award
2010	**Arthur F. Church Graduate Scholarship in Mechanical Engineering ($5,000)** University of Waterloo Academic and Research Award
2009 – 2010	**Mechanical Engineering Outstanding TA Award x3 ($150)** University of Waterloo Teaching Award
2009 – 2010	**President's Graduate Scholarship ($10,000)** University of Waterloo Academic Award
2009 – 2010	**NSERC Alexander Graham Bell Canada Graduate Scholarship ($17,500)** National Scholarship, University of Waterloo
2009 – 2010	**Ontario Graduate Scholarship (Declined) ($15,000)** Provincial Scholarship, University of Waterloo
2009 – 2010	**Graduate Research Scholarship x5 ($3,750)** University of Waterloo Research Award
2008	**Undergraduate Upper Year Scholarship ($1,000)** University of Waterloo Award for Academic Ranking of 1st out of 87 students
2003	**Ontario Scholarship ($500)** Provincial Academic Award

PUBLICATIONS and PRESENTATIONS

A   Peer Reviewed Journal Manuscripts
In Preparation for Submission

1. Johnson, A.J., **Langohr, G.D.G.**, King, G.J.W., Johnson, J.A. The Effect of Material Selection on Radial Head Hemiarthroplasty Joint Contact Mechanics Using Patient Specific Geometry. *For Submission to The Journal of Clinical Biomechanics 2015.*

2. Khayat, A,. **Langohr, G.D.G.**, Lalone, E.A., Willing, R., Medley, J.B., King, G.J.W., Johnson, J.A. The Effect of Pin Geometry on Early Cartilage Wear in Linear Reciprocal Motion. *For Submission to Engineering in Medicine 2015.*

3. Knowles, N.K., **Langohr, G.D.G.**, Athwal, G.S.A., Ferreira, L.M. A Finite Element Analysis of Augmented Glenoid Components. *For Submission to The Journal of Shoulder and Elbow Surgery 2015.*

4. Razfar, N., Reeves, J., **Langohr, G.D.G.**, Willing, R., Athwal, G.S, Johnson, J.A. Comparison of Proximal Humeral Bone Stresses Between Stemless, Short and Standard Stem Length. *Submitted to The Journal of Shoulder and Elbow Surgery 2015*.

5. Reeves, J., Razfar, N., **Langohr, G.D.G**., Athwal, G.A., King, G.J.W., Johnson, J.A. The Effect of Positioning of Partial Joint Resurfacing Implants on the Contact Mechanics of the Mating Cartilage. *For Submission to Clinical Biomechanics 2015.*

Submitted
1. **Langohr, G.D.G.,** Athwal, G.S.A., Johnson, J.A., Medley, J.B. Wear Simulation Strategies for the Reverse Shoulder Implant. *For Submission to The Journal of Engineering in Medicine 2015*

Published and in press
1. **Langohr, G.D.G.**, Willing, R., Medley, J.B., Athwal, G.S.A., Johnson, J.A. Contact Mechanics of Reverse Total Shoulder Arthroplasty During Abduction: The Effect of Head-Neck / Neck-Shaft Angle, Humeral Cup Depth, and Glenosphere Diameter. *Accepted with Revisions to the Journal of Shoulder and Elbow Surgery.*

2. **Langohr, G.D.G.**, Willing, R., Medley J.B., King, G.J.W., Johnson, J.A. The Effect of Radial Head Hemiarthroplasty Geometry on Proximal Radioulnar Joint Contact Mechanics. *Accepted with Revisions to the Journal of Shoulder and Elbow Surgery*.

3. Giles, J.W.G., **Langohr, G.D.G.**, Johnson, J.A., Athwal, G.S.A. The Influence of Reverse Shoulder Arthroplasty Implant Geometric Variables on Deltoid Muscle Activation, Joint Load and Shoulder Function- An In-vitro Study. *Accepted to the Journal of Clinical Orthopedics and Related Research.*

4. **Langohr, G.D.G.**, Willing, R., Medley, J.B., King, G.J.W., Johnson, J.A. Contact Analysis of the Native Radiocapitellar Joint Compared with Axisymmetric and Non-Axisymmetric Radial Head Hemiarthroplasty. *Accepted to the Journal of Shoulder and Elbow Surgery 2014.*

5. **Langohr, G.D.G.**, Giles, J.W.G., Athwal, G.S.A., Johnson, J.A. The Effect of Glenosphere Diameter in Reverse Shoulder Arthroplasty on Muscle Force, Joint Load, and Range of Motion. *Accepted to the Journal of Shoulder and Elbow Surgery 2014.*

6. Irish, S.E., **Langohr, G.D.G.**, Willing, R., King, G.J.W., Johnson, J.A. Implications of Radial Head Hemiarthroplasty Dish Depth on Radiocapitellar Contact Mechanics. *Accepted to The Journal of Hand Surgery 2014.*

7. Abdulla, I., **Langohr, G.D.G.**, Gladwell, M., Yeung, C., Faber, K.J., King, G.J.W., Athwal, G.S. Optimizing the Sizing of Radial Head Implants. *Accepted to The Journal of Shoulder and Elbow Surgery 2014*.

8. Teeter MG, **Langohr GDG**, Medley JB, Holdsworth DW (2014) Nondestructive Microimaging During Preclinical Pin-on-Plate Testing of Novel Materials for Arthroplasty. Proc IMechE, Part H, Journal of Engineering in Medicine, 228, 2,159-64.

9. **Langohr, G.D.G.**, Austin, H.A., Medley, J.B. (2011) Wear performance of all-polymer PEEK articulations for a cervical total level arthroplasty system. *IMechE Part J: J Eng Tribology 2011*, 225(6), pp 499-513.

B Refereed Abstracts and Conference Presentations

1. **Langohr, G.D.G.**, Willing, R., Medley, J.B., Medley, J.B., Johnson, J.A., King, G.J.W. (2014) The Effect of Radial Head Hemiarthroplasty Geometry on Proximal Radioulnar Joint Contact Mechanics, Paper #32. *American Shoulder and Elbow Surgeons (ASES) 2015 Closed Meeting*, October 8-11, Asheville, NC.

2. **Langohr, G.D.G.**, Willing, R., Medley, J.B., Athwal, G.S.A., Johnson, J.A. The Effect of Reverse Total Shoulder Implant Neck-Shaft Angle, Cup Depth, and Size on Contact Mechanics. 2015 2nd Annual Pan Pacific Orthopaedic Congress, July 22-25, Hawaii, US.

3. **Langohr, G.D.G.**, Giles, J.W., Athwal, G.S., Johnson, J.A., King, G.J.W. (2015) An In-Vitro Study of the Effect of Reverse Shoulder Arthroplasty Glenosphere Size on Joint Load, Muscle Force, and Range of Motion. 60th *Meeting of the Orthopaedic Research Society*, March 28-31, Las Vegas, NV.

4. Giles, J.W., **Langohr, G.D.G.**, Athwal, G.S., Johnson, J.A., King, G.J.W. (2015) The Influence of Reverse Shoulder Arthroplasty Implant Variables on Muscle Activation and Joint Load. 60th *Meeting of the Orthopaedic Research Society*, March 28-31, Las Vegas, NV.

5. Khayat, A., **Langohr, G.D.G.**, Lalone, E.A., Willing, R., Medley, J.B., King, G.J.W., Johnson, J.A. (2015) The Effect of Pin Geometry on Early Cartilage Wear in Linear Reciprocal Sliding. 60th *Meeting of the Orthopaedic Research Society*, March 28-31, Las Vegas, NV.

6. Razfar, N., Reeves, J., **Langohr, G.D.G.**, Willing, R., Athwal, G.S., Johnson, J.A. (2015) The Effect of Humeral Component Length of Bone Stresses: A Finite Element (FE) Analysis. 60th *Meeting of the Orthopaedic Research Society*, March 28-31, Las Vegas, NV.

7. Reeves, J., Razfar, N., **Langohr, G.D.G.**, Athwal, G.S., King, G.J.W., Johnson, J.A. (2015) The Effect of Material Selection and Implant Positioning on Cartilage Stresses Following Partial Joint Resurfacing: A Finite Element Study. 60th *Meeting of the Orthopaedic Research Society*, March 28-31, Las Vegas, NV.

8. **Langohr, G.D.G.**, Willing, R., Medley, J.B., Medley, J.B., Johnson, J.A., King, G.J.W. (2015) Contact Mechanics of Axisymmetric & Non-Axisymmetric Radial Head Hemiarthroplasty Compared to the Native Joint, Paper #23. *2015 AAOS Annual Meeting*, March 24-28, Las Vegas, NV.

9. **Langohr, G.D.G.**, Giles, J.W.G., Athwal, G.S.A., Johnson, J.A. The Effect of Glenosphere Size on Joint Load, Muscle Force, and Range of Motion in Reverse Shoulder Arthroplasty. 2015 Canadian Orthopaedic Research Society Meeting, June 17-20, Vancouver, Canada.

10. Abdulla, I.M.D., **Langohr, G.D.G.,** Giles, J.W., Johnson, J.A., Athwal, G.S. The Effect of Humeral Cup Constraint in Reverse Shoulder Arthroplasty: An In-Vitro Cadaveric Study. 2015 Canadian Orthopaedic Research Society Meeting, June 17-20, Vancouver, Canada.

11. Abdulla, I.M.D., **Langohr, G.D.G.**, Giles, J.W., Johnson, J.A., Athwal, G.S. The Effect of Fracture Comminution on the Reliability and Accuracy of Radial Head Sizing. 2015 Canadian Orthopaedic Association Annual Meeting, June 17-20, Vancouver, Canada.

12. Johnson, A.J., **Langohr, G.D.G.**, King, G.J.W., Johnson, J.A. The Effect of Material Selection on Radial Head Hemiarthroplasty Joint Contact Mechanics Using Patient Specific Geometry. 2015 Canadian Orthopaedic Association Annual Meeting, June 17-20, Vancouver, Canada.

13. Khayat, A,. **Langohr, G.D.G.**, Lalone, E.A., Willing, R., Medley, J.B., King, G.J.W., Johnson, J.A. The Effect of Contact Geometry on Early Cartilage Wear in Linear Reciprocal Motion. 2015 Canadian Orthopaedic Association Annual Meeting, June 17-20, Vancouver, Canada.

14. Razfar, N., Reeves, J., **Langohr, G.D.G.**, Willing, R., Athwal, G.S., Johnson, J.A. Comparison of Proximal Humeral Bone Stresses for Stemless, Short and Standard Stem Humeral Components for Shoulder Arthroplasty - A Finite Element Study. 2015 Canadian Orthopaedic Association Annual Meeting, June 17-20, Vancouver, Canada.

15. Reeves, J., Razfar, N., **Langohr, G.D.G.,** Athwal, G.A., King, G.J.W., Johnson, J.A. The Effect of Positioning of Partial Joint Resurfacing Implants on the Contact Mechanics of the Opposing Cartilage: A Finite Element Study. 2015 Canadian Orthopaedic Association Annual Meeting, June 17-20, Vancouver, Canada.

16. Abdulla, I.M.D., **Langohr, G.D.G.,** Giles, J.W., Johnson, J.A., Athwal, G.S. The Effect of Humeral Cup Constraint in Reverse Shoulder Arthroplasty: An In-Vitro Cadaveric Study. 2015 Canadian Orthopaedic Residents Association Meeting, June 17, Vancouver, Canada.

17. **Langohr, G.D.G.**, Willing, R., Medley, J.B., Medley, J.B., Johnson, J.A., King, G.J.W. (2014) The Effect of Radial Head Hemiarthroplasty Geometry on Radiocapitellar Joint Contact Mechanics, Paper #23. *American Shoulder and Elbow Surgeons (ASES) 2014 Closed Meeting*, October 9-12, Pinehurst, NC.

18. Abdulla, I.N., **Langohr, G.D.G.**, Giles, J.W., Johnson, J.A., Athwal, G.S.A. (2014) The Effect of Humeral Cup Constraint in Reverse Shoulder Arthroplasty: A Cadaveric In-Vitro Study. 2014 London Health Sciences Resident Research Day (Best Paper Award), October 7, London, ON.

19. **Langohr, G.D.G.**, Giles, J.W.G., Johnson, J.A., Athwal, G.S.A. An In-Vitro Study of the Effect of Reverse Shoulder Arthroplasty Sizing on Active and Passive Abduction and Internal-External Rotation. *Imperial College Annual Bioengineering Meeting,* 10-11 Sept 2014, Imperial College, London, UK.

20. Giles, J.W.G., **Langohr, G.D.G.**, Johnson, J.A., Athwal, G.S.A. The Influence of Reverse Shoulder Arthroplasty Implant Variables on Muscle Activation and Joint Load. *Imperial College Annual Bioengineering Meeting,* 10-11 Sept 2014, Imperial College, London, UK.

21. **Langohr, G.D.G.**, Willing, R., Medley, J.B., King, G.J.W., Johnson, J.A. (2014) Comparison of the Native Radiocapitellar Joint to Axisymmetric and Non-Axisymmetric

Radial Head Hemiarthroplasty Using Finite Element Contact Analysis. *Meeting of the Canadian Orthopaedic Association,* June 17-21, Montreal, QC.

22. **Langohr, G.D.G.**, Willing, R., Medley, J.B., Athwal, G.S.A., Johnson, J.A. (2014) Effects of Head-Neck Angle on the Contact Mechanics of Reverse Shoulder Arthroplasty. *Meeting of the Canadian Orthopaedic Association,* June 17-21, Montreal, QC

23. Irish, S.E., **Langohr, G.D.G.**, Willing, R., King, G.J.W., Johnson, J.A. (2014) Implications of Radial Head Hemiarthroplasty Dish Depth on Contact Mechanics: A Finite Element Analysis. *Meeting of the Canadian Orthopaedic Association,* June 17-21, Montreal, QC.

24. **Langohr, G.D.G.**, Willing, R., Medley, J.B., King, G.J.W., Johnson, J.A. (2014) The Effect of Radial Head Hemiarthroplasty Shape on Proximal Radioulnar Joint Contact. *Meeting of the Canadian Orthopaedic Association,* June 17-21, Montreal, QC.

25. Reeves, J., Razfar, N., **Langohr, G.D.G.**, Athwal, G.S.A., King, G.J.W., Johnson, J.A. (2014) The Effect of Material Selection and Position of Partial Joint Replacement Prostheses on Articular Contact Mechanics: A Finite Element Study. *Meeting of the Canadian Orthopaedic Association,* June 17-21, Montreal, QC.

26. **Langohr, G.D.G.**, Willing, R., Medley, J.B., Athwal, G.S.A., Johnson, J.A. (2014) Contact Mechanics of Reverse Total Shoulder Arthroplasty During Abduction: The Effect of Head-Neck Angle and Humeral Cup Depth. *2nd Meeting of the International Conference on BioTribology (ICoBT),* May 11-14, Toronto, ON.

27. Bobo, A.B.I., **Langohr, G.D.G.**, Medley, J.B., De Wet, D.D. (2014) Static Friction Forces for Porous Surfaced Cobalt-Chromium Alloys Against Simulated Trabecular Bone. *2nd Meeting of the International Conference on BioTribology (ICoBT),* May 11-14, Toronto, ON.

28. **Langohr, G.D.G.**, Willing, R., Medley, J.B., King, G.J.W., Johnson, J.A. (2014) Finite Element Contact Analysis of the Native Radiocapitellar Joint Compared to Axisymmetric and Non-Axisymmetric Radial Head Hemiarthroplasty. *59th Meeting of the Orthopaedic Research Society*, March 15-18, New Orleans, LA.

29. **Langohr, G.D.G.**, Willing, R., Medley, J.B., King, G.J.W., Johnson, J.A. (2014) The Effect of Radial Head Hemiarthroplasty Shape on Proximal Radioulnar Joint Contact Mechanics: A Finite Element Contact Analysis. *59th Meeting of the Orthopaedic Research Society*, March 15-18, New Orleans, LA.

30. Irish, S.E., **Langohr, G.D.G.**, Willing, R., King, G.J.W., Johnson, J.A. (2014) Finite Element Analysis of Radial Head Hemiarthroplasty: Implications of Dish Depth on Contact Mechanics. *59th Meeting of the Orthopaedic Research Society*, March 15-18, New Orleans, LA.

31. Razfar, N., Reeves, J., **Langohr, G.D.G.**, Willing, R., Athwal, G.S.A., Johnson, J.A. The Effect of Shoulder Humeral Component Length on Bone Stresses: A Finite Element Analysis. *22nd Annual Symposium on Computational Methods in Orthopaedic Biomechanics*, March 14, New Orleans, LA.

32. **Langohr, G.D.G.**, Willing, R., Medley, J.B., King, G.J.W., Johnson, J.A. (2013) Finite Element Contact Analysis of Axisymmetric and Non-Axisymmetric Radial Head Hemiarthroplasty. *58th Meeting of the Orthopaedic Research Society*, January 26-29, San Antonio, Texas.

33. **Langohr G.D.G.**, Teeter, M.G., Agarwal, M., Holdsworth, D.W., Medley, J.B. (2013) Comparison of Gravimetric and Micro-CT Wear Assessment Methods for Metal-on-PEEK Pin-on-Plate Testing. *58th Meeting of the Orthopaedic Research Society*, January 26-29, San Antonio, Texas.

34. **Langohr, G.D.G.**, Willing, R., Medley, J.B., King, G.J.W., Johnson, J.A. (2013) Finite Element Contact Analysis of Axisymmetric and Non-Axisymmetric Radial Head Hemiarthroplasty. *19th Canadian Connective Tissue Conference*, May 29-June 1, Montreal, QC.

35. **Langohr G.D.G.**, Teeter, M.G., Maheshwari, N., Agarwal, M., Holdsworth, D.W., Medley, J.B. (2012) Using Micro-CT to Determine the Wear of PEEK in Pin-on-Plate Testing. *57th Meeting of the Orthopaedic Research Society*, February 4-7, San Francisco, California.

36. **Langohr, G.D.G.**, Medley, J.B. (2012) Conceptual Design of a Cervical Disc and Facet Joint Arthroplasty System made from PEEK. *25th Annual Meeting of the International Society for Technology in Arthroplasty*, October 3-6, Sydney, Australia.

37. **Langohr, G.D.G.**, Willing, R., Medley, J.B., King, G.J.W., Johnson, J.A. (2012) A Finite Element Contact Analysis of Axisymmetric and Anatomical Radial Head Hemiarthroplasty. *Meeting of the Canadian Orthopaedic Association,* June 8-10, Ottawa, ON.

38. Gawel, H.A., **Langohr, G.D.G.**, Harper, M.L., Medley, J.B. (2012) Some tribology of self-mating PEEK articulations for cervical disc arthroplasty. *International Conference on BioTribology*, September 18-21, Imperial College, London, UK.

39. Medley, J.B., Maheshwari, N., **Langohr, G.D.G.**, Yao, M., de Wet, D. (2012) A new cobalt-based alloy for metal-metal hip implants? *International Conference on BioTribology*, September 18-21, Imperial College, London, UK.

40. **Langohr G.D.G.**, Teeter, M.G., Maheshwari, N., Agarwal, M., Holdsworth, D.W., Medley, J.B. (2012) Using Micro-CT to Determine the Wear of PEEK in Pin-on-Plate Testing. *London Health Research Day*, January 20, London, ON.

41. **Langohr, G.D.G.** (2011) Wear Assessment and Improvement of Upper Extremity Joint Replacements. *CIHR Joint Motion Training Program in Musculoskeletal Health Research and Leadership: Annual Retreat*, June 2011, The University of Western Ontario, London, ON.

42. **Langohr, G.D.G.**, Gawel, H.A., Maheswari, N., Medley, J.B. (2011) Carbon-Fiber Reinforced PEEK for Cervical Disc Arthroplasty. *Society for Biomaterials Annual Meeting and Exposition*, April 13-16, Orlando, FL.

43. **Langohr, G.D.G.**, Gawel, H.A., Maheswari, N., Medley, J.B. (2011) CFR PEEK and it's application for Cervical Disc Arthroplasty. *Schulich School of Medicine and Dentistry Margaret Moffat Research Day*, March 29, London, Ontario, Canada.

44. **Langohr, G.D.G.**, Gawel, H.A., Maheshwari, N., Harper, M.L., Medley, J.B. (2011) Tribology of all-polymer PEEK articulations for cervical spine arthroplasty. *18th International Conference on Wear of Materials,* April 3-7, Philadelphia, PA.

45. **Langohr, G.D.G.**,Maheshwari, N., Medley, J.B. (2011) Wear Performance of Self Mating Unfilled and Carbon Fiber Reinforced PEEK Articulations. *56th Meeting of the Orthopaedic Research Society*, January 13-16, Long Beach, California.

46. **Langohr, G.D.G.**, Austin, H.A., Medley, J.B. (2010) Cervical Total Level Arthroplasty System with All-Polymer PEEK Articulations. *Proc. 37th Leeds-Lyon Symposium on Tribology*, September 7-10, The University of Leeds, Leeds, UK.

47. **Langohr, G.D.G.**, Medley, J.B. (2010) Design of a Total Level Spinal Arthroplasty (TLSA) for the Cervical Spine: Consideration of Kinematics and Materials. *Proc. 28th Canadian Biomaterials Society Conference*, June 2-4, Kingston, ON.

48. Austin, H., **Langohr, G.D.G.,** Harper, M.L., Medley, J.B. (2009) Performance of PEEK All-Polymer Articulations for Spinal Applications. *Proc. 56th Meeting of the Orthopaedic Research Society*, March 6-9, New Orleans, Louisiana.

49. Austin, H., Harper, M.L., Medley, J.B. and **Langohr, G.D.G.** (2009) Exploring the wear of a PEEK all-polymer articulation for spinal applications. *Society for Biomaterials Annual Meeting and Exposition*, April 22-25, San Antonio, TX.

50. Austin, H., Harper, M.L., Medley, J.B. and **Langohr, G.D.G.** (2009) Wear and surface damage of a PEEK all-polymer articulation for spinal applications. *Proc. 27th Canadian Biomaterials Society Conference*, May 20-23, Québec City, QC.

C   Non-Refereed Contributions

1. **Langohr, G.D.G.** (2010) Cervical Total Level Spinal Arthroplasty System With PEEK All-Polymer Articulations. MASc Thesis, University of Waterloo, 230 pages.

2. **Langohr, G.D.G.,** Medley, J.B. (2009) Design of an Implant System for Both Disc and Facet Joint Arthroplasty in the Cervical Spine. Submitted to A. Kinbrum, Invibio Ltd., Thornton-Cleveleys, Lancashire, UK, 46 Pages.

3. **Langohr, G.D.G.** (2009) The Effects of Young's Modulus and Poisson's Ratio on Spinal Disc Load Response. CIVE 701: Tissue Engineering Final Project Report, 50 Pages.

4. **Langohr, G. Daniel G.** (2007) Cervical Spine Implant Wear Simulator: Conversion of MATCO Hip Simulator. Prepared for Dr. John Medley, University of Waterloo, Manufacture and Implementation Report, 62 Pages.

5. **Langohr, G. Daniel G.** (2006) Cervical Spine Implant Wear Simulator: Conversion of MATCO Hip Simulator. Prepared for Dr. John Medley, University of Waterloo, Final Design Report, 54 Pages.

EXTRA ACTIVITES

1. **Guest Lecture: Implant Design and Failure (MME 4469)**
    The University of Western Ontario, London ON (March 2015)

2. **Biomedical Engineering Research Day Invited Talk: Reverse Total Shoulder Arthroplasty: Putting a Shoulder Replacement in Backwards has its Advantages and Disadvantages**
    The University of Western Ontario, London ON (Oct 2014)

3. **Engineering Biomechanics (ME 598/CIVE 460) Guest Lecture: Biomechanics of the Upper Limb**
    University of Waterloo, Waterloo ON (Jan 2014)

4. **Advcd Topics in Mechanical Engineering (MME 4427) Guest Lecture: Implant Design and Failure**
    The University of Western Ontario, London ON (Feb 2012)

5. **FIRST Lego League Team #2042 Expert Guest Speaker**
    Guest lectured grade school students on biomedical engineering topics and careers (Nov 2010)

6. **'ExpecTAtions' Seminar**
    Delivered a two-day seminar on being an effective Teaching Assistant to new graduate students (2009)

PROFESSIONAL & SOCIETY MEMBERSHIPS

2013-   Orthopedic Research Society Associate Member (ORS)

2008-   Canadian Biomaterials Society (CBS)

2008-   Society for Biomaterials (SFB)

2009-   Orthopaedic Research Society Student Member (ORS)

2008-   Professional Engineers of Ontario (PEO) Student Member

RESEARCH SUPERVISION

A   Co-op Students
1. Mr. Nick Asapu (2015)
    The Effect of RSA Size on Abduction Range of Motion (Co-Supervised with J. Johnson)

2. Mr. Andre Bodo (2013)
    Friction of Bone-Porous Metal Constructs (Co-Supervised with J. Medley)

3. Ms. Micky Agarwal (2011)
    Pin-on-Plate wear testing of self-mating CoCR articulations (Co-Supervised with J. Medley)

4. Ms. Nupur Maheswari (2010)
    Wear of Medical Implant Materials (Co-Supervised with J. Medley)

B Undergraduate Fourth Year Projects

1. Mr. Daniel Tovbis (2015)
    The Effect of Deltoid Line of Action on Scapular Stress with Special Interest in Acromial Fractures (Co-Supervised with J. Johnson)

2. Mr. Nathan Law (2013)
    Investigation of Patient Specific Radial Head Hemiarthroplasty Implants (Co-Supervised with J. Johnson)

3. Mr. Andre Bodo (2012)
    Wear Testing of Nitinol Wire for Cardiac Applications (Co-Supervised with J. Medley)

4. Ms. Joyce Lam (2009)
    Wear of Medical Implant Materials (Co-Supervised with J. Medley)

C Undergraduate Research Assistants

1. Mr. Jakub Szmit (2015)
    Optimization of the Geometry of Radial Head Hemiarthroplasty Implants (Co-Supervised with J. Johnson)

2. Mr. Murray Wong (2015)
    Investigation of the Impact of Reverse Shoulder Arthroplasty on Acromial Stresses (Co-Supervised with J. Johnson)

3. Ms. Elizabeth Irish (2014)
    The Effect of Radial Head Hemiarthroplasty Dish Depth (Co-Supervised with J. Johnson)

4. Mr. Andrew Johnson (2014)
    Investigation of the Effect of Radial Head Hemiarthroplasty Stiffness (Co-Supervised with J. Johnson)

5. Mr. Andre Bodo (2012)
    Friction of Various Porous Coated Metals (Co-Supervised with J. Medley)

5. Ms. Elizabeth Irish (2013)
    Elbow Joint FEA Contact Analysis (Co-Supervised with J. Johnson)

6. Mr. Andrew Johnson (2013)
    Mechanical Engineering (Co-Supervised with J. Johnson)

D Research Assistants

1. Mr. Michael Griffiths (2015)
    Wear Studies of Reverse Shoulder Implants (Co-Supervised with J. Johnson & J.B.Medley)

VOLUNTEER EXPERIENCE

2013 – Present	**Student Chair, Biomedical Engineering Student Committee** The University of Western Ontario, London ON
2013 – Present	**Representative, Schulich School of Medicine and Dentistry Graduate Committee** The University of Western Ontario, London ON
2013 – 2014	**Engineering Summer Academy Organizer/Instructor, Western Student Outreach** The University of Western Ontario, London ON
2012 – 2013	**Treasurer, Biomedical Engineering Student Committee** The University of Western Ontario, London ON
2011 – 2012	**Engineering Summer Academy Instructor, Western Student Outreach** The University of Western Ontario, London ON
2008 – 2010	**International Graduate Student Academic Mentor** University of Waterloo, Waterloo ON